REPORT DOCUMENTATION PAGE

Form Approved
OMB No. 0704-0188

1. AGENCY USE ONLY (Leave blank)	2. REPORT DATE	3. REPORT TYPE AND DATES COVERED
	Mar 94	Final 11 May 87 - 10 May 92

4. TITLE AND SUBTITLE
Stress-State Effects on Strength and Fracture of Partially-Stabilized Zirconia

5. FUNDING NUMBERS
DAAL03-87-K-0060

6. AUTHOR(S)
Dinesh K. Shetty

7. PERFORMING ORGANIZATION NAME(S) AND ADDRESS(ES)
University of Utah
Department of Materials Science and Engineering
304 EMRO
Salt Lake City, UT 84112

8. PERFORMING ORGANIZATION REPORT NUMBER

9. SPONSORING/MONITORING AGENCY NAME(S) AND ADDRESS(ES)
U. S. Army Research Office
P. O. Box 12211
Research Triangle Park, NC 27709-2211

10. SPONSORING/MONITORING AGENCY REPORT NUMBER
ARO 24583.11-MS

11. SUPPLEMENTARY NOTES
The view, opinions and/or findings contained in this report are those of the author(s) and should not be construed as an official Department of the Army position, policy, or decision, unless so designated by other documentation.

12a. DISTRIBUTION/AVAILABILITY STATEMENT
Approved for public release; distribution unlimited.

12b. DISTRIBUTION CODE

13. ABSTRACT *(Maximum 200 words)*

Stress-state effects on the transformation yield stresses of commercial-grade ceria-partially-stabilized zirconia/alumina (Ce-TZP/Al_2O_3) composite and MgO-partially-stabilized zirconia (Mg-PSZ) were studied in various biaxial tests and in hydraulic compression tests. The yield envelopes in tension-tension and tension-compression stress quadrants and the pressure sensitivity of the yield stress in uniaxial compression were rationalized by a hypothesis where stress-induced transformation is triggered by a critical value of the interaction energy calculated according to the method of Eshelby. Crack-tip transformation zone shapes and sizes and rising crack-growth-resistance behaviors were stuided in Ce-TZP/Al_2O_3. The shape of the crack-tip transformation zones was not consistent with the derived yield criterion; however, the crack shielding developed by the elongated zones could be explained by zone shielding theories that took into account the observed zone shape and the variations in the monoclinic content within the zones. The variation of the R-curves with the sintering temperature was consistent with the efects of transformation zone shape and size on zone shielding. The Ce-TZP/Al_2O_3 composites were also shown to exhibit a genuine fatigue crack-growth phenomenon. Characteristics of their fatigue behavior included higher crack-growth rates in tension-tension cyclic loading as compared to crack-growth rates in peak sustained loads, lower threshold stress intensity for initiation of crack growth in fatigue and a systematic decrease of the thresholds with increasing transformation yield stress.

14. SUBJECT TERMS
Partially-Stabilized Zirconia, Transformation Yielding, Crack-Growth Resistance Behavior

15. NUMBER OF PAGES

16. PRICE CODE

17. SECURITY CLASSIFICATION OF REPORT	18. SECURITY CLASSIFICATION OF THIS PAGE	19. SECURITY CLASSIFICATION OF ABSTRACT	20. LIMITATION OF ABSTRACT
UNCLASSIFIED	UNCLASSIFIED	UNCLASSIFIED	UL

STRESS-STATE EFFECTS ON STRENGTH AND FRACTURE OF PARTIALLY-STABILIZED ZIRCONIA

Final Report

Prof. Dinesh K. Shetty

March, 1994

U. S. ARMY RESEARCH OFFICE

Grant Number : DAAL03-87-K-0060

University of Utah
Department of Materials Science and Engineering
304 EMRO
Salt Lake City, Utah 84112

Approved for Public Release
Distribution Unlimited

TABLE OF CONTENTS

LIST OF APPENDIXES

INTRODUCTION

Partially-stabilized zirconia ceramics that exhibit significant transformation plasticity and high fracture toughness display strong influence of stress state on strength and fracture. This stress-state influence is due to the dilatation and the shear components of the strain associated with the metastable tetragonal to the equilibrium monoclinic phase transformation in partially-stabilized zirconia and their interaction with the components of the applied stress. This interaction between the transformation strain components and the applied stress components, i.e., the stress-induced transformation, determines the transformation yield stress in a given stress state. Stress states with strong hydrostatic tension promote the transformation and lower the transformation yield stress, while hydrostatic compression suppresses the transformation and increases the transformation yield stress. This influence of the stress state on the transformation yield stress also affects the size and the shape of the transformation zones at crack tips. The growth of these transformation zones with increasing crack-driving force, i.e., the applied stress intensity, in the wake of the crack produces the rising crack-growth-resistance or R-curve behavior of partially-stabilized zirconia. R-curves for surface or internal (microstructural) flaws define the ultimate strength of zirconia ceramics via a crack-stability criterion. Thus, a fundamental understanding of the stress-state influence on transformation yielding is essential to the understanding of the stress-state effects on strength and fracture of partially-stabilized zirconia ceramics.

STATEMENT OF THE PROBLEM STUDIED

Partially-stabilized zirconia ceramics that possess high strength and high fracture toughness are used in structural applications wherein they are subjected to complex multiaxial stress states. But the current understanding of the mechanical behavior of zirconia ceramics is largely limited to simple uniaxial stress state. The potential applications of zirconia ceramics highlight an area of limited understanding, i.e., the effects of stress state on transformation yielding and fracture strength.

RESEARCH OBJECTIVES

The objectives of this research were to conduct critical experiments and develop a theoretical basis for formulating stress-state effects on transformation yield stress of a high toughness partially-stabilized zirconia and use the resulting yield criterion

to study crack-tip transformation zones and rising crack-growth-resistance (R-curve) behavior.

RESEARCH APPROACH

Commercial-grades of ceria-partially-stabilized-zirconia-alumina composite[§] (Ce-TZP/Al_2O_3) and MgO-partially-stabilized zirconia[¶] that exhibit pronounced transformation plasticity and R-curve behavior at ambient temperature were selected for this study. Test specimens suitable for measuring transformation yield stresses in various biaxial stress states (uniaxial tension, uniaxial compression, equibiaxial tension and tension-compression) and fracture mechanics specimens (compact tension and single-edge-notch beam) suitable for studying crack-tip transformation zones and measuring R-curves and subcritical crack growth rates were fabricated from sintered billets. The billets of the Ce-TZP/Al_2O_3 were prepared in-house from premixed and spray-dried powder by die-pressing, isopressing and sintering of powder compacts. The sintering temperature was varied in the range 1425 to 1525 °C to vary the grain size of the metastable tetragonal zirconia and the transformation yield stress. Sintered billets of the MG-PSZ were purchased from the vendor. Well-defined transformation yield points associated with abrupt transition from the elastic to the plastic regime were measured on Ce-TZP/Al_2O_3 with strain gauges. Stable crack growth was monitored in compact specimens using traveling microscopes and/or microcircuit grids. In addition, under a subcontract with Southwest Research Institute selected uniaxial compression tests were conducted at high strain rates in compression (Hopkinson pressure bar tests) and in confining hydraulic pressure to study the strain-rate sensitivity and the pressure sensitivity of transformation yielding, respectively.

SUMMARY OF THE MOST IMPORTANT RESULTS

Details of the experimental results and the theoretical analyses are given in appendixes A through F. Summaries of the most important results are given here in three sections :

---

§ Grade Z-65, Ceramatec, Inc., Salt Lake City, Utah 84119

¶ TS grade, Nilcra Ceramics (USA) Inc., St. Charles, IL 60174

(1) Stress-State Effects on the Transformation Yield Stress of Partially-Stabilized Zirconias (Appendices A and B)

(a) Transformation yield envelopes in tension-tension and tension-compression biaxial stress quadrants were established for commercial grades of Ce-TZP/Al_2O_3 and a MgO-partially-stabilized zirconia (Mg-PSZ) via the measurements of stress-induced transformation yield points in four different mechanical tests. A high yield stress in compression relative to that in tension (approximately 4 times) was the significant feature of the envelopes for transformation yielding. This result is consistent with the dilatation and the shear components of the tetragonal to monoclinic transformation strain and their interaction with the applied stress components.

(b) A theoretical analysis of the stress-state effect on transformation yielding was developed by applying Eshelby's inclusion theory. The basis for formulating the yield envelope was the criterion that the same critical interaction energy was attained in different stress states at the yielding stress. The interaction energy, which is a function of the applied stress, stress state and transformation strains (both dilatation and shear), was maximized with respect to the orientation of the martensite habit plane. The pertinent equations derived for yield criteria in tension-tension ($k > 0$) and tension-compression ($k < 0$) stress states were as follows :

Tension-Tension

$$\sigma_y^k = \frac{\sigma_y^T}{1 + k\left(\dfrac{\frac{\Delta}{3}}{\frac{\Delta}{3} + \xi \cos^2\beta^* + s \cos\beta^* \sin\beta^*}\right)}$$

Tension-Compression :

$$\sigma_y^k = \frac{\sigma_y^T}{1 + k\left[\dfrac{\frac{\Delta}{3} + \xi \sin^2\beta^* - S \cos\beta^* \sin\beta^*}{\frac{\Delta}{3} + \xi \cos^2\beta^* + S \cos\beta^* \sin\beta^*}\right]}$$

where

σ_y^k = transformation yield stress in a stress state characterized by $k = \sigma_2/\sigma_1$, where σ_1 and σ_2 are principal stresses,

σ_y^T = transformation yield stress in uniaxial tension,

Δ = dilatation strain,

ξ= component of out of plane strain,

β^* = orientation of habit plane normal for maximum interaction energy.

The yield criteria as developed above have been found to adequately describe measured yield envelopes for both Ce-TZPs and Mg-PSZs.

(c) The transformation yield stress of Ce-TZP/Al_2O_3 in uniaxial compression was found to increase linearly with confining hydrostatic pressure according to the equation :

$$\sigma_y^p = \sigma_y^c + \alpha^c p$$

where σ_y^p is the yield stress in compression under a confining pressure, p, σ_y^c is the yield stress in uniaxial compression and α_c is the pressure sensitivity of the yield stress. The theoretical analysis of stress-state effect based on Eshelby's inclusion theory was extended to treat transformation yielding under hydrostatic pressure by modifying the interaction energy by the dilatation strain energy, $p\Delta$. The analysis predicted the following equation for α^c :

$$\alpha^c = \frac{\Delta}{S \cos\beta^* \sin\beta^* - \frac{\Delta}{3} - \xi \sin^2\beta^*}$$

For type II A Ce-TZP/Al_2O_3, $(\sigma_y^T/\sigma_y^C) = 4.0$, $S = 0.075$, $\Delta = 0.04$, $\beta^* = 37.5$ degrees and $\xi = 0.02$. For these values of the parameters, above equation predicts $\alpha^c = 2.584$. This predicted value is within the 90 % confidence interval for the pressure sensitivity measured in experiments .

(d) The effects of strain rate on the transformation yield stress and the ultimate stress of Ce-TZP/Al_2O_3 composite (type A) in uniaxial compression were studied in collaboration with Dr. James Lankford as part of a subcontract from University of Utah to Southwest Research Institute. In the strain rate range, 10^{-5} to 1 (s^{-1}), Ce-TZP/Al_2O_3 exhibited distinct yield-point behavior, but the upper yield stress was insensitive to the strain rate. Tests above 1 s^{-1} (up to 2400 s^{-1}) were conducted using Hopkinson pressure bar apparatus. These tests showed elastic-plastic behavior, but no distinct yield point was observed. The ultimate stress corresponding

to the maximum sustained load showed a modest increase with increasing strain rate in the entire strain rate range.

(2) Transformation zone Size, Shape and R-Curve Behavior of Ce-TZP/Al_2O_3 Composites (Appendixes B, C, D & E).

(a) A systematic increase in the transformation yield stress with decreasing size of the metastable tetragonal zirconia grains (varied by varying the sintering temperature) in the Ce-TZP/Al_2O_3 was shown to be consistent with 'end point' thermodynamic analysis of stability involving volume (chemical free energy & strain energy) and surface (interface and twin/microcrack) energies. The analysis predicted the observed inverse relationship between grain size and the transformation yield stress.

(b) Ce-TZP/Al_2O_3 composites of different grain sizes and transformation yield stresses have been shown to exhibit rising-crack-growth-resistance (R-Curve) behavior. A number of significant results have been obtained in this area : (i) Ce-TZP/Al2O3 composites exhibited thin elongated transformation zones, not the circular zones expected from the shear/dilatation yield criterion. (ii) Composites of varying yield stresses exhibited widely differing crack-tip transformation zone sizes and, yet, their R-curves were remarkably similar. (iii) Transformation zone lengths at crack tips followed the classical Dugdale strip zone model.

(c) The crack-growth-resistance behavior of Ce-TZP/Al_2O_3 composites was analyzed using transformation zone shielding theory. The analysis took into account the observed shapes and local variations within the transformation zones of volume fraction of monoclinic phase determined by Raman spectroscopy. The results indicated that the insensitivity of the fracture toughness and the R-curves to the zone size variations was due to a compensating zone-shape effect. Smaller zones were associated with greater wake length to zone width ratio and a correspondingly higher normalized shielding stress intensity, κ. Transformation zone shielding accounted for roughly 60 % of the measured fracture toughness of Ce-TZP/Al_2O_3 composites.

(3) Fatigue Crack Growth Behavior of Ce-TZP/Al_2O_3 (Appendix F).

Fatigue crack growth measurements showed that Ce-TZP/Al_2O_3 composites exhibited a genuine fatigue crack growth phenomenon. Characteristics of their fatigue behavior included higher crack growth rates in tension-tension cyclic loading

as compared to crack growth rates at peak sustained loads, lower threshold stress intensity for initiation of crack growth in fatigue as compared to the thresholds under sustained loads and a systematic decrease of the stress-intensity thresholds with increasing transformation yield stress.

LIST OF PUBLICATIONS AND REPORTS

List of Publications :

1. C-S. Yu and D. K. Shetty, " Transformation Zone Shape, Size, and Crack-Growth-Resistance (R-Curve) Behavior of Ceria-Partially-Stabilized Zirconia Polycrystals, " Journal of the American Ceramic Society, Vol.72, No.6, pp.921-28 (1989).
2. C-S. Yu and D. K. Shetty, " Transformation Yielding, Plasticity and Crack-Growth-Resistance (R-Curve) Behavior of CeO_2-TZP, " Journal of Materials Science, Vol.25, pp.2025-35 (1990).
3. J-F. Tsai, C-S. Yu and D. K. Shetty, " Fatigue Crack Propagation in Ceria-Partially-Stabilized Zirconia (Ce-TZP)-Alumina Composites, " Journal of the American ceramic Society, Vol.73, No.10, pp.2992-3001 (1990).
4. J-F. Tsai, C-S. Yu and D. K. Shetty, " Role of Autocatalytic Transformation in Zone Shape and Toughening of Ceria-Tetragonal-Zirconia-Alumina (Ce-TZP/Al_2O_3) Composites, " Journal of the American Ceramic Society, Vol.74, No.3, pp.678-81 (1991).
5. C-S. Yu, D. K. Shetty, M. C. Shaw and D. B. Marshall, " Transformation Zone Shape Effects on Crack Shielding in Ceria-Partially-Stabilized Zirconia (Ce-TZP)-Alumina Composites, " Journal of the American Ceramic Society, Vol.75, No.11, pp.2991-94 (1992).

List of Theses and Reports

1. " Stress-State Effects on Transformation Yield Stress and Fracture Toughness of Zirconia Ceramics, " Ph. D. thesis of Dr. Cheng-Sheng Yu, University of Utah, March, 1991.
2. " Stress-State Effects on the Transformation Yield Stress of Ceria-Partially-Stabilized Tetragonal Zirconia/Alumina (Ce-TZP/Al_2O_3) Composites, ", Technical Report attached to this final report as Appendix A.

LIST OF PARTICIPATING SCIENTIFIC PERSONNEL

1. Dr. Dinesh K. Shetty, Professor of Materials Science and Engineering, University of Utah, Principal Investigator on the project.
2. Dr. Cheng-Sheng Yu. Dr. Yu received a Ph.D. in March, 1991 while working on the project as a research assistant.
3. Mr. Jing-Fong Tsai was partially supported on the project while working on his Ph.D. as a research assistant.
4. Dr. James Lankford, Institute Scientist, Southwest Research Institute collaborated on the project in the areas of high strain rate testing of the zirconia ceramics.

APPENDIXES

Appendixes A through F are attached to this report.

Appendix A

Stress-State Effects On The Transformation Yield Stress Of Ceria-Partially-Stabilized Tetragonal Zirconia/Alumina (Ce-TZP/Al_2O_3) Composites

Cheng-Sheng Yu and Dinesh K. Shetty
Department of Materials Science and Engineering
University of Utah
Salt Lake City, Utah 84112

ABSTRACT

Partially-stabilized zirconia ceramics that exhibit significant transformation plasticity and high fracture toughness display strong influence of stress state on strength and fracture. This stress-state influence is due to the dilatation and the shear components of the tetragonal to monoclinic transformation strain and their interaction with the components of the applied stress. A ceria-partially-stabilized zirconia/alumina (Ce-TZP/Al_2O_3) composite was employed in a study of the stress-state effects on transformation yield stress at room temperature (25 °C). Distinct yield points corresponding to abrupt transition from elastic to plastic regimes were measured on stress-strain records in three-point bending (uniaxial tension), compression (uniaxial compression), biaxial flexure (equibiaxial tension) and diametral compression (tension-compression) tests. The stress-state influence was manifested by high yield stress in uniaxial compression, low yield stress in biaxial tension and increase of the yield stress in compression with superposed hydrostatic pressure. The yield-stress envelope in the biaxial stress state and the pressure sensitivity of the yield stress were satisfactorily explained by a theoretical analysis based on the hypothesis that stress-induced transformation yielding is triggered at the same critical value of the maximum interaction energy. Eshelby's theory of the transforming inclusion was used to formulate the interaction energy in an arbitrary biaxial stress state in terms of the applied stress and the transformation strain components.

I. Introduction

The potential applications of zirconia ceramics highlight an area of limited understanding, i.e. the effects of stress state on strength and fracture toughness. Fracture strengths of ceramics are usually assessed in uniaxial bending or tension, whereas they are required to operate under complex multiaxial stress states in structural applications. There are two fundamental reasons for the stress-state dependence of the strength of conventional brittle ceramics. One is the statistical flaw effect in which the effective flaw severity due size and orientation of the strength-controlling critical flaw may be different in different stress states. The other is that Griffith's fracture criterion can be modified for a flaw subjected to normal and shear stresses parallel to the crack plane. In other words, the fracture criterion depends on the interaction of the principal stresses and the flaws. Statistical fracture theories, such as the classical Weibull theory[1] or the more recent fracture-mechanics based treatments of Batdorf [2,3], Evans [4] and Shetty [5], treat this aspect of stress-state effect on strength.

The fracture behavior of the zirconia ceramics that exhibit high fracture toughness differs from that of the conventional ceramics in two ways. First, there is significant transformation plasticity and inelastic deformation from microcracking preceding the final fracture [6-9]. Secondly, zirconia ceramics exhibit rising crack-growth-resistance or R-curve behavior[10-12], i.e. resistance to crack growth increases with increasing crack length, due to the formation and growth of a transformation zone around the crack tip. As a result, the conventional concepts of fracture mechanics and statistics of ceramic strengths cannot be directly applied to analyze the effects of stress-state on the strength of partially-stabilized zirconia. Zirconia ceramics can exhibit stress-state effects on strength for two reasons. First, the critical stress for transformation yielding is strongly dependent on the stress state due to the interaction of the applied stress components with the dilatation and the shear components of the transformation strain. Secondly, the R-curve behavior of zirconia ceramics, which governs the fracture strength and originates from the crack-tip transformation zones, is likely to be affected by the stress state. Both of these phenomena have attracted attention of researchers in recent years.

Chen and Reyes-Morel[13,14] studied stress-state effects on transformation yielding in MgO-partially-stabilized zirconia (Mg-PSZ) and CeO_2-partially-stabilized tetragonal zirconia polycrystal (Ce-TZP) in uniaxial compression with superposed hydrostatic pressure. They proposed a phenomenological yield criterion incorporating two

yield stress parameters, a characteristic equivalent stress and a characteristic mean stress. The proposed yield criterion accounted for the trends in the transformation yield stress in uniaxial compression and uniaxial tension and the effect of the superposed hydrostatic pressure on the yield stress in uniaxial compression.

The present paper reports the experimental results and the theoretical analyses of the stress-state effects on the transformation yield stress of a commercial-grade Ce-TZP/Al_2O_3 composite. The experiments included uniaxial (uniaxial compression and three-point bending), biaxial (biaxial flexure and diametral compression) and hydrostatic compression tests on Ce-TZP/Al_2O_3 sintered at different temperatures. The transformation yield stresses measured in different stress states were analyzed using a critical interaction energy criterion wherein the interaction energy is calculated using Eshelby's methodology of the transforming inclusion. The transformation yield envelope that emerges from this simple yield criterion is in good agreement with the experimental results and the phenomenological yield criterion.

II. Ce-TZP/Al_2O_3 Ceramics and Test Procedures

(1) Ce-TZP/Al_2O_3 Ceramics

A Ce-TZP/Al_2O_3 powder of the nominal composition, 88 wt % of Ce-TZP (12 mol % CeO_2 and 88 mol % ZrO_2) and 10 wt % Al_2O_3 and 2 wt % of proprietary dopants was obtained from a commercial source[#]. Billets of the Ce-TZP/Al_2O_3 were prepared by die-pressing, isopressing and sintering compacts from two powder lots (I and II). Test specimens sintered at five different temperatures 1525, 1500, 1475, 1450 and 1425 °C for 2 hours are referred to as type AA, type A, type B, type C and type D, respectively. The as-sintered billets were cut and ground to the required specimen dimensions and annealed at 1000 °C for 30 minutes before using them for different mechanical tests. The characterization of the microstructures, phase contents, and phase stability of the Ce-TZP/Al_2O_3 composites have been reported in recent papers[15-17].

(2) Mechanical Tests for Different Stress States

Several loading schemes that generated either uniaxial or biaxial stress states were used to assess the transformation yield stresses of the Ce-TZP/Al_2O_3 ceramics. Figure 1 illustrates the loading configurations and the specimen geometries and the

[#] Grade Z-65, Ceramatec, Salt Lake City, UT.

corresponding principal stress ratio, k ($k = \sigma_2/\sigma_1$, where σ_2, and σ_1 are the principal stresses) that can be obtained in each of the tests. The three-point bend test and the uniaxial compression test provided uniaxial stress states. A tension-compression stress state with a principal stress ratio $k = -3$ was achieved with diametral compression of disks. An equibiaxial tension stress state (principal stress ratio, $k = 1$) was obtained in a disk specimen supported on a concentric discrete points support and subjected to transverse pressure. Different cross-head speeds were selected for different test geometries in order to obtain the same initial elastic strain rate (1.5×10^{-5}/s).

(a) Three-Point Bending Test : Transformation yielding and plasticity in tension were characterized in three-point bending using beam specimens with dimensions 4 x 5 x 45 mm and 40 mm support span. Yu and Shetty[15,16] have described the test procedures and results in detail.

(b) Uniaxial Compression Test : Right circular cylinders, with diameter of 6.35 mm (0.25 inches) and length of 12.7 mm (0.5 inches) were used in uniaxial compression tests. The cylindrical specimens were loaded between two cylindrical alumina platens with diameter of 12.7 mm (0.5 inches) and length of 19.05 mm (0.75 inches). The contacting surfaces of both the specimens and the alumina platens were polished to 0.05 μm to reduce the effects of end friction. Strain gauges were placed along the axial and the hoop directions on the cylinder surface. The same type of specimens were also used in the studies of strain rate effects and confining pressure effects on the stress-strain behavior of the Ce-TZP/Al_2O_3 composites. The high strain rate tests using the Hopkinson pressure bar apparatus and the confining pressure experiments were conducted at Southwest Research Institute, San Antonio, Texas, under the direction of Dr. James Lankford. The compression tests were conducted at strain rates ranging from 0.97×10^{-5} to 2.423×10^{3} s^{-1}; low and intermediate rates were achieved using a standard servo-controlled test machine, while the high strain rates were obtained in the Hopkinson pressure bar system. In addition, uniaxial compression tests with an independently controlled confining hydrostatic pressure were conducted.

(c) Diametral Compression Test : The diametral compression test is also known as the Brazilian test or splitting tension test [18]. In this test method, a thin cylindrical (circular disk) specimen is compressed diametrally between two platens. Before testing, strain gauges were placed at the centers of the flat surfaces of the disks (31.75 mm in diameter by 2.5 mm thick). One strain gauge was aligned perpendicular to the loading axis to assess the indirect tensile stress, the other was aligned along the loading axis to measure the

compressive stress, thus recording the load and strain variations for both stress states at the same time.

(d) Biaxial Flexure Test : Biaxial tension was achieved in disk specimens by subjecting them to radially symmetrical bending forces. A hydraulic test cell that applies uniform lateral pressure on disk specimens supported on concentric ball support was used for biaxial flexure. A detailed description of the design of this biaxial flexure test was reported by Shetty et al. [19]. The disk specimen with diameter of 50.8 mm (2 inches) and thickness of 3.175 mm (0.125 inches) was supported on 40 ball bearings, 2.4 mm in diameter, placed along a circle 49.53 mm (1.95 inches) in diameter. A balanced biaxial tension stress state develops at the center of the disk. A strain gauge was placed at the center of the disk specimens and this maximum strain was monitored as a function of the applied pressure.

III. Experimental Results

(1) Tetragonal to Monoclinic Transformation in Ce-TZP/Al_2O_3

Figure 2 shows a transmission electron micrograph of type II A Ce-TZP-Al_2O_3 specimen. The micrograph shows a transformed grain consisting of many monoclinic laths that is surrounded by alumina particles and microcracks. Microcracks may have been formed during phase transformation or nonuniform deformation during sample preparation. These morphologies are similar to the observations in 12 mol % Ce-TZP by Hannink and Swain [20]. Monoclinic laths and microcracks at the lath terminations were observed to result from stress-induced tetragonal to monoclinic transformation.

(2) Transformation Yielding in Three-Point Bending Test

Figure 3 shows the stress-strain curves corresponding to the six different types of Ce-TZP-Al_2O_3 designated I A, II AA, II A, II B, II C and II D. The only difference among these was the average grain size of the tetragonal Ce-TZP phase due to the different sintering temperatures. Small differences in grain size produced significant differences in both the transformation yield stress and the total strain to fracture. The stress-strain records showed sharp transition from elastic to plastic regime with well-defined yield points. The yield stress increased from 176 to 390 MPa and the total strain to fracture decreased from 1.5 to 0.23 % with a decrease in grain size from 2.18 to 1.47 μm [16]. A yield plateau followed the yield point due to the sudden formation of a primary transformation band on the tension surface. A detailed description of the formation of these transformation bands

and nucleation of surface cracks within the bands leading to final fracture has been previously reported[16].

(2) Transformation Yielding in Uniaxial Compression Test

Figure 4 shows stress-strain curves measured in the axial and the hoop directions on a type II A cylindrical compression specimen. The strain in the axial direction is negative, while the hoop strain is positive. For convenience of comparison, the two stress-strain curves are plotted in the same stress-strain quadrant. The transformation strain plateau at the yield point in the hoop direction was about 3.34 times that in the axial direction. Beyond the yield plateau, the stress-strain curves were similar for the two directions. These results suggest that deformation in the hoop direction was preferred over deformation in the axial direction at yielding. This is an indication that transformed grains may have a preferred orientation in the initial stage of transformation. This preferred orientation can be further demonstrated by analyzing the phases on the as-yielded specimens in the axial and radial directions. The intensities of the monoclinic reflections, $(11\bar{1})_m$ and $(111)_m$, in the axial direction were reversed as compared to those in the radial direction. These observations suggest that a texture of the monoclinic phase (transformed phase) was developed in the as-yielded compression specimens. A similar preferred orientation in a 12 mol % Ce-TZP cylindrical specimens was shown by Bowman et al. [21]. In their study, a pole figure goniometer was employed to detect the fraction of transformed grains over a range of orientation with respect to the compression axis. They found that maximum transformation occurred at 35° in the initial stage of transformation. This preferred orientation changed as the sample was further deformed. Reyes-Morel and Chen [14] also observed the formation of transformation bands at an angle of 33° relative to the compression axis in cylindrical specimens subjected to hydraulic compression.

(3) Transformation Yielding in Biaxial Tension

The stress-strain curves measured in the biaxial flexure test on the five types of Ce-TZP/Al_2O_3 are shown in Figure 5. Again, systematic variations of well-defined transformation yield stress and plasticity with mean grain size were obtained. The magnitudes of the transformation yield stress in biaxial tension for all five types of Ce-TZP/Al_2O_3 were less than those in the three-point bending test. Transformation bands were observed at the center of the tensile surfaces of the disk specimens, the location of maximum tension in this loading configuration.

(4) Transformation Yielding in Diametral-Compression Test

The stress-strain curves measured in the transverse tension and the diametral compression directions for type II A Ce-TZP/Al_2O_3 in the diametral-compression test are shown in Figure 6. Also included in the figure are the stress-strain curves measured in the biaxial flexure, the three-point bend, and the uniaxial compression tests. Nearly perfect plasticity was observed in the transverse tension direction of the diametral-compression test. Transformation bands nucleated and grew along the diametral loading line on both surfaces of the right circular thin cylinder.

Table 1 summarizes the yield stresses measured in the four different test geometries on the five types of Ce-TZP/Al_2O_3. The data reported for each test includes an average and standard deviation based on at least six specimens. The yield stress in uniaxial compression is much higher than those in uniaxial tension and biaxial tension stress states. Systematic increase in yield stress as the mean grain size decreased was observed in all the stress states. All of the tests were conducted at a strain rate of 1.5×10^{-5} sec^{-1}. All of these data will be used to establish a transformation yield criterion in a later section.

(5) Pressure Sensitivity of Compression Yield Stress in Hydraulic Compression Tests

Pressure sensitivity (α^c) of yield stress in uniaxial compression was assessed in hydraulic compression tests. In a hydraulic compression test, a uniaxial compression loading was applied in a pressure vessel at constant confining pressure, P. Figure 7 shows the variation of the yield stress in compression as a function of the confining pressure. The yield stress increased linearly with the confining pressure P. The pressure sensitivity α^c, i.e., the slope of the plot in Figure 7, assessed by linear regression was 1.6 ± 0.6.

(6) Strain Rate Effects on the Yielding and Fracture of Ce-TZP-Al_2O_3

The variation of the transformation yield stress and the fracture strength with strain rate in uniaxial compression tests on type II A Ce-TZP/Al_2O_3 specimens are shown in Figure 8. All the data in this plot were obtained from the measurements of stress-strain curves at different strain rates at room temperature. The transformation yield stress did not change as the strain rate increased from 1×10^{-5} s^{-1} to 1.19 s^{-1}, while the ultimate strength increased from 1822 MPa to 2450 MPa. The insensitivity of the transformation yield stress to the applied strain rate observed here for the Ce-TZP/Al_2O_3 ceramic is different from the observations reported for Mg-PSZ [7]. Transformation yield stress increases slightly with strain rate for Mg-PSZ[7].

(7) Transformation Yield Envelopes

Figures 9 shows the yield envelopes for three types of Ce-TZP/Al_2O_3. Also included are the yield envelopes corresponding to the following phenomenological yield criterion proposed by Chen and Reyes-Morel [13,14]. The procedure for calculating the yield envelopes in the tension-tension and tension-compression stress quadrants has been described by Yu and Shetty [15]. The characteristic yield parameters, the characteristic equivalent stress, σ_e^* and the characteristic mean stress, σ_m^*, were assessed from the measured yield stresses in uniaxial tension and uniaxial compression. The experimental data plotted for Ce-TZP-Al_2O_3 were the well-defined yield stresses measured in uniaxial tension (three-point bending), tension-compression (diametral compression), biaxial tension (biaxial flexure) and uniaxial compression tests. The higher yield stress measured in the uniaxial compression test relative to the yield stress in the uniaxial tension test in these materials reflects the combined influence of the dilatational (hydrostatic) and shear (deviatoric) stress components in transformation yielding as compared to the pure shear yielding in metals. As pointed out before, the phenomenological yield envelopes were assessed by the yield stresses in compression and tension. A comparison of this envelope with the measured yield stresses in biaxial tension and tension-compression stress states reveals some discrepancies judges the effectiveness of the yield criterion. For Ce-TZP/Al_2O_3 ceramic, the phenomenological yield criterion slightly underestimates the yield stress in biaxial tension.

IV. DISCUSSIONS

Transformation of a ZrO_2 grain in a ceramic matrix from tetragonal to monoclinic symmetry may occur whenever the total free energy of the system (grain plus matrix) can be decreased, i.e. the net change of total free energy, ΔG_T, has a negative value. The total free energy change consists of changes of chemical free energy, ΔG_{chem}, strain energy, ΔU_{str}, interaction energy, ΔU_{int} and interfacial energy, $\Delta \gamma_i$:

$$\Delta G_T = \Delta V (- \Delta G_{chem} + \Delta U_{str} - \Delta U_{int}) + \Sigma_i \Delta A_i \Delta \gamma_i \qquad (1)$$

ΔA_i is the interface area associated with the interface energy, $\Delta\gamma_i$, in a transformed volume ΔV. ΔA_i may simply be the surface area of the transformed volume if there are no additional interfaces, such as twin boundaries within the transformed volume. Both chemical free energy and strain energy depend on the transformed volume. The change of chemical free energy depends on composition and the degree of super cooling below the

equilibrium transformation temperature (T_e) at which tetragonal and monoclinic ZrO_2 have the same chemical free energy. The strain energy change ΔU_{str} is due to the volume and shape change associated with the transformation. Instead of super cooling, external applied stresses or internal stresses can reduce the strain energy by supplying interaction energy ΔU_{int} and increase the driving force for transformation. Schematics of a ZrO_2 grain under a biaxial stress before, during and after transformation are shown in Figures 10 (A), (B) and (C). In the final state of Figure 10 (C), the monoclinic grain is fully twinned. As shown in Figure 8, the transformation yield stress was independent of the strain rate; the tetragonal to monoclinic phase transformation in Ce-TZP-Al_2O_3 is essentially a stress-induced transformation.

(1) Transformation Yield Envelopes

The interaction energy due to the external applied stress (uniaxial stress state) in martensitic transformation has been treated by Eshelby [22,23]. Thus, we use Eshelby's inclusion theory to establish a transformation yield criterion and yield envelope. Since tetragonal to monoclinic phase transformation is accompanied by both dilatation and shear strains, the coupling between the applied stress and these strains which give rise to the interaction energy, thus depends on the applied stress state. It is well known that applied stress state [24] influence martensite formation in metals. The coupling of applied stress with transformation strains in a homogeneous system has been expressed by Eshelby [22,23] as

$$\Delta U_{int} = W_{int} = \sigma_{ij}^{A} e_{ij}^{T} \qquad (2)$$

where σ_{ij}^{A} is the applied stress in the tensor notation which can be expanded in the generalized coordinate system i and j. e_{ij}^{T} is the generalized stress-free transformation strain. Each type of Ce-TZP-Al_2O_3 can be regarded as a homogeneous system since the elastic modulus of the monoclinic grains (transformed phase) is only slightly different from that of the tetragonal grains (parent phase). Mecartney and Ruhle [25] have shown that a single monoclinic (martensite) lath can form at grain boundaries in Y-TZP. Thus, the applied stresses coupled with the transformation strains of single monoclinic product is the basic model of analysis of the interaction energy. In martensitic transformation, there exists one habit plane between the product phase and the parent phase, and the invariant plane strain (IPS) condition on the habit plane is usually followed. The orientation relation of the applied stress coupled with the habit plane is shown in Figure 11. In-plane distortion is assumed isotropic in the plane, and the coordinate system of the applied stress

is denoted by X_1, Y_1, Z_1. The coordinate system X_2, Y_2, Z_2 is defined relative to the habit plane, as in the geometrical construction for the one dimensional analysis given by Eshelby. OX_1, OZ_2 and OX_2 are assumed to be on the same plane and the angle between OZ_2 and OX_1 is defined as β, the projection of OX_2 on the OY_1Z_1 plane is OP, the angle between OP and OZ_1 is defined as ϕ. Eshelby's expression for the interaction energy of a transformed-inclusion for a uniaxial stress state can then be expanded to

$$W_{int} = \Delta U_{int} = \sigma_{ij}^{A} e_{ij}^{T} = \sigma_{x_2 x_2} e_{x_2 x_2}^{T} + \sigma_{x_2 y_2} e_{x_2 y_2}^{T} + \sigma_{x_2 z_2} e_{x_2 z_2}^{T} +$$

$$\sigma_{y_2 x_2} e_{y_2 x_2}^{T} + \sigma_{y_2 y_2} e_{y_2 y_2}^{T} + \sigma_{y_2 z_2} e_{y_2 z_2}^{T} + \sigma_{z_2 x_2} e_{z_2 x_2}^{T} +$$

$$\sigma_{z_2 y_2} e_{z_2 y_2}^{T} + \sigma_{z_2 z_2} e_{z_2 z_2}^{T} \qquad (3)$$

The transformation strain, e_{ij}^{T}, for a transformed monoclinic phase, is composed of three components only. One is the shear transformation strain e_{x2z2}^{T} on the habit plane, which is made up of a shear parallel to the habit plane through an angle S

$$e_{x_2 z_2}^{T} = e_{z_2 x_2}^{T} = \frac{S}{2} \qquad (4)$$

and a second component, the in-plane dilatation strains, e_{x2x2}^{T}, and e_{y2y2}^{T}. These are related to the uniform volume dilatation strain Δ according to

$$e_{x_2 x_2}^{T} = e_{y_2 y_2}^{T} = \frac{\Delta}{3} \qquad (5)$$

The third component is the strain normal to the plane, e_{z2z2}^{T} defined in Equation (6). ξ is the extension normal to the habit plane; for tetragonal to monoclinic phase transformation in zirconia this is related to the dilatation strain Δ by $\xi = \Delta/2$ [14]. Specifically, $\xi + \Delta$ represents the net dilatation (such that the strain normal to the disc is $\xi + \Delta/3$, and the in-plane strains are $\Delta/3$ [23]. All the other strains are zero.

$$e_{z_2 z_2}^{T} = \xi + \frac{\Delta}{3} \qquad (6)$$

These notations for constrained transformation strains were suggested by Eshelby [22], and later proved by Christian [26] in the formation of martensite. These strains also follow the invariant plane strain condition (IPS) in the crystallographic theories of martensite suggested by Bowles and Mackenzie [27]. A uniform dilatation strain, $\Delta = 0.04$, was calculated from the volume change of unit cell from tetragonal to monoclinic structure. In

the plane stress biaxial stress state, $\sigma_{x_1x_1} = \sigma$, $\sigma_{y_1y_1} = k\,\sigma_{x_1x_1}$, and all the other stresses, $\sigma_{z_1z_1}$, $\sigma_{y_1y_1}$, $\sigma_{y_1z_1}$, $\sigma_{z_1x_1}$, etc., are equal to zero. After transforming the coordinate system X_1, Y_1, Z_1 of applied stress into the coordinate system X_2, Y_2, Z_2 of the transformation strain, the general expression for the interaction energy is

$$W_{int} = \sigma\left[(1+k)\frac{\Delta}{3} + (\cos^2\beta + k\sin^2\beta\sin^2\phi)\xi + (\cos\beta\sin\beta)(1 - k\sin^2\phi)S\right] \tag{7}$$

Note that the interaction energy, W_{int}, is a function of the stress σ, stress state parameter, k, orientation angles, β and ϕ, and transformation strains, Δ, S, and ξ. The expression of Equation (7) for interaction energy in biaxial stress state can correctly reduce to that given by Eshelby for uniaxial tension [23]. It is assumed that the transformation occurs in those tetragonal grains most favorably oriented for maximum interaction energy. The condition for maximum interaction energy is

$$\frac{\partial W_{int}}{\partial\beta} = 0\,,\ \frac{\partial^2 W_{int}}{\partial\beta^2} < 0\,,\ \frac{\partial W_{int}}{\partial\phi} = 0\,,\ \frac{\partial^2 W_{int}}{\partial\phi^2} < 0 \tag{8}$$

The critical angle β^* for maximum interaction energy is defined by Equation (9). ϕ^* can be defined similarly and $\phi^* = \pi/2$ for $k < 0$ and $\phi^* = 0$ for $k \geq 0$.

$$\tan 2\beta^* = \frac{S}{\xi} \tag{9}$$

The corresponding expressions for maximum interaction energy in uniaxial tension (k =0), uniaxial compression ($k = -\infty$) and biaxial tension (k = 1) are given by Equations (10), (11) and (12) respectively :

$$(W_{int}^{max})_T = \sigma_c^T\left(\frac{\Delta}{3} + \xi\cos^2\beta^* + S\cos\beta^*\sin\beta^*\right) \tag{10}$$

$$(W_{int}^{max})_C = \sigma_c^C\left(\frac{\Delta}{3} + \xi\sin^2\beta^* - S\cos\beta^*\sin\beta^*\right) \tag{11}$$

$$(W_{int}^{max})_{BT} = \sigma_c^{BT}\left(\frac{2\Delta}{3} + \xi\cos^2\beta^* + S\cos\beta^*\sin\beta^*\right) \tag{12}$$

σ_c^T, σ_c^C and σ_c^{BT} are the critical transformation stresses which are set equal to the well-defined transformation yield stresses σ_y^T, σ_y^C and σ_y^{BT} in uniaxial tension, uniaxial compression and biaxial tension, respectively; i.e., $\sigma_c^T = \sigma_y^T$, $\sigma_c^C = \sigma_y^C$ and $\sigma_c^{BT} = \sigma_y^{BT}$. Since transformation is assumed to be governed by the same total free energy

change which is dependent on properties of material only, it is reasonable to assume that the maximum interaction energy takes the same critical value at yielding in different stress states. Then, the yield envelope can be defined by equating the interaction energies in different stress states as indicated in Equation (13) :

$$(W_{int}^{max})_{k=0} = (W_{int}^{max})_{k<0} = (W_{int}^{max})_{k>0} \tag{13}$$

and substituting the values of ϕ^* for $k < 0$ and $k > 0$ in Equations (7) and (13). This leads to the following two general expressions for the yield envelope for two ranges of the stress states parameter k :

$$k<0 \ , \ \sigma_y^k = \frac{\sigma_y^T}{1 + k\left(\dfrac{\frac{\Delta}{3} + \xi \sin^2\beta^* - S\cos\beta^* \sin\beta^*}{\frac{\Delta}{3} + \xi \cos^2\beta^* + S\cos\beta^* \sin\beta^*}\right)} \tag{14}$$

$$k>0 \ , \ \sigma_y^k = \frac{\sigma_y^T}{1 + k\left(\dfrac{\frac{\Delta}{3}}{\frac{\Delta}{3} + \xi \cos^2\beta^* + S\cos\beta^* \sin\beta^*}\right)} \tag{15}$$

where $\sigma_y{}^k$ is the yield stress in a stress state defined by k. For a grain as a whole, the shear strain is partially accommodated by the twinning, or microcracking processes, during the formation of martensite. This means that the full transformation shear strain ($S = 0.16$) is reduced to a macroscopic shear strain. Therefore, the shear strain, S, and orientation angle, β^*, are regarded as unknown parameters. The dilatation strain, Δ, and normal strain, ξ, are assumed to be 0.04 and 0.02, respectively. The magnitudes of the shear strain S and β^* can be found by using the ratio of yield stresses in tension and compression tests, the specific condition of orientation angle β^* in Equation (9), and ϕ^*. For different materials, the ratio of the yield stresses in uniaxial tension and uniaxial compression is different. This combined with the common condition Equation (9) will be used to calculate specific value of S and preferred orientation β^* for each material. Table 2 lists the yield stress ratio in uniaxial tension and uniaxial compression and corresponding shear strain S and preferred orientation β^* for different types of Ce-TZP-Al_2O_3. The preferred orientation β^* is believed to be the reason that lead to the development of texture in uniaxial compression.

Using these values of S and β^* in Equations (14) and (15), the yield envelope for each type material can be derived. Equations (16) and (17) describe the yield envelopes of type II A Ce-TZP-Al_2O_3 in the tension-tension and the tension-compression stress states

At $k < 0$;

$$\sigma_y^k = \frac{\sigma_y^T}{1 - 0.2496\,k} \tag{16}$$

At $k > 0$;

$$\sigma_y^k = \frac{\sigma_y^T}{1 + 0.2144\,k} \tag{17}$$

The theoretical yield envelopes derived on the basis of Eshelby's inclusion transformation theory are compared in Figures 12 with experimental yield stress data for types I A, II A, and II C Ce-TZP-Al_2O_3. Figure 12 shows plots of two yield envelopes that are based on Equations (16) and (17), and the yield stresses measured in different stress-states for three types specimen. There is good agreement between the theoretical envelopes and the experimental results. Only the yield stress of type II C in diametral-compression test showed deviation from the theoretical prediction. One possible reason for the discrepancy is that the crack and the transformation band reach the center of the disk at the same time for type II C specimen. This may cause the yield stress to be less than the prediction of the yield criteria.

(2) Pressure Sensitivity of Transformation Yield Stress in Hydraulic Compression

Pressure sensitivity measured in hydraulic compression tests was shown in Figure 7. Since the confining pressure, P, was applied independently of the uniaxial compression, the interaction energy in hydraulic compression can be simply equated to the sum of the interaction energy from uniaxial compression given by Equation (11) and the interaction energy from the confining pressure P. The confining pressure is assumed to interact only with the uniform dilatational transformation strain Δ. The interaction between P and nonuniform macroscopic normal strain ξ was assumed negligible. Therefore, the interaction energy from the confining pressure P is equal to $P \times \Delta$ [14]. Then, the maximum interaction energy in hydraulic compression stress state is

$$\left(W_{int}^{max} \right)_{HC} = \sigma_y^{HC}\left(\frac{\Delta}{3} + \xi \sin^2\beta^* - S\cos\beta^*\sin\beta^* \right) + P\,\Delta \tag{18}$$

where $(\sigma_y)^{HC}$ is the compression-yield stress in hydraulic compression. Again, assuming that the maximum interaction energy in hydraulic compression equals that in uniaxial compression, then

$$\sigma_y^{HC}(\frac{\Delta}{3} + \xi \sin^2\beta^* - S \cos\beta^* \sin\beta^*) + P\Delta = \sigma_y^C (\frac{\Delta}{3} + \xi \sin^2\beta^* - S \cos\beta^* \sin\beta^*) \quad (19)$$

then, Equation (19) is equivalent to

$$\sigma_y^{HC} = \sigma_y^C + \frac{P\Delta}{S \cos\beta^* \sin\beta^* - \frac{\Delta}{3} - \xi \sin^2\beta^*} \quad (20)$$

where the pressure sensitivity $\alpha^C = d\sigma_y^{HC} / dP$, that is

$$\alpha^C = \frac{\Delta}{S \cos\beta^* \sin\beta^* - \frac{\Delta}{3} - \xi \sin^2\beta^*} \quad (21)$$

As shown in Table 2, for type II A specimens the shear strain S = 0.075 and $\beta^* = 37.526°$, a pressure sensitivity $\alpha^C = 2.58$ is calculated from Equation (21). This prediction is slightly higher than the experimental results, i.e. $\alpha^C = 1.6 \pm 0.6$. For different types Ce-TZP-Al_2O_3, the predictions of pressure sensitivity range from 1.88 for type II D to 2.95 for type I A specimen. The pressure sensitivity increases as shear strain, S, decreases in Equation (21). This tendency is similar to the prediction using the phenomenological yield criterion suggested by Chen and Reyes-Morel [13,14]. However, the magnitude of pressure sensitivity predicted by the phenomenological yield criterion for type II A Ce-TZP-Al_2O_3 is 4.5, which is much higher than the experimental results.

V. CONCLUSIONS

1. Transformation Yielding in Ce-TZP-Al_2O_3 follows a combined dilatation/shear yield criterion. This is consistent with a stress-assisted tetragonal to monoclinic phase transformation that involves both volume expansion and shear strains.
2. Transformation yield envelopes can be interpreted by employing Eshelby's inclusion theory for stress-induced transformation in a general biaxial stress-state.
3. Tetragonal to monoclinic transformation in Ce-TZP-Al_2O_3 is consistent with preferred orientations for habit planes and partially accommodated shear strains.

Acknowledgments

This paper is based on research supported by the Army Research Office under contract DAAL03-87-0060 at the University of Utah. The authors are grateful to Dr. James Lankford of Southwest Research Institute for his contribution to this study.

REFERENCES

1. W. Weibull, " A Statistical Theory of the Strength of Materials, "*Ingenioersvetenskapsakad. Handl.*, **151**, 1-45 (1939).

2. S. B. Batdorf and J. G. Crose, " A Statistical Theory for the Fracture of Brittle Structures Subjected to Nonuniform Polyaxial Stresses," *J. of Appl. Mech.*, **41**, 459-65 (1974).

3. S. B. Batdorf and H. L. Heinisch, Jr., " Weakest Link Theory Reformulated for Arbitrary Fracture Criterion," *J. Am. Ceram. Soc.*, **61** [7-8], 355-58 (1978).

4. A. G. Evans, " A General Approach for the Statistical Analysis of Multiaxial Fracture," *J. Am. Ceram. Soc.*, **61** [7-8], 302-308 (1978).

5. D. K. Shetty, " Mixed-Mode Fracture Criteria for Reliability Analysis and Design with Structural Ceramics ", ASME *Journal of Engineering for Gas Turbines and Power*, **109** [3] 282-289 (1987).

6. J. Lankford, " Plastic Deformation of Partially-Stabilized Zirconia," *J. Am. Ceram. Soc.*, **66** [11], C-212-213 (1983).

7. J. Lankford, " The Influence of Temperature and Loading rate on Flow and Fracture of Partially-Stabilized Zirconia," *J. Mater. Sci.* **20**, 53-59 (1985).

8. M. V. Swain, " Inelastic Deformation of Mg-PSZ and Its Significance for Strength-Toughness Relationship of Zirconia-Toughened Ceramics," *Acta. Metall.*, **33** [11] 2083-91 (1985).

9. D. B. Marshall, " Strength Characteristic of Transformation-Toughened Zirconia," *J. Am. Ceram. Soc.*, **69** [3], 173-80 (1986).

10. M. V. Swain, " R-Curve Behavior of Magnesia Partially Stabilized Zirconia and Its Significance to Thermal Shock "; pp. 355-70 in *Fracture Mechanics of Ceramics*, Vol. **6**. Edited by R. C. Bradt, A. G. Evans, D. P. H. Hasselman and F. F. Lange. Plenum Press, New York (1983).

11. M. V. Swain and R. H. J. Hannink, " R-Curve Behavior in Zirconia Ceramics," *Adv. Ceram.*, **12**, 225-39 (1984).

12. M. J. Ready, A. H. Heuer, and R. W. Steinbrech, " Crack Propagation in Mg-PSZ "; pp.107-20, in *Advanced Structural Ceramics*, Vol. **78**, Materials Research Society Symposia Proceedings. Edited by P. F. Becher, M. V. Swain and S. Somiya. Materials Research Society, Pittsburgh, Pennsylvania (1987).

13. I-W. Chen and P. E. Reyes-Morel, " Implications of Transformation Plasticity in Containing Ceramics : I, Shear and Dilatation Effects," *J. Am. Ceram. Soc.*, **69** [3], 181-89 (1986).

14. P. E. Reyes-Morel and I-W. Chen, "Transformation Plasticity of CeO_2-Stabilized Tetragonal Zirconia Polycrystals : I, Stress Assistance and Autocatalysis," *J. Am. Ceram. Soc.*, **71** [5], 343-53 (1988).

15. C-S. Yu and D. K. Shetty, " Transformation Zone Shape, Size, and Crack-Growth-Resistance (R-Curve) Behavior of Ceria-Partially-Stabilized Zirconia Polycrystals," *J. Am. Ceram. Soc.*, **72** [6] 921-28 (1989).

16. C-S. Yu and D. K. Shetty, " Transformation Yielding, Plasticity and Crack-Growth-Resistance (R-Curve) Behavior of CeO_2-TZP," *J. Mater. Sci.*, **25**, 2025-2035 (1990).

17. J-F. Tsai, C-S. Yu and D. K. Shetty, " Fatigue Crack Propagation in Ceria-Partially-Stabilized Zirconia Polycrystals (Ce-TZP)-Alumina Composites," *J. Am. Ceram. Soc.*, **73** [10] 2992-3001 (1990).

18. A. Rudnick, A. R. Hunter and F. C. Holden, " An Analysis of the Diametral-Compression Test," *Materials Research & Standards*, **3** [4], 283-89 (1963).

19. D. K. Shetty, A. R. Rosenfield, W. H. Duckworth, and P. R. Held, "A Biaxial-Flexure Test for Evaluating Ceramic Strengths," J. Am. Ceram. Soc., **66** [1], 36-42 (1983).

20. R. H. Hannink and M. V. Swain, "Metastability of the Martensitic Transformation in a 12 mol% Ceria-Zirconia Alloy : I, Deformation and Fracture Observations," J. Am. Ceram. Soc., **72** [1], 90-98 (1989).

21. K. J. Bowman, P. E. Reyes-Morel, and I-W. Chen, "Texture from Deformation of Zirconia-Containing Ceramics," 811-16 in Proceedings of the Eighth International Conference on Texture of Materials, Santa Fe, NM, Sept. (1987).

22. J. D. Eshelby, "The Determination of the Elastic Field of An Ellipsoidal Inclusion, and Related Problem," Proc. R. Soc., A **241**, pp376-96 (1957).

23. J. D. Eshelby, "Elastic Inclusions and Inhomogeneities," Progress in Solid Mechanics, Edited by I. N. Sneddon and R. Hill, Vol **2**, pp 89-140 (1961).

24. J. P. Patel and M. Cohen, "Criterion for the Action of Applied Stress in the Martensitic Transformation," Acta. Metall., 1 [9], 531-38 (1953).

25. M. L. Mecartney and M. Ruhle, "In Situ Transmission Electron Microscopy Observations of the Monoclinic to Tetragonal Phase Transformation in Tetragonal ZrO_2," Acta Metall., **37** [7], 1859-64 (1989).

26. J. W. Christian, "Accommodation Strains in Martensitic Formation, and the Use of a Dilatation Parameter," Acta Metall., **6** [3], 377-79 (1958).

27. J. S. Bowles and J. K. Mackenzie, "The Crystallography of Martensite Transformation I," Acta Metall., **2** [1], 129-37 (1954).; "The Crystallography of Martensite Transformation II," ibid., 138-47 (1954).

Figure Captions

Figure 1. Test geometries and corresponding stress state parameter k of different mechanical tests.

Figure 2. Twins and microcracks in Ce-TZP/Al_2O_3 composites (arrows indicate the microcracks).

Figure 3. Nominal elastic stress-strain curves measured in three-point bending for Ce-TZP/Al_2O_3 composites sintered at different temperatures.

Figure 4. Stress-strain curves of type II A Ce-TZP/Al_2O_3 composites assessed in axial and hoop direction in uniaxial compression test.

Figure 5. Stress-strain curves for five types of Ce-TZP/Al_2O_3 composites obtained in biaxial flexure test.

Figure 6. Stress-strain curves of type II A Ce-TZP/Al_2O_3 composite obtained in three-point bending, uniaxial compression, diametral-compression and biaxial flexure tests.

Figure 7. Transformation yield stress versus confining pressure p for type II A Ce-TZP/Al_2O_3 in hydraulic compression tests.

Figure 8. Variation of yield stress and ultimate strength of type II A specimen with the strain rates in uniaxial compression test.

Figure 9. Transformation yield stress envelopes for type I A, II A, and II C Ce-TZP/Al_2O_3 composites in the tension-tension and tension-compression quadrants.

Figure 10 Schematics of the transformation of a constrained tetragonal ZrO_2 at (A) initial, (B) intermediate and (C) final states under an applied biaxial stress.

Figure 11. Applied stresses coupled with the transformation strains in habit plane between two coordinate systems.

Figure 12. Theoretical transformation yield envelopes (derived from the Eshelby's inclusion theory) and experimental yield stresses for types I A, II A, II C Ce-TZP/Al_2O_3 composites in tension-tension and tension-compression quadrants.

Table 1. Transformation yield stresses in three-point bending, uniaxial compression, biaxial flexure, and diametral-compression tests for type I A, II A, II B, II C, and II D Ce-TZP-Al_2O_3

Materials	Yield Stress in Three-Point Bending	Yield Stress in Uniaxial Compression	Yield Stress in Biaxial Flexure	Yield Stress in Diametral-Compression (Tension)
	σ_y^T	σ_y^C	σ_y^{BT}	σ_y^{DC}
	(MPa)	(MPa)	(MPa)	(MPa)
I A	190 ± 5	842 ± 14	164 ± 3	107 ± 3
II A	236 ± 13	946 ± 30	193 ± 14	117 ± 12
II B	280 ± 6	1101 ± 10	235 ± 9	—
II C	326 ± 9	1127 ± 19	286 ± 9	125 ± 4
II D	390 ± 4	1248 ± 11	320 ± 8	—

Table 2. Yield stress ratio in uniaxial compression and tension tests, shear strains S, preferred orientations β^* and mean grain sizes for Ce-TZP-Al_2O_3

Materials	Mean Grain Size (μm)	Yield Stress Ratio($\lvert\sigma_y^C\rvert/\sigma_y^T$)	Shear Strain S	Preferred Orientation β^*(°)
I A	1.91	4.43	0.071	37.146
II A	1.87	4.00	0.075	37.526
II B	1.73	3.93	0.076	37.620
II C	1.52	3.46	0.082	38.165
II D	1.47	3.20	0.087	38.514

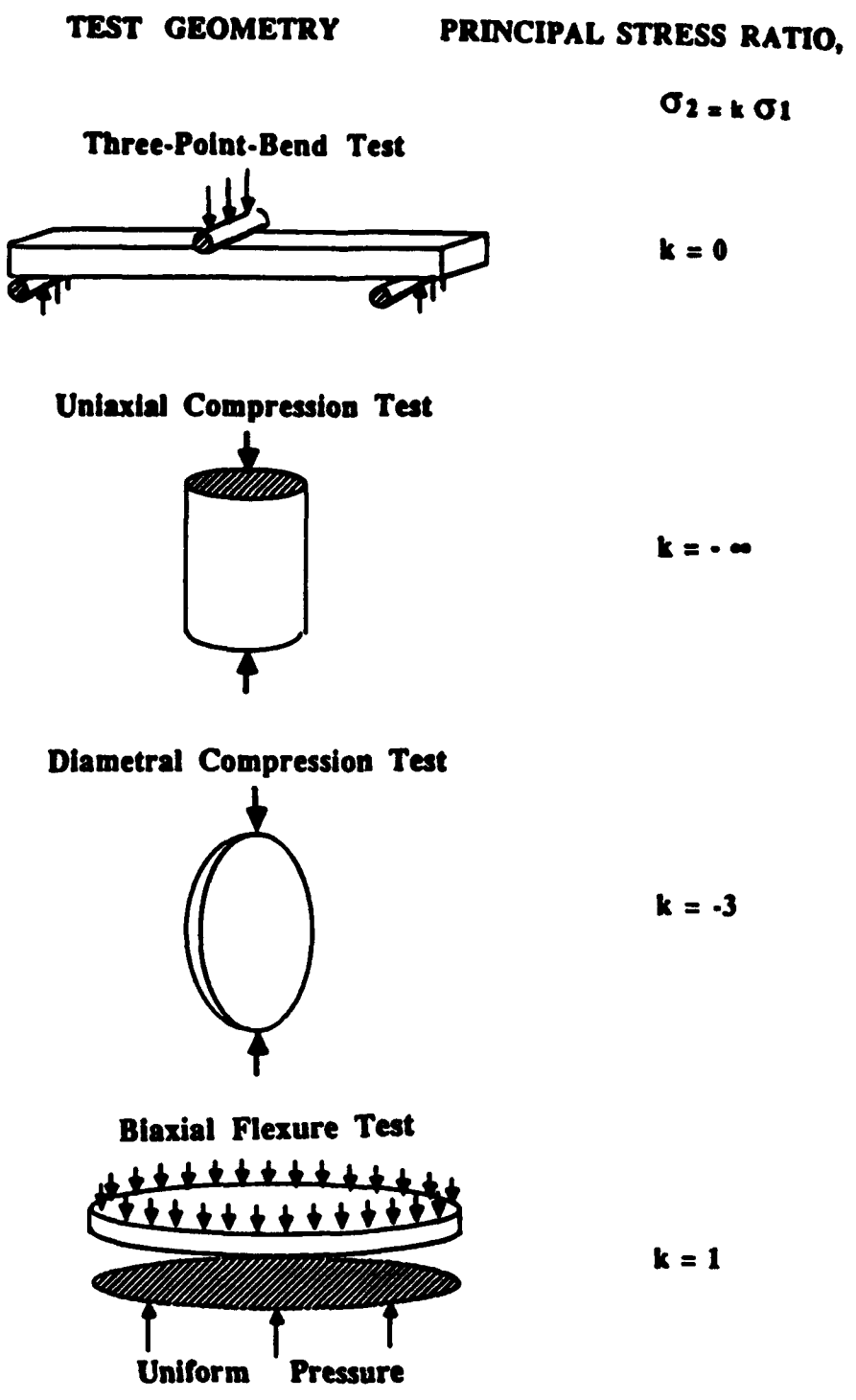

Figure 1. Test geometries and corresponding stress state parameter k of different mechanical tests.

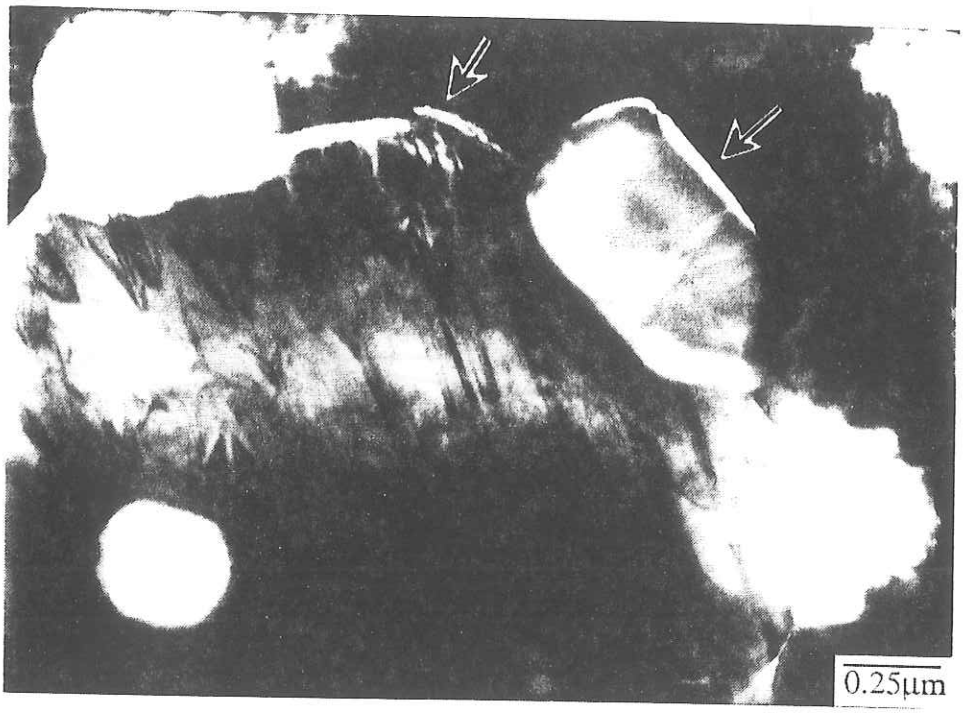

Figure 2. Twins and microcracks in Ce-TZP/Al_2O_3 composites (arrows indicate the microcracks).

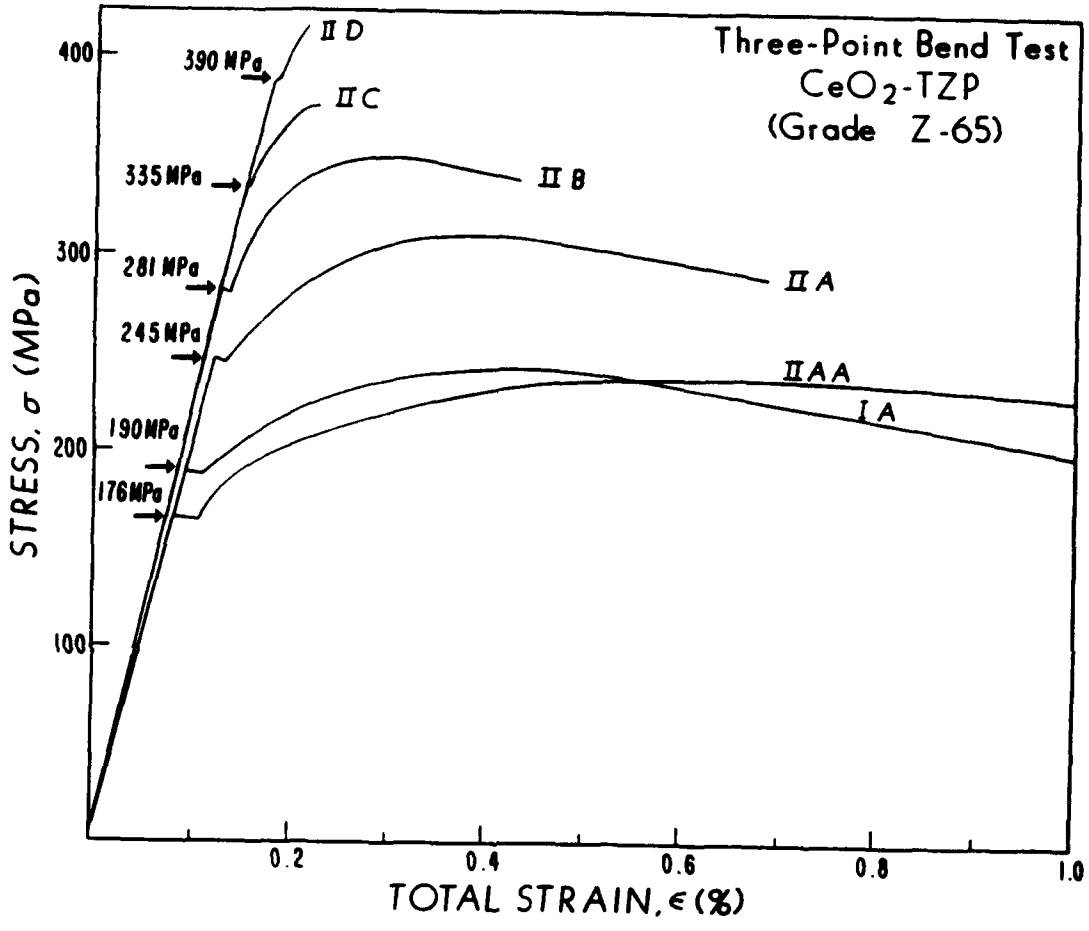

Figure 3. Nominal elastic stress-strain curves measured in three-point bending for Ce-TZP/Al_2O_3 composites sintered at different temperatures.

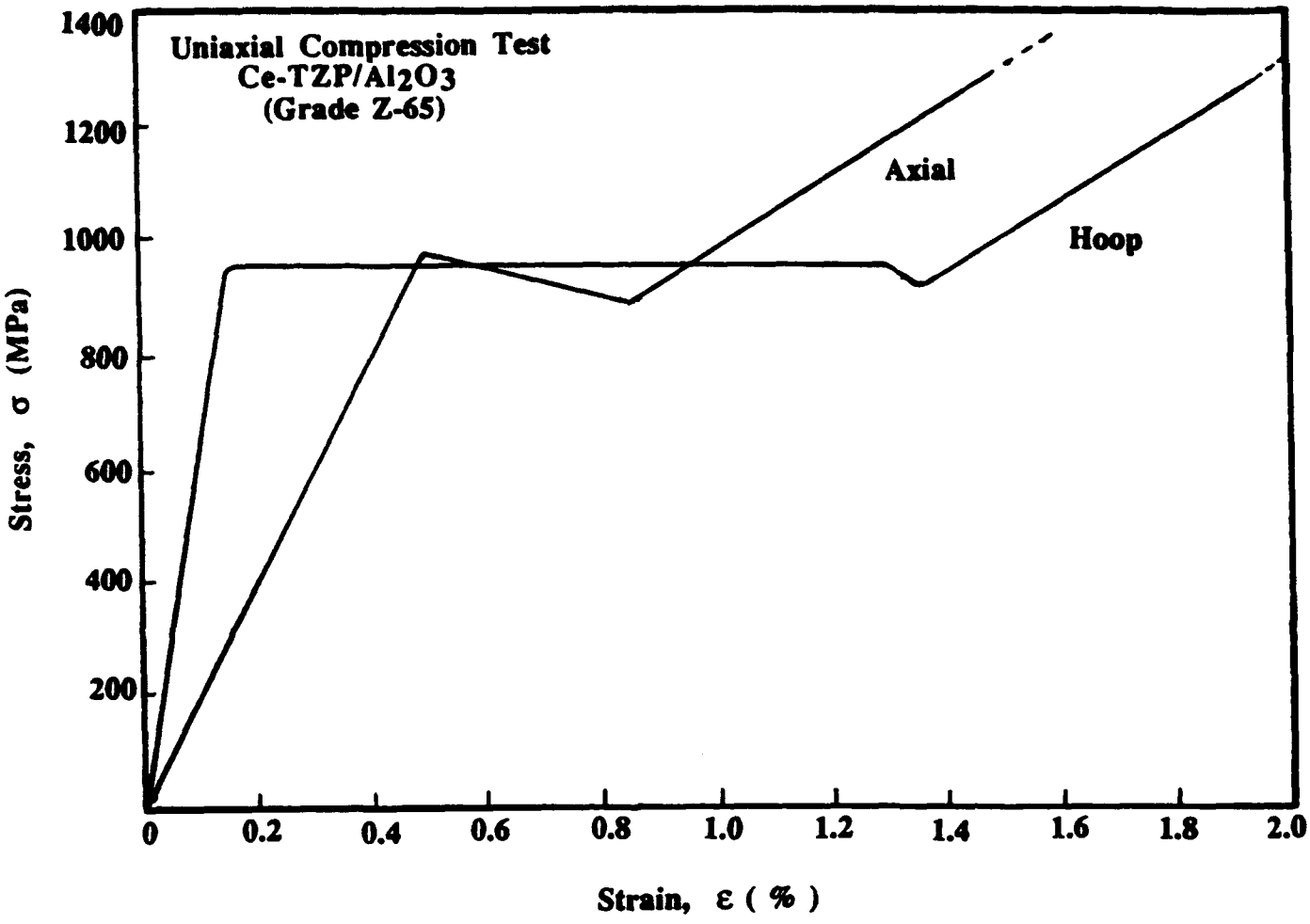

Figure 4. Stress-strain curves of type II A Ce-TZP/Al_2O_3 composites assessed in axial and hoop direction in uniaxial compression test.

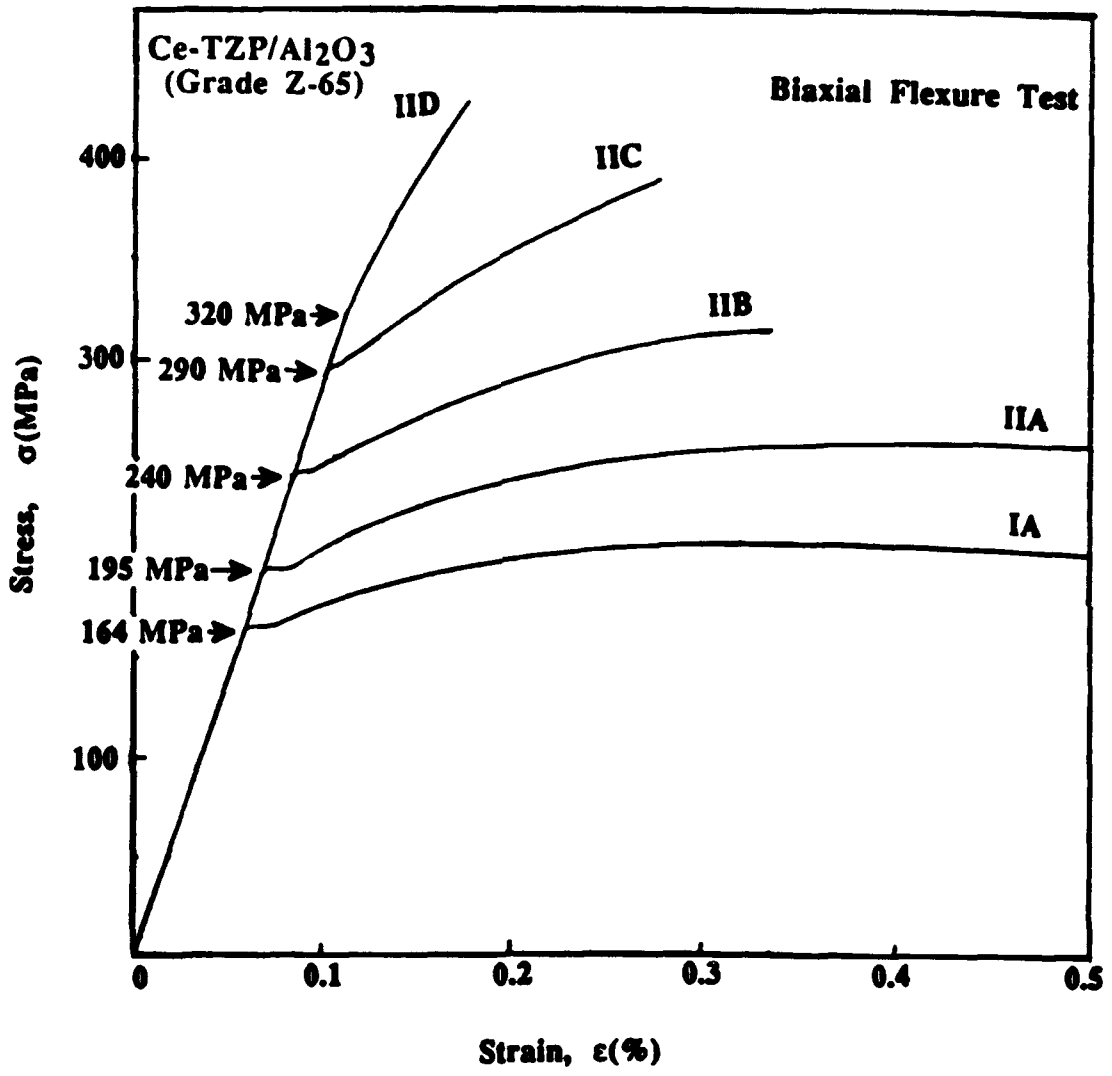

Figure 5. Stress-strain curves for five types of Ce-TZP/Al_2O_3 composites obtained in biaxial flexure test.

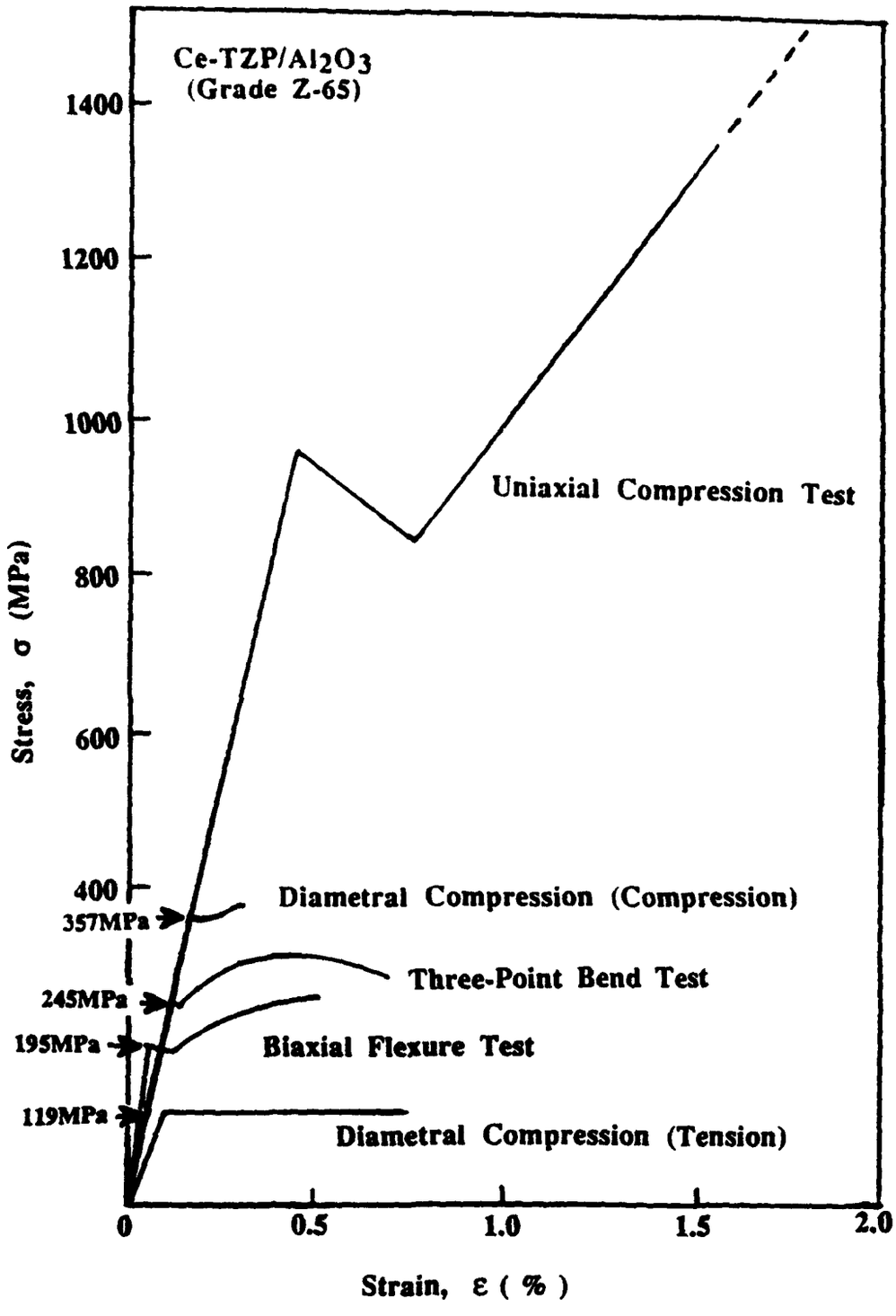

Figure 6. Stress-strain curves of type II A Ce-TZP/Al_2O_3 composite obtained in three-point bending, uniaxial compression, diametral-compression and biaxial flexure tests.

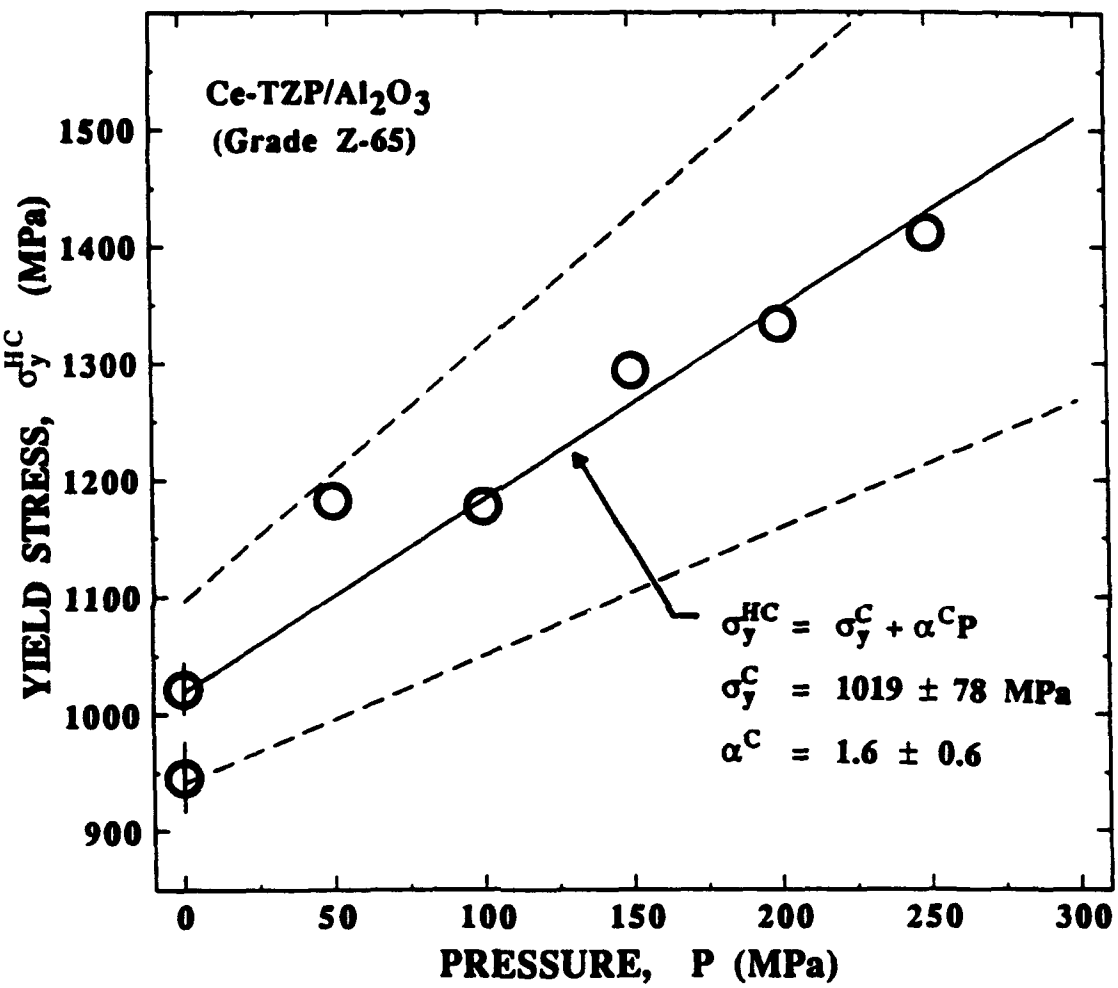

Figure 7. Transformation yield stress versus confining pressure p for type II A Ce-TZP/Al_2O_3 in hydraulic compression tests.

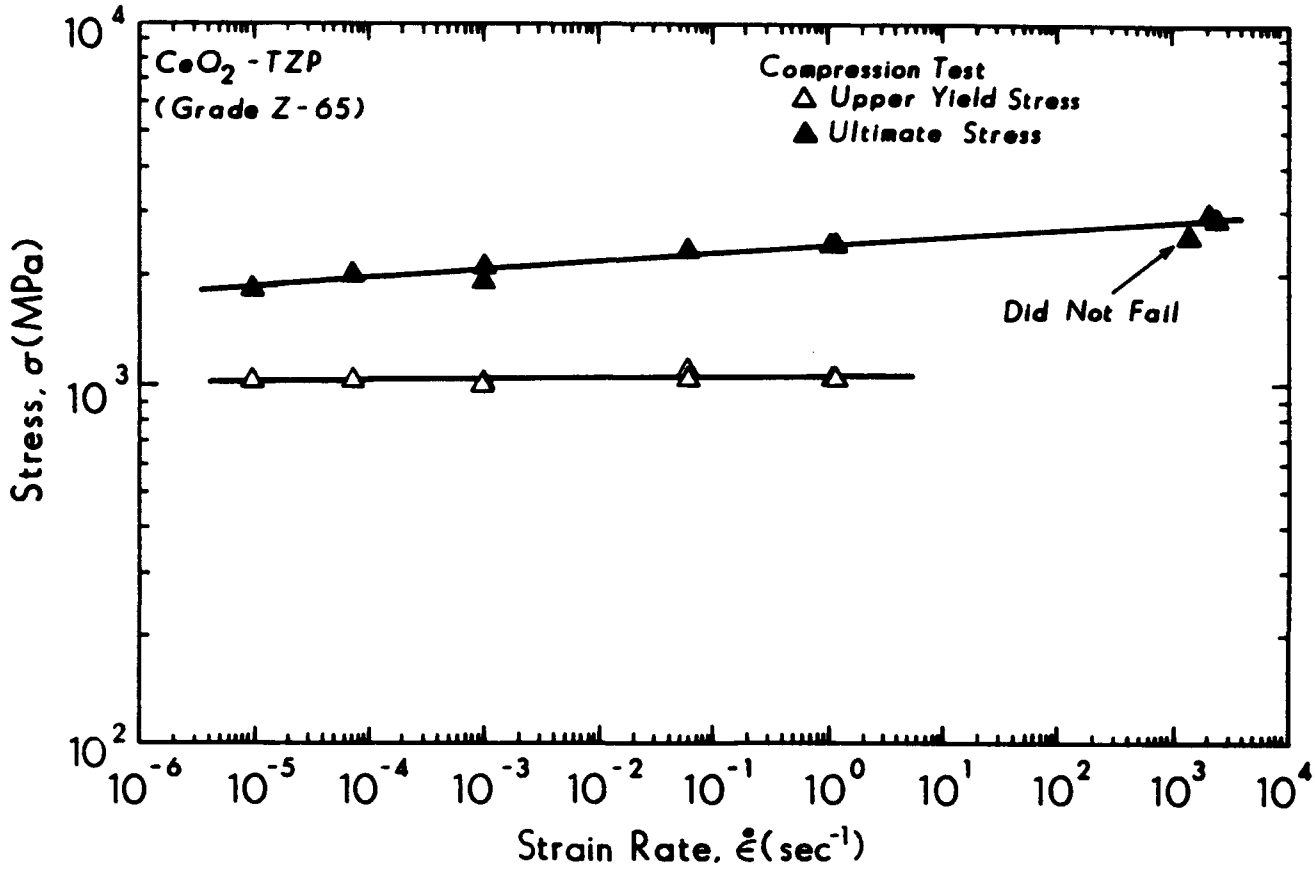

Figure 8. Variation of yield stress and ultimate strength of type II A specimen with the strain rates in uniaxial compression test.

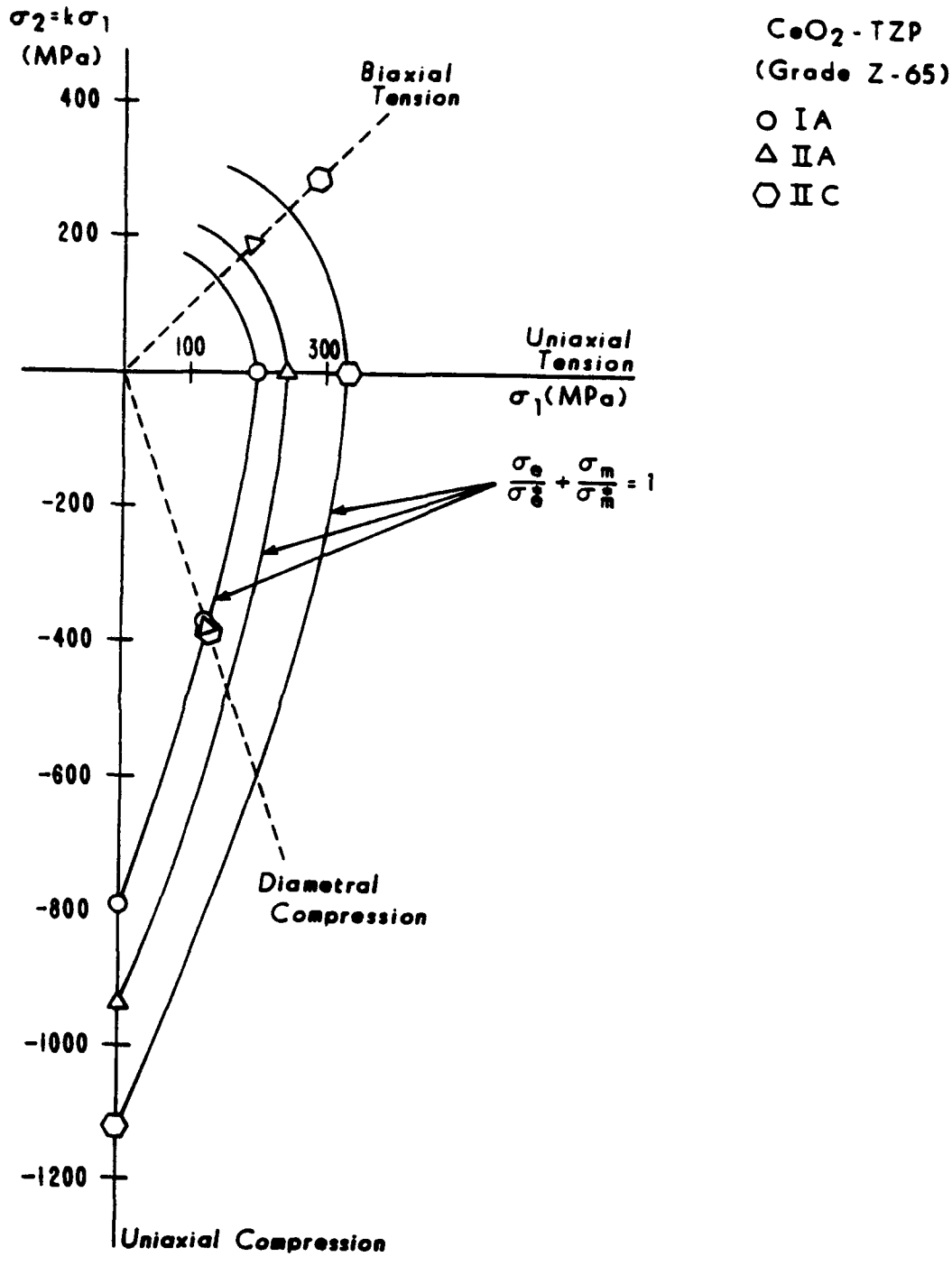

Figure 9. Transformation yield stress envelopes for type I A, II A, and II C Ce-TZP/Al_2O_3 composites in the tension-tension and tension-compression quadrants.

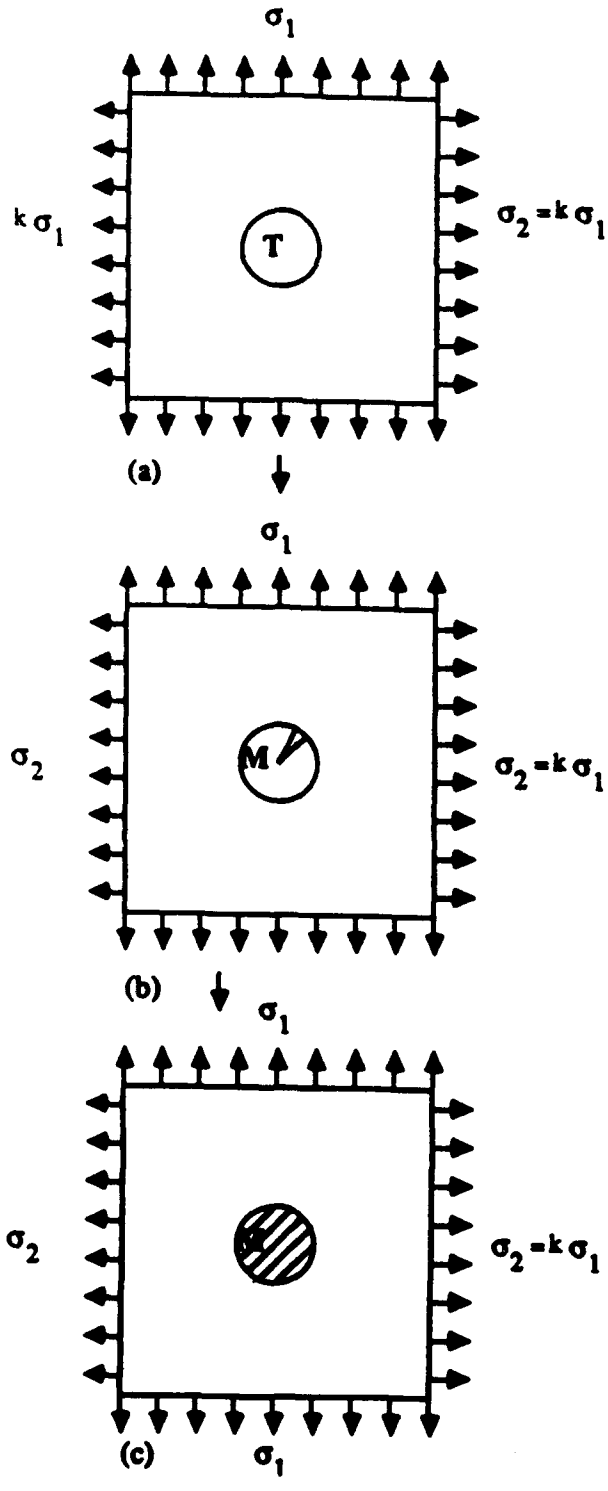

Figure 10 Schematics of the transformation of a constrained tetragonal ZrO_2 at (A) initial, (B) intermediate and (C) final states under an applied biaxial stress.

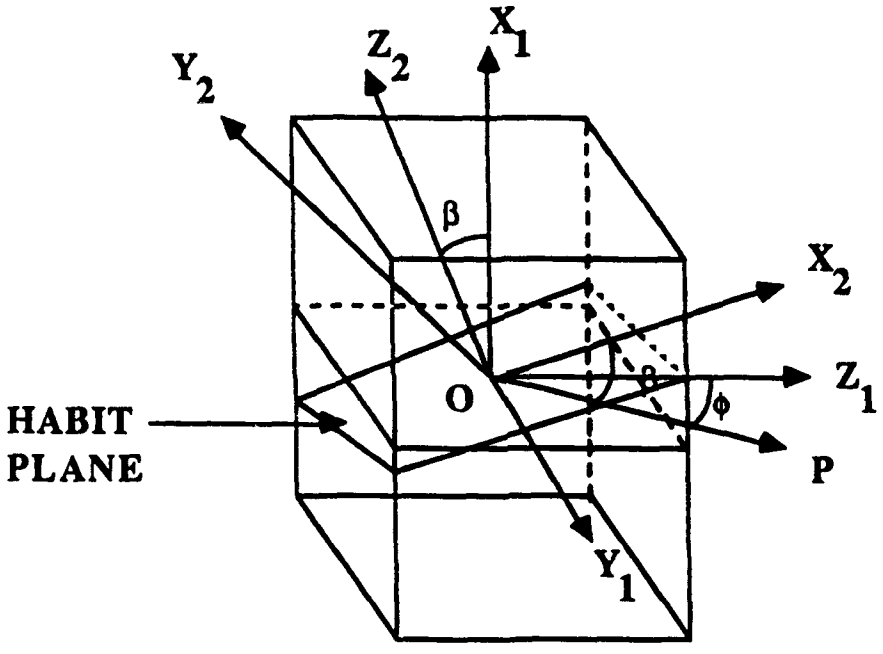

Figure 11. Applied stresses coupled with the transformation strains in habit plane between two coordinate systems.

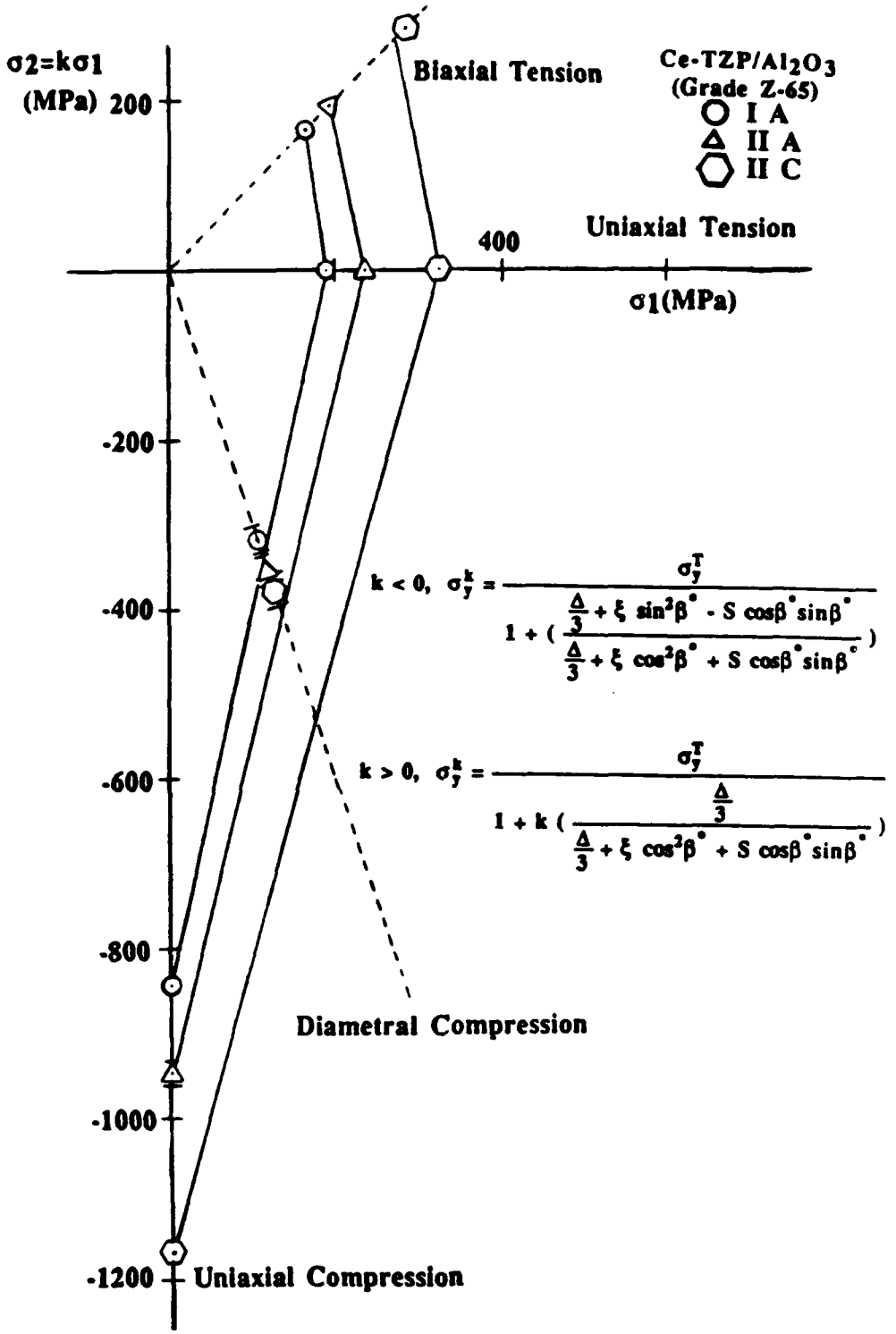

Figure 12. Theoretical transformation yield envelopes (derived from the Eshelby's inclusion theory) and experimental yield stresses for types I A, II A, II C Ce-TZP/Al_2O_3 composites in tension-tension and tension-compression quadrants.

journal

Appendix B

J. Am. Ceram. Soc., 72 [6] 921-28 (1989)

Transformation Zone Shape, Size, and Crack-Growth-Resistance (*R*-Curve) Behavior of Ceria-Partially-Stabilized Zirconia Polycrystals

Cheng-Sheng Yu* and Dinesh K. Shetty*

Department of Materials Science and Engineering, University of Utah, Salt Lake City, Utah 84112

Transformation zone shape, size, and crack-growth-resistance (*R*-curve) behavior were studied in precracked and annealed single-edge notch bend specimens of commercial-grade ceria-partially-stabilized zirconia polycrystals as a function of applied load. Well-defined transformation zones with a characteristic elongated shape in the plane of the crack were observed. It is shown that the observed zone shape is significantly different from the shape predicted by a combined shear/dilatation yield criterion and the stress field of the crack prior to the transformation. The length of the transformation zone directly ahead of the crack tip is in better agreement with the prediction of the Dugdale plastic strip zone model. The fracture toughness increment showed the characteristic square root dependence on the transformation zone width, but the magnitude of the toughness increment was not consistent with the predictions of the theoretical models of transformation toughening. [Key words: zirconia, ceria, *R* curve, mechanical properties, cracks.]

R. W. Rice — contributing editor

Manuscript No. 199013. Received July 11, 1988; approved November 8, 1988.
Presented at the 90th Annual Meeting of the American Ceramic Society, Cincinnati, OH, May 4, 1988 (Basic Science Division, Paper No. 188-B-88).
Supported by the Army Research Office under Contract No. DAAL03-87-0060 at the University of Utah.
*Member, American Ceramic Society.

I. Introduction

THE transformation zone formed in the stress fields of cracks in ceramics containing metastable tetragonal phase of ZrO_2 has a central role in the crack-shielding mechanism of transformation toughening.[1,2] To date, transformation zones have been studied and the zone widths have been quantitatively measured in MgO-partially-stabilized zirconia (MgO-PSZ) and Y_2O_3-partially-stabilized zirconia (Y_2O_3-TZP) ceramics using transmission electron microscopy[3] and X-ray diffraction[4,5] techniques. The small zone sizes (due to the limited transformation plasticity) and the diffused nature of the zone boundary in these ceramics do not permit a precise evaluation of the zone shapes and sizes using direct optical or scanning electron microscope observations. Recent development of ceria-partially-stabilized zirconia polycrystal (CeO_2-TZP) ceramics that exhibit high fracture toughness[6,7] and significant transformation plasticity[8,9] has made it possible to directly examine the transformation zones more quantitatively.[10,11]

Results of an investigation of the shapes and sizes of transformation zones and their relation to the *R*-curve behavior obtained in a commercial-grade CeO_2-TZP using precracked and annealed single-edge notch beam specimens are discussed in this paper. The zone shape was quantitatively compared to profiles predicted on the basis of a yield criterion established using biaxial tests and the stress field of the crack before transformation. The relations between the characteristic dimensions of the transformation zone,

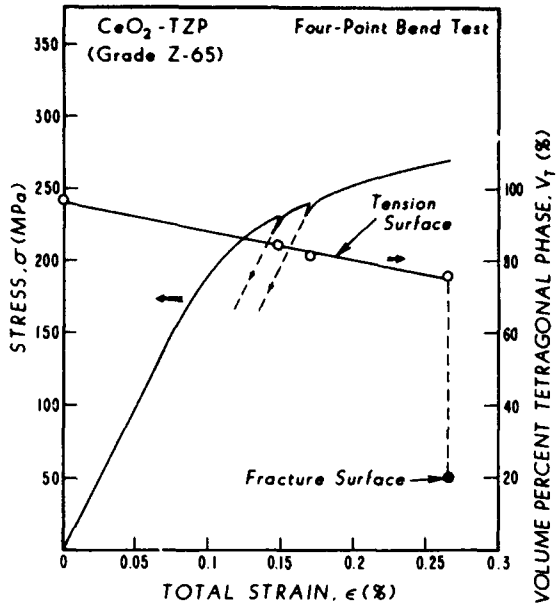

Fig. 1. Stress–strain curve for CeO_2-TZP obtained in four-point bending at 20°C and strain rate $\dot{\varepsilon} = 1.4 \times 10^{-5}$/s. The volume percent of the tetragonal phase on the tension face and on the fracture surface are also plotted.

i.e., zone width, w, measured normal to the crack and the zone length, l, measured ahead of the crack tip in the plane of the crack, and the rising fracture toughness obtained in the R-curve behavior were examined in terms of both the crack shielding models of transformation toughening and the Dugdale plastic strip zone model. It is shown that CeO_2-TZP exhibits several characteristic behaviors that are different from those of MgO-PSZ and Y_2O_3-TZP. Possible reasons for these deviations are discussed.

II. Test Material and Procedures

The CeO_2-TZP ceramic used in the present study was obtained in powder form from a commercial source.† Nominally, it is a partially stabilized zirconia with 12 mol% CeO_2 and small amounts of proprietary additives. The as-received powder was first sieved through a 70-μm screen. The screened powder was first pressed in a uniaxial die press at 34.5 MPa, followed by isostatic pressing at 207 MPa. The as-pressed compacts were sintered in air at 1500°C for 2 h. The average grain size of the sintered zirconia was 2 μm, and phase analysis by an X-ray diffraction technique[12] showed that the as-sintered ceramic contained 98 to 100 vol% of the tetragonal phase.

Single-edge notch bend specimens of the geometry defined in the American Society for Testing and Materials Standard E 399-83[13] were fabricated from the sintered billets by cutting with diamond blades and grinding with diamond wheels. The final dimensions of the specimen were support span (S) = 60, specimen width (W) = 15, and specimen thickness (B) = 7.5 mm. This relatively large specimen size was used to meet the minimum size requirements specified in ASTM E 399-83 based on the expected range of fracture toughness and the yield stress of the material. All specimens were first notched in the center of the beam to a depth of 1.5 mm, loaded in a universal testing machine to precrack to a total depth of 3.0 to 3.5 mm, and subsequently annealed at 1000°C for 30 min. There was no detectable change in the phase content after annealing. The precracked and annealed bend specimens were loaded incrementally and unloaded, and the transformation zone dimensions (zone width, w, and zone length, l) and the crack extension (Δa) were measured with a stereo microscope and a micrometer stage. The measurements were repeated as a function of applied load and crack length. The shapes of the transformation zones were photographed with an optical microscope using the Nomarski interference contrast technique.

In addition to the single-edge notch bend specimens, four-point-bend, uniaxial-compression, and diametral-compression specimens were also fabricated and tested for studying the stress-state dependence of transformation yield stress and plasticity. Details of these test specimens, procedures, and results will be discussed in a separate paper.[14] Only the results relevant to the discussion of the transformation zone shape and size are presented in the following section.

III. Experimental Results and Analysis

(1) Transformation Yield Stress and Plasticity in Four-Point Bending

The CeO_2-TZP ceramic used in the present study has a relatively low yield stress and shows significant amount of transformation plasticity. Figure 1 shows a typical stress–strain curve obtained in four-point bending at room temperature. The strain plotted was measured on the tension surface in the center span using a strain gage. The initial elastic strain rate of the outer fibers during bending was 1.4×10^{-5}/s. The stress was calculated from the load using the conventional elastic bending formula. The yield stress, defined as the stress corresponding to an offset strain of 0.05%, was 192 MPa. The total strain at failure in bending ranged from 0.25% to 0.45%. It should be noted, however, that the four-point-bend specimens did not deform uniformly on the tension face. Transformation strain was localized in a number of discrete bands that were normal to the specimen axis.[14] The strain measured was the average strain in the gage section of the strain gage.

Also plotted in Fig. 1 is the volume percent of the tetragonal phase determined by X-ray diffraction on the tension surface (open circles) and the fracture surface (filled circle). The volume percent tetragonal phase on the tension surface decreased monotonically with the total strain from an initial value of about 98% to approximately 76% at fracture. On the fracture surface, the volume percent of the retained tetragonal phase was about 20. This difference in the tetragonal-phase contents on the tension surface and the fracture surface is also due to the nonuniform distribution of the transformation strain. On the tension surface, X-ray diffraction analysis samples both the transformation bands as well as the untransformed regions in between. The fracture surface of the bend specimen is presumed to be located in one of the localized transformation bands and the tetragonal-phase content measured on the fracture surface is believed to be representative of the degree of transformation within such a band.

(2) Transformation Zone Shapes in Single-Edge Notch Bend Specimens

Figures 2(A) through (F) show a series of optical photographs of the initial precrack and the transformation zone at the crack tip in a single-edge notch bend specimen as a function of the applied stress intensity, K_I. The stress-intensity relationship given in ASTM E-399[13] was used to calculate K_I from the applied bending load, specimen and loading geometry, and the crack length. Figure 2(A) shows the initial crack emanating from the tip of a machined notch. Figures 2(B) through (F) show optical photographs of the specimen surface in the vicinity of the crack tip. A well-defined transformation zone could be observed with Nomarski interference contrast. A surprising feature of the transformation zone was its shape. The zone is elongated in the plane of the crack, with the zone length ahead of the crack tip being much greater than the zone width. Rose and Swain[10] have recently made similar observations in a CeO_2-TZP. The schematic of the transformation zone in Fig. 2(G) defines the two characteristic dimensions of the transformation zone, the zone length ahead of the crack tip, l, and the zone width normal to the crack plane at

†Tentative grade Z-65, Ceramatec Inc., Salt Lake City, UT.

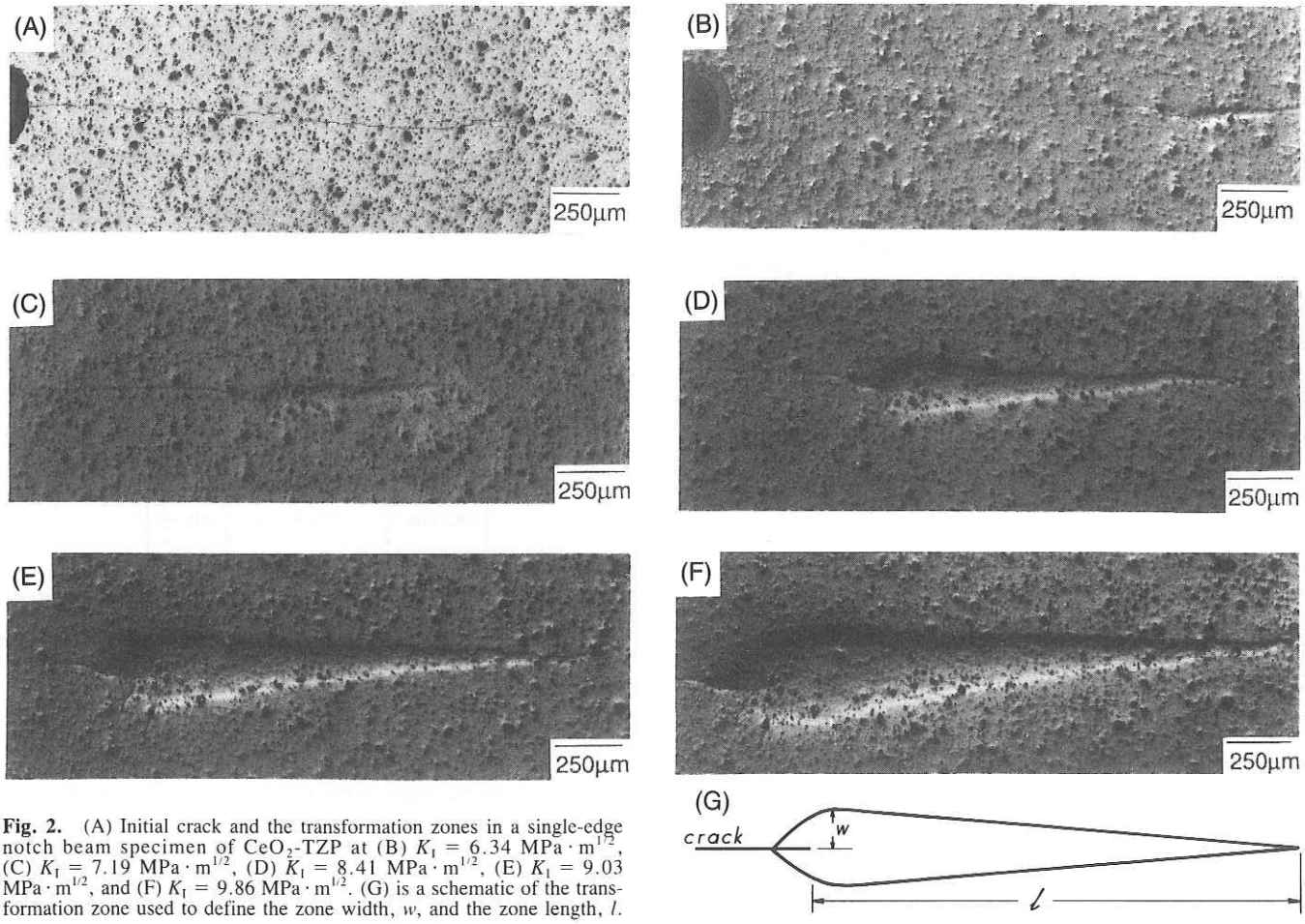

Fig. 2. (A) Initial crack and the transformation zones in a single-edge notch beam specimen of CeO_2-TZP at (B) $K_I = 6.34$ MPa · $m^{1/2}$, (C) $K_I = 7.19$ MPa · $m^{1/2}$, (D) $K_I = 8.41$ MPa · $m^{1/2}$, (E) $K_I = 9.03$ MPa · $m^{1/2}$, and (F) $K_I = 9.86$ MPa · $m^{1/2}$. (G) is a schematic of the transformation zone used to define the zone width, w, and the zone length, l.

the crack tip, w. Table I summarizes the measurements of the transformation zone dimensions and the crack extension (Δa) at the different loading conditions shown in Figs. 2(A) through (F).

The shape of the transfomation zone observed on the CeO_2-TZP specimen was unexpected because yield criteria that incorporate both the shear and the dilatational effects on transformation yield do not predict the elongated shape of the transformation zone. This can be demonstrated by the following exercise. As part of a study of the stress-state effects on transformation yield, plasticity, and fracture toughness of CeO_2-TZP, experiments are being conducted in uniaxial (four-point bend and uniaxial compression) and biaxial (diametral compression and biaxial tension) stress states.[14] Partial results obtained to date are shown in Fig. 3. Figure 3 shows a yield envelope for the CeO_2-TZP plotted in the tension–tension and tension–compression quadrant. The experimental data plotted are the 0.05% offset yield stress measured in uniaxial tension (four-point bend), tension–compression (diametral compression), and uniaxial-compression stress states. A nearly constant initial elastic strain rate of 1.4×10^{-5}/s was employed in all of the tests. The yield stress increased from 192 MPa measured in four-point bending to 635 MPa in uniaxial compression, and the diametral-compression tests gave intermediate values. This trend of the higher yield stress in uniaxial compression relative to the yield stress in uniaxial tension reflects the combined influence of the dilatational (hydrostatic) and shear stress components in transformation yielding as compared to the pure shear yielding in metals. A similar trend has been observed in MgO-PSZ,[15–17] although the magnitudes of the yield stresses are higher and the ratio of the yield stresses in compression and tension is smaller for MgO-PSZ as compared to CeO_2-TZP.

Chen and Reyes-Morel[9,17] have suggested the following yield criterion to describe the combined shear and dilatation effects on transformation yield and plasticity for both MgO-PSZ and CeO_2-TZP:

$$\frac{\sigma_e}{\sigma_e^*} + \frac{\sigma_m}{\sigma_m^*} = 1 \tag{1}$$

In Eq. (1), σ_e and σ_m are the equivalent stress and the mean hydrostatic stress, respectively, and in terms of the principal stresses — σ_1, σ_2, and σ_3 — they are given by the following equations:

$$\sigma_e = \frac{1}{\sqrt{2}}[(\sigma_1 - \sigma_2)^2 + (\sigma_2 - \sigma_3)^2 + (\sigma_3 - \sigma_1)^2]^{1/2} \tag{2}$$

$$\sigma_m = \frac{1}{3}(\sigma_1 + \sigma_2 + \sigma_3) \tag{3}$$

Table I. Characteristic Dimensions of the Transformation Zone and Crack Extension in Single-Edge Notch Beam Specimen of CeO_2-TZP

Figure	K_I (MPa · $m^{1/2}$)*	w (μm)†	l (μm)‡	Δa (μm)§	l/w
2(A)	0	0	0	0	
2(B)	6.34	29	351	0	12.1
2(C)	7.19	52	716	0	13.8
2(D)	8.41	88	1190	0	13.5
2(E)	9.03	125	1580	123	12.6
2(F)	9.89	166	1961	180	11.8

*Stress intensity. †Zone width. ‡Zone length. §Crack extension.

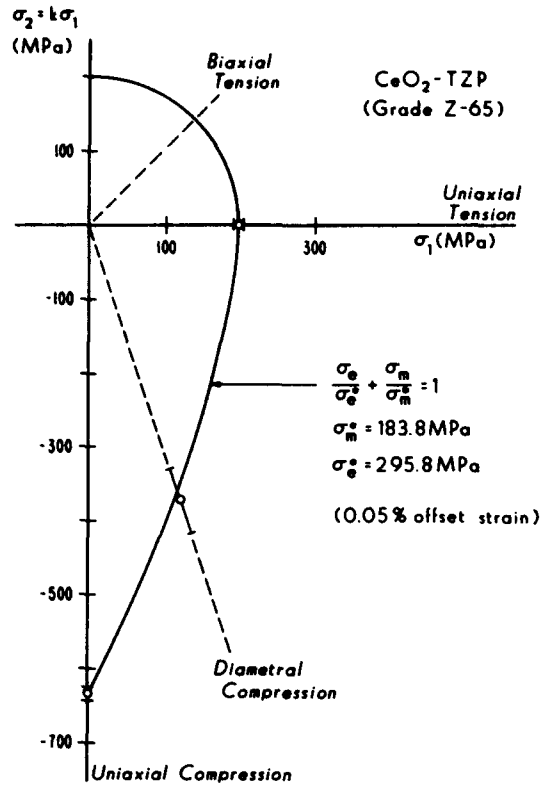

Fig. 3. Transformation yield stress envelope for CeO_2-TZP in the tension–tension and tension–compression stress quadrants. The experimental data plotted are yield stresses corresponding to 0.05% offset strain.

and σ_e^* and σ_m^* are the characteristic yield stress parameters independent of the stress state. For a general biaxial stress state defined by the principal stresses, $\sigma_1 = \sigma_1$ and $\sigma_2 = k\sigma_1$, the yield envelope corresponding to the yield criterion of Eq. (1) is given by the following equation:

$$\sigma_1 = \frac{1}{\frac{1+k}{3\sigma_m^*} + \frac{(1-k+k^2)^{1/2}}{\sigma_e^*}} \tag{4}$$

The yield envelope corresponding to Eq. (4), which is equivalent to Eq. (1) in the biaxial stress state, is shown in Fig. 3. To plot this envelope, the characteristic yield stress parameters, σ_e^* and σ_m^*, were calculated from the yield stresses measured in four-point-bend and uniaxial-compression tests using Eqs. (1) through (3). The yield stress parameters calculated in this manner were $\sigma_e^* = 296$ MPa and $\sigma_m^* = 184$ MPa. It is seen in Fig. 3 that the yield stress measured in the diametral compression test is consistent with this envelope. Thus, the yield criterion proposed by Chen and Reyes-Morel[9,17] for the combined shear/dilatation effects appears to account for the stress-state influence on yielding of the CeO_2-TZP employed in this study. It is interesting to note in Fig. 3 that the yield envelope based on Eq. (1) predicts a lower yield stress in biaxial tension as compared to the yield stress in uniaxial tension or tension–compression stress states. In the equibiaxial tension stress state ($k = 1$), for example, Eq. (4) predicts a yield stress of 140 MPa. Experiments are currently under way using biaxial disk bending tests to verify this prediction.

Although Eq. (1) provides an accurate description of the stress-state dependence of the transformation yield stress in biaxial stress states, it does not predict the elongated shape of the transformation zone observed in the CeO_2-TZP. Chen and Reyes-Morel[17] used Eq. (1) and the plane strain stress field of a crack in an untransformed material to calculate the transformation zone profiles. In the following, similar calculated profiles are compared with the observed zone shapes. The calculations were, however, made for the plane stress condition for comparison with the transformation zone profile measured on the surface of the single-edge notch beam specimen. For the plane stress condition, the principal stresses are given by the following equations:

$$\sigma_1 = \frac{K_I}{\sqrt{2\pi r}} \cos\frac{\theta}{2}\left(1 + \sin\frac{\theta}{2}\right) \tag{5}$$

$$\sigma_2 = \frac{K_I}{\sqrt{2\pi r}} \cos\frac{\theta}{2}\left(1 - \sin\frac{\theta}{2}\right) \tag{6}$$

$$\sigma_3 = 0 \tag{7}$$

Equations (5) through (7), when combined with the yield criterion of Eq. (1), give the following equation for the transformation zone boundary:

$$r(\theta) = \left[\frac{2K_I \cos\frac{\theta}{2}}{3\sqrt{2\pi}\,\sigma_m^*} + \frac{\sqrt{2}K_I \cos\frac{\theta}{2}\sin\frac{\theta}{2}}{\sqrt{\pi}\,\sigma_e^*}\right]^2 \tag{8}$$

Figure 4 compares the transformation zone shape calculated from Eq. (8) (identified as the shear/dilatation boundary) using the yield stress parameters obtained in biaxial tests with the experimental observation at $K_I = 9$ MPa · $m^{1/2}$. Equation (8) predicts much larger zone width (w) normal to the crack than the zone length (l) ahead of the crack. Also shown in Fig. 4 are the zone boundaries calculated on the basis of pure shear and pure dilatation yield criteria. None of the yield criteria predict the elongated shape of the transformation zone observed in the CeO_2-TZP.

It should be noted that the transformation zone boundary defined by Eq. (8) is based on the elastic stress field of the crack (Eqs. (5) through (7)) in the absence of transformation yielding at the crack tip. The onset of yielding at the crack tip reduces the stresses within the transformation zone and increases the stresses in the elastic zone due to load shedding. This stress redistribution causes the plastic zone size to be larger than the calculated zone size based on Eq. (8). The calculations based on the elastic stress distribution only serve to qualitatively illustrate the significant difference between the observed and the expected transformation zone shapes.

(3) Transformation Zone Size and Crack-Growth-Resistance (R-Curve) Behavior

Despite the disagreement between the observed zone shape and the zone shape calculated from the macroscopic yield criterion, the relationship among the measured zone size (w), crack extension (Δa), and fracture toughness is of interest. According to the crack-shielding models of transformation toughening, the zone width, w, and the extent of crack growth into the transformed zone, Δa, to form a transformation wake behind the crack tip are important parameters (among others) that determine the degree of toughening and the R-curve behavior. The model of McMeeking and Evans,[1] for example, gives the following equation for the toughness increment, ΔK_I, as a function of the normalized crack length increment, $\Delta a/w$:

$$\Delta K_I = \frac{Ee^T V_f \sqrt{w}}{1-\nu}\kappa(\Delta a/w, \nu) \tag{9}$$

where E is the elastic modulus of the matrix containing the zirconia particles, e^T the transformation strain, V_f the volume fraction of transformed zirconia particles, and ν Poisson's ratio. $\kappa(\Delta a/w, \nu)$ is a function whose value increases with the relative crack extension and approaches an asymptotic value at $\Delta a \sim 5w$. The function κ, in effect, describes the crack-growth-resistance behavior. The magnitude of the asymptotic value is 0.215 according to the model of McMeeking and Evans,[1] who considered only the dilatational component of transformation strain. Lambropoulos[18] has proposed a model that includes both

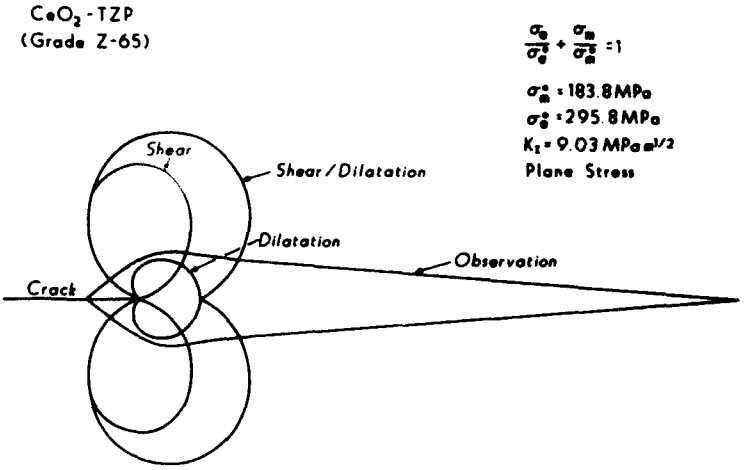

Fig. 4. Comparison of the calculated and observed transformation zone profiles in a single-edge notch beam specimen of CeO_2-TZP at $K_I = 9.03$ MPa · $m^{1/2}$.

shear and dilatational strain contributions during nucleation, and the predicted asymptotic value for κ in his model is $0.55(1 - \nu)$. Swain[19] and Swain and Rose[20] have shown that measurements of the saturation fracture toughness and the zone size in Y_2O_3-TZP and MgO-PSZ ceramics are in good agreement with the above two models, respectively.

Figure 5 shows plots of the fracture toughness of the CeO_2-TZP as a function of the crack length normalized by the single-edge notch beam specimen width. The specimen was unloaded twice just before instability set in and subjected to two intermediate annealing treatments (1000°C, 30 min) and the fracture toughness measurements were repeated on the same specimen. The annealing treatment eliminated the transformation zone at the crack tip and completely recovered the specimen to its initial state. The R curves for all three measurement cycles were nearly identical and there was no apparent dependence on a/W. Several features of the R curves in Fig. 5 are noteworthy and are different from theoretical expectations. A significant amount of the toughness increment was associated with an increase in the size of the transformation zone (both w and l) without an increase in the crack length. This is also evident in Table I. The zone size continued to increase with the initiation of crack extension and stable growth, approaching a zone width $w = 340$ μm at a maximum stress-intensity factor of about $K_I = 14.5$ MPa · $m^{1/2}$. The R curves did not show evidence of a saturation fracture toughness; instability set in when the fracture toughness was still increasing. The beginning of the instability coincided with a maximum in the load; this occurred at about the same fracture toughness in all three measurement cycles and it appeared to be associated with a critical size of the transformation zone.

It should be noted that the maximum value of the fracture toughness measured in the CeO_2-TZP is comparable to the maximum toughness measured in MgO-PSZ.[19] However, the maximum zone width measured in this study in CeO_2-TZP is more than an order of magnitude greater than the maximum zone width measured in the MgO-PSZ (~20 μm). As a consequence, the dependence of the fracture toughness on the transformation zone width in CeO_2-TZP is not in quantitative agreement with the crack-shielding models discussed above. This is easily seen by substituting the appropriate material properties and the zone size in Eq. (9). For material properties appropriate for CeO_2-TZP, $E = 200$ GPa, $e^T = 0.05$, $V_f = 0.8$ (measured on the fracture surface of the single-edge notch bend specimen), $\nu = 0.3$, Eq. (9) predicts a maximum toughness increment, $\Delta K_I = 45$ MPa · $m^{1/2}$ for $w = 340$ μm, and $\kappa = 0.214$. The total fracture toughness for the CeO_2-TZP is only 14.5 MPa · $m^{1/2}$. Other models of crack shielding give even greater discrepancy between the measured and expected toughness increments.

However, the fracture toughness of the CeO_2-TZP does exhibit an excellent linear dependence on $w^{1/2}$ in its R-curve behavior.

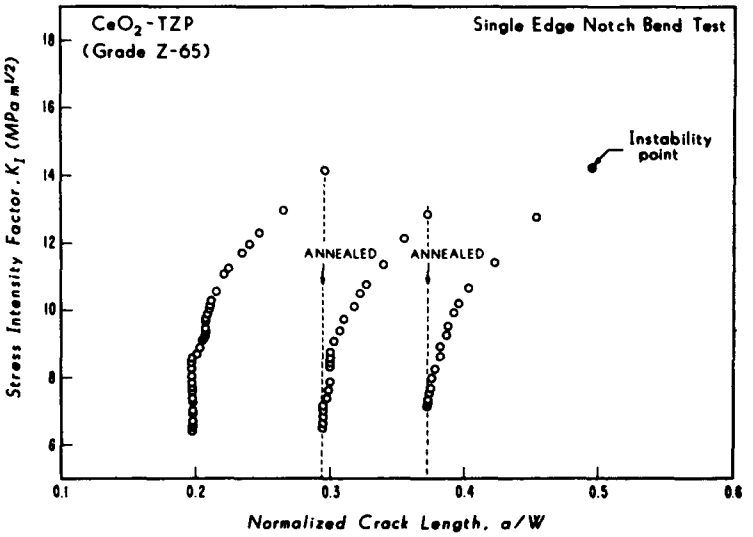

Fig. 5. Crack-growth resistance (R curves) for CeO_2-TZP measured with a single-edge notch beam specimen.

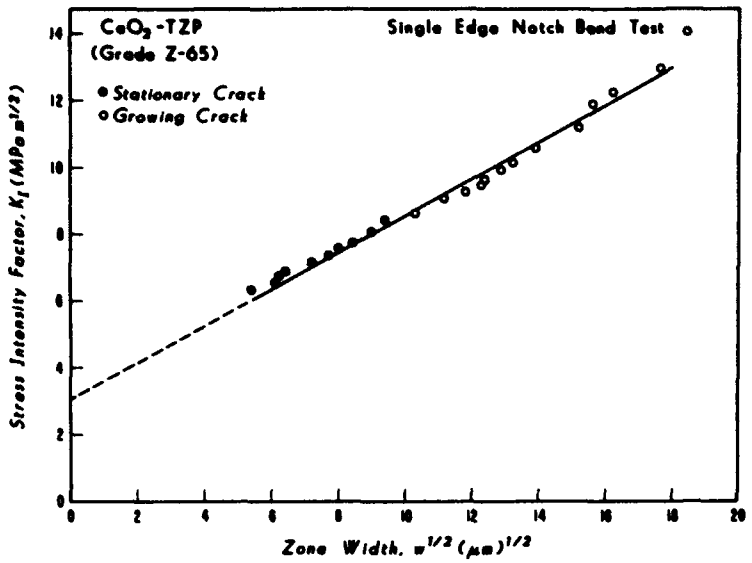

Fig. 6. Relation between the applied stress intensity (K_I) and the transformation zone width, w, in single-edge notch beam specimen of CeO_2-TZP.

This is illustrated in Fig. 6. It is interesting to note in Fig. 6 that the linear relationship covers both the stationary crack regime as well as the stable crack growth regime of the *R*-curve behavior. It will be shown later in Section IV that the $w^{1/2}$ dependence of the fracture toughness does not necessarily imply conformance with the crack-shielding models. It is a more general consequence of the dependence of the transformation (plastic) zone on the applied load under the condition of an invariable zone shape.

(4) Analysis of the Transformation Zone Length in Terms of the Dugdale Plastic Strip Zone Model

Since the transformation zones in the CeO_2-TZP are thin elongated strips, they resemble the plastic strip zones envisaged in the classic Dugdale model.[21] It was, therefore, of interest to examine the zone length as a function of the applied load in terms of the Dugdale model. Rose and Swain[10] recently employed a modified Dugdale model to analyze their results on CeO_2-TZP. By rewriting the original Dugdale equation, which was developed for a center-cracked panel under uniform tension, in terms of the elastic stress intensity factor (assuming small-scale yielding condition prevails) for the single-edge notch beam specimen, we get the following equation for the transformation zone length ahead of the crack tip:

$$\frac{l}{a+l} = 2\sin^2\left[\frac{\pi K_I}{4\sigma_y\sqrt{\pi a}}\right] \tag{10}$$

In Eq. (10), σ_y is the yield stress measured in uniaxial tension. Figure 7 compares the prediction of Eq. (10) with the zone length measurements in the CeO_2-TZP. To plot the experimental points in Fig. 7, the transformation zone lengths (l), crack lengths (a), and the applied stress intensity (K_I) measured at different stages of both the stationary and the stably growing crack were used. The 0.05% offset yield stress, σ_y = 192 MPa, measured in four-point bending was used in these calculations. Considering that no adjustable parameters are involved in the theoretical prediction shown in Fig. 7, the agreement between the experimental measurements on the CeO_2-TZP and the Dugdale model prediction is very good.

IV. Discussion

Several results of this study on CeO_2-TZP warrant additional discussion. The large transformation zone and its elongated shape, unexpected from theoretical considerations, are two of the most noteworthy results. Rose and Swain[10] have also observed thin, elongated zones in double-cantilever-beam specimens of a CeO_2-TZP, although the maximum dimensions of the transformation zone obtained at room temperature (20°C) in their material (w = 30 to 40 μm, l = 200 μm) are significantly smaller than those measured in this study. These zone size differences can be rationalized as being due to differences in the compositions of the two CeO_2-TZPs. The CeO_2-TZP used in this study appears to have a higher M_s temperature and, as a consequence, a greater propensity for transformation than the CeO_2-TZP studied by Rose and Swain.[10] This argument is supported by the fact that Rose and Swain obtained yield stress ($\sigma_y \sim$ 200 MPa), fracture toughness ($K_{Ic} \sim$ 16 MPa · m$^{1/2}$), and transformation zone sizes in their material at −40°C comparable to the properties of the present CeO_2-TZP at room temperature. However, the CeO_2-TZP of this study did not exhibit the characteristic branching shear bands that were observed by Rose and Swain at −10° and −40°C.

The reasons for the elongated shape of the transformation zones are not clear. The transformation zone shapes should be, ideally, predicted by an appropriate yield criterion that properly accounts for both the dilatational and shear effects on the transformation yield and the local stress field of the crack in the untransformed material. There are two possible reasons why this approach does not explain the zone shape in CeO_2-TZP. First, the transformation strain in the uniaxial and biaxial test specimens used to establish the yield criterion is nonuniform and localized in bands. The yield criterion for this localized deformation, which prevails at a crack tip, may be different from the one that governs macroscopic yield behavior. Secondly, fracture surface observations in this study and transformation zone observations by Rose and Swain[10] in their material using scanning electron microscopy have revealed evidence of intergranular microcracks. The crack-tip zone in CeO_2-TZP may combine the characteristics of a transformation and a damage zone for which the governing constitutive law may be different from the one established with macroscopic tests. It is also interesting to note that the same elongated transformation zone shape was observed in two different test geometries, single-edge notch beam specimens of this study and the double-cantilever-beam specimens of Rose and Swain.[10] Thus, the zone shape is not governed by the specimen geometry.

Although the transformation zones obtained in the CeO_2-TZP are more than an order of magnitude larger than the transformation zones in optimally aged MgO-PSZ,[19,20] the measured fracture toughnesses are comparable. This suggests that the transformation zone in the CeO_2-TZP is not as efficient in developing crack shielding via the compressive tractions at the zone boundary as the zones in MgO-PSZ. As was illustrated in a previous section, if the transformation zones in CeO_2-TZP behaved in the same manner as those in MgO-PSZ, the expected fracture toughness increment from the crack-shielding effect would be 3 times the measured fracture toughness. Part of this discrepancy could be

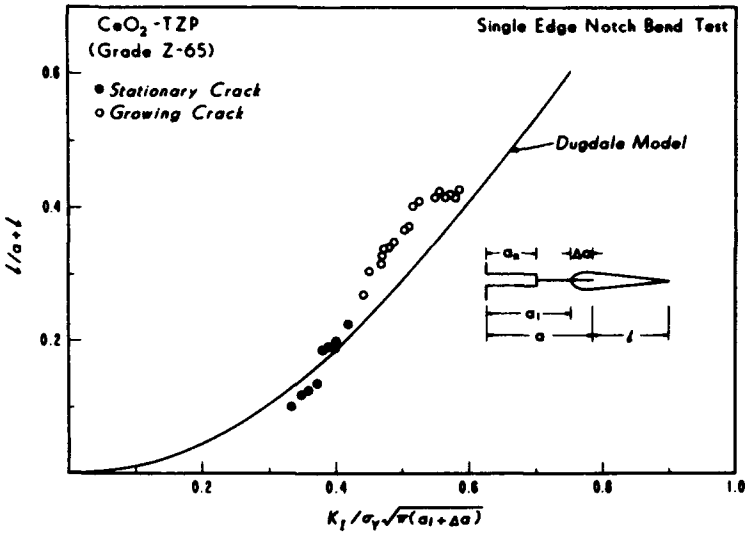

Fig. 7. Comparison of the dependence of the transformation zone length on the applied stress intensity in CeO_2-TZP with the Dugdale plastic strip zone model.

due to an overestimation of the volume fraction transformed, V_f. The value, $V_f = 0.8$, was based on X-ray diffraction analysis of the fracture surface. The actual volume fraction transformed in the transformation zone may well be lower. It may also vary with position within the transformation zone. Secondly, since the CeO_2-TZP has a range of grain sizes for the tetragonal grains as opposed to the very uniformly sized tetragonal precipitates in the MgO-PSZ, the transformation zone size at any load can be expected to be a function of this grain size distribution. The zone size would also be expected to vary with the applied load. The simplified transformation toughening model, as represented by Eq. (9), does not take these effects into account. Equation (9), for example, is based on the premise that transformation zone size is uniquely determined by the intrinsic matrix toughness and the critical transformation stress. As a result, w is assumed to be constant independent of the applied load and crack extension. These assumptions are clearly not valid in the case of CeO_2-TZP.

The linear dependence of the fracture toughness on $w^{1/2}$ seemingly suggests at least a qualitative agreement with the crack-shielding models. However, it should be recognized that the plot shown in Fig. 6 is intrinsically different from similar plots reported for MgO-PSZ and Y_2O_3-TZP.[19,20] These latter plots were constructed by correlating the *saturation* fracture toughness with the zone size measured on the fracture surface using the X-ray diffraction technique. Thus, different fracture toughness values were obtained on different specimens subjected to different heat treatments or processing conditions. On the other hand, the plot of Fig. 6 corresponds to measurements on the same CeO_2-TZP specimen and reflects the growth of the transformation zone during the rising crack growth resistance behavior. This relationship can be rationalized in the following way. A simplified form of the Dugdale model gives the following equation for the plastic zone length, l:[22]

$$l = \frac{\pi}{8}\left(\frac{K_I}{\sigma_y}\right)^2 \tag{11}$$

Since the shape of the transformation zone remains approximately constant (see Table I), Eq. (11) implies that $K_I \propto w^{1/2}$. Thus, the linear relationship seen in Fig. 6 can be expected since the transformation zone size follows the Dugdale plastic strip zone model (Fig. 7).

The agreement obtained between the zone length measurements and the Dugdale strip zone model is intriguing. Rose and Swain[10] have also rationalized their results in terms of a modified Dugdale–Bilby–Cottrell–Swinden (DBCS) model. Of course, this agreement in itself does not explain the behavior of CeO_2-TZP completely. The Dugdale model was developed by replacing the elastic singularity at the crack tip by a constant yield stress zone whose length is governed by the yield stress in uniaxial tension. It does not account for the stress-state effects on the yield stress and it does not define the length of the yield zone in a direction other than along the plane of the crack. In this sense, the agreement with the Dugdale model is logical, but it does not provide any insight into the origin of the elongated transformation zones in CeO_2-TZP. It is also interesting to note that the original Dugdale model[21] was verified by plastic zone size measurements in thin steel sheets. One question that remains to be investigated is whether the observation of the elongated transformation zone is a characteristic of only the surface, where plane stress conditions prevail, or whether it is representative of the bulk. This investigation is currently under way.

V. Conclusions

(1) Precracked and annealed single-edge notch beam specimens of CeO_2-TZP exhibit thin, elongated transformation zones with a shape that is nearly independent of the applied stress intensity. This shape is inconsistent with the zone profile predicted on the basis of a shear/dilatation yield criterion and the stress field of the crack in the untransformed material.

(2) The transformation zone size measured for the CeO_2-TZP is more than an order of magnitude greater than the zone sizes reported for MgO-PSZ, but the maximum fracture toughness for the CeO_2-TZP is comparable to that of MgO-PSZ. As a result, crack-shielding models which adequately explain the fracture toughness of MgO-PSZ overestimate the fracture toughness of CeO_2-TZP.

(3) The dependences of the zone width and the zone length on the applied load are consistent with the Dugdale plastic strip zone model.

Acknowledgments: Helpful discussions with Prof. Anil V. Virkar are gratefully acknowledged.

References

[1]R. M. McMeeking and A. G. Evans, "Mechanics of Transformation-Toughening in Brittle Materials," *J. Am. Ceram. Soc.*, **65** [5] 242–46 (1982).

[2]B. Budiansky, J. W. Hutchinson, and J. C. Lambropoulos, "Continuum Theory of Dilatant Transformation Toughening in Ceramics," *Int. J. Solids Struct.*, **19** [4] 337–55 (1983).

[3]A. H. Heuer, "Transformation Toughening in ZrO_2-Containing Ceramics," *J. Am. Ceram. Soc.*, **70** [10] 689–98 (1987).

[4]T. Kosmac, R. Wagner, and N. Claussen, "X-Ray Determination of Transforma-

tion Depths in Ceramics Containing Tetragonal ZrO_2," *J. Am. Ceram. Soc.*, **64** [4] C-72–C-73 (1981).

[5]R. C. Garvie, R. H. J. Hannink, and M. V. Swain, "X-Ray Analysis of the Transformed Zone in Partially-Stabilized Zirconia (PSZ)," *J. Mater. Sci. Lett.*, **1**, 437–40 (1982).

[6]K. Tsukuma and M. Shimada, "Strength, Fracture Toughness and Vickers Hardness of CeO_2-Stabilized Tetragonal ZrO_2 Polycrystals," *J. Mater. Sci.*, **20**, 1178–84 (1985).

[7]R. L. K. Matsumoto, R. J. Mayhew, and A. V. Virkar, "Strength and Toughness of Modified Ceria-Doped Polycrystalline Tetragonal Zirconia"; presented at the 90th Annual Meeting of the American Ceramic Society, Cincinnati, OH, May 4, 1988.

[8]I-W. Chen and P. E. Reyes-Morel, "Transformation Plasticity and Transformation Toughening in Mg-PSZ and Ce-TZP"; pp. 75–88 in Advanced Structural Ceramics. Edited by P. F. Becher, M. V. Swain, and S. Somia. Materials Research Society Symposium Series, Materials Research Society, Pittsburgh, PA, 1986.

[9]P. E. Reyes-Morel and I-W. Chen, "Transformation Plasticity of CeO_2-Stabilized Tetragonal Zirconia Polycrystals: I, Stress Assistance and Autocatalysis," *J. Am. Ceram. Soc.*, **71** [5] 343–53 (1988).

[10]L. R. F. Rose and M. V. Swain, "Transformation Zone Shape in Ceria-Partially-Stabilized Zirconia," *Acta Metall.*, **36** [4] 955–62 (1988).

[11]C.-S. Yu and D. K. Shetty, "Transformation Plasticity and Crack Growth Resistance Behaviors of CeO_2-TZP"; presented at the 90th Annual Meeting of the American Ceramic Society, Cincinnati, OH, May 4, 1988.

[12]H. Toraya, M. Yoshimura, and S. Somiya, "Calibration Curve for Quantitative Analysis of the Monoclinic–Tetragonal ZrO_2 System by X-Ray Diffraction," *J. Am. Ceram. Soc.*, **67** [9] C-119–C-121 (1984).

[13]ASTM E 399-83, "Standard Test Method for Plane Strain Fracture Toughness of Metallic Materials"; Annual Book of ASTM Standards, Section 3, Vol. 03.01. American Society for Testing and Materials, Philadelphia, PA, 1984.

[14]C.-S. Yu and D. K. Shetty, "Stress-State Effects on Transformation Yielding and Plasticity in CeO_2-TZP"; unpublished work.

[15]J. Lankford, "Plastic Deformation of Partially-Stabilized Zirconia," *J. Am. Ceram. Soc.*, **66** [11] C-212–C-213 (1983).

[16]D. B. Marshall, "Strength Characteristics of Transformation-Toughened Zirconia," *J. Am. Ceram. Soc.*, **69** [3] 173–80 (1986).

[17]I-W. Chen and P. E. Reyes-Morel, "Implications of Transformation Plasticity in ZrO_2-Containing Ceramics: I, Shear and Dilatation Effects," *J. Am. Ceram. Soc.*, **69** [3] 181–89 (1986).

[18]J. C. Lambropoulos, "Effect of Nucleation on Transformation Toughening," *J. Am. Ceram. Soc.*, **69** [3] 218–22 (1986).

[19]M. V. Swain, "Inelastic Deformation of Mg-PSZ and Its Significance for Strength–Toughness Relationship in Zirconia-Toughened Ceramics," *Acta Metall.*, **33** [11] 2083–91 (1985).

[20]M. V. Swain and L. R. F. Rose, "Strength Limitations of Transformation-Toughened Zirconia Alloys," *J. Am. Ceram. Soc.*, **69** [7] 511–18 (1986).

[21]D. S. Dugdale, "Yielding of Steel Sheets Containing Slits," *J. Mech. Phys. Solids*, **8**, 100–104 (1960).

[22]H. L. Ewalds and R. J. H. Wanhill, Fracture Mechanics; pp. 60–61. Arnold, London, England, 1984. □

JOURNAL OF MATERIALS SCIENCE 25 (1990) 2025-2035

Transformation yielding, plasticity and crack-growth-resistance (R-curve) behaviour of CeO_2–TZP

CHENG-SHENG YU, D. K. SHETTY
Department of Materials Science and Engineering, University of Utah, Salt Lake City, Utah 84112, USA

Transformation yield and plasticity, transformation zone sizes at crack tips and rising crack-growth-resistance (R-curve) behaviours were studied in a commercial-grade ceria partially stabilized zirconia polycrystalline material (CeO_2–TZP). The yield stresses measured in three-point bending decreased from 390 to 176 MPa when the sintering temperature was varied from 1425 to 1525° C. The corresponding total plastic strain to fracture increased with decreasing yield stress. Crack-tip transformation zones in precracked, annealed and loaded single-edge-notch-bend specimens decreased significantly in size with increasing transformation yield stress; however, the R-curves were relatively insensitive to the yield stresses or the transformation zone sizes. The measured zone sizes and R-curves were examined in terms of both crack shielding and plastic yield strip zone models.

1. Introduction

Crack shielding models [1–3] have been successfully used to explain many aspects of transformation toughening in MgO–partially stabilized zirconia (MgO–PSZ), Y_2O_3–partially stabilized zirconia (Y_2O_3–TZP) and zirconia-toughened alumina ceramics. Thus, for example, the rising crack-growth-resistance (R-curve) measured in MgO–PSZ by Swain and Hannink [4] and Marshall and Swain [5] is qualitatively consistent with the R-curve behaviour predicted by the crack shielding models due to the transformation wake behind the advancing crack tip. Further, Swain [6] and Swain and Rose [7] have successfully correlated the saturation fracture toughness of MgO–PSZ and Y_2O_3–TZP with the square root of the widths of the transformation zones in accordance with the crack shielding models. The transformation zone sizes in the above studies were, however, measured indirectly on fracture surfaces using X-ray diffraction techniques [8, 9], because the zones are not sufficiently well defined for observation in optical or scanning electron microscopes.

Recent development of certain grades of ceria–partially stabilized zirconia (CeO_2–TZP) ceramics that exhibit pronounced transformation plasticity has permitted direct observation of the shapes and sizes of the transformation zones in precracked fracture mechanics test specimens [10, 11]. A quantitative comparison of the observed shapes and sizes of the transformation zones and the measured R-curve behaviour with the theoretical predictions by Yu and Shetty [10] revealed several interesting anomalies in CeO_2–TZP. First, the transformation zone was elongated in the plane of the crack, i.e. the zone length ahead of the crack was much greater than the zone width normal to the crack plane. This zone shape was shown to be inconsistent with the prediction of a combined shear/dilatation yield criterion established in macroscopic biaxial tests. Secondly, even though the maximum transformation zone widths measured in CeO_2–TZP ($> 300\,\mu m$) were more than an order of magnitude larger than the transformation zone widths in MgO–PSZ ($\sim 25\,\mu m$), the maximum fracture toughness measured in the two materials were comparable ($K_c \sim 14$ to $15\,MPa\,m^{1/2}$). Finally, both the transformation zone sizes and the R-curves measured with precracked and annealed single-edge-notch-bend (SENB) specimens of CeO_2–TZP did not show evidence of saturation, i.e. both the transformation zone dimensions and the crack-growth-resistance were increasing up to the point of instability.

The present paper summarizes the results of an investigation in which the transformation yield stress of a CeO_2–TZP was systematically varied by varying the sintering temperature. The objective was to examine the effect of the varying yield stress on transformation plasticity, the crack-tip transformation zone size and the R-curve behaviour in the context of crack shielding and plastic strip zone models.

2. Test material and procedures

The CeO_2–TZP ceramic used in the present study was obtained in powder form from a commerical source (tentative grade Z-65, Ceramatec Inc., Salt Lake City, Utah 84119, USA). Nominally, it is partially-stabilized zirconia with 12 mol% CeO_2 and small amounts of proprietary additives. The as-received powder was first sieved through a $70\,\mu m$ screen. The

0022–2461/90 $03.00 + .12

TABLE I Sintering temperatures, average grain sizes, phase contents and yield stresses for CeO_2-TZP specimens

Type	Sintering temperature (°C)	Grain size (μm)	Phase content (as-annealed) V_T (%)	Yield stress (MPa)	Phase content (fracture surface) V_T (%)
IA	1500	1.91	98	190	15
IIAA	1525	2.18	98	176	15
IIA	1500	1.87	98	245	18
IIB	1475	1.73	99	281	19
IIC	1450	1.52	99	335	22
IID	1425	1.47	99	390	27

screened powder was pressed in a uniaxial die press at 34.5 MPa, followed by isostatic pressing at 207 MPa. The as-pressed compacts were sintered in air at temperatures ranging from 1425 to 1525°C for 2 h. Test specimens were from two powder lots I and II and were sintered at five different temperatures: 1525°C (type AA), 1500°C (type A), 1475°C (type B), 1450°C (type C) and 1425°C (type D); these are listed in Table I along with the corresponding average grain sizes, phase contents (volume per cent of the tetragonal phase) and yield stresses measured in three-point bend tests. The CeO_2-TZP powders of lots I and II differed slightly in their composition and this was reflected in the different grain sizes and properties of specimens of types IA and IIA, even though these specimens were sintered at the same temperature. The grain sizes were determined by intercept length measurements on scanning electron micrographs of polished and thermally etched surfaces. Approximately 700 grain intercept lengths were measured for each material to obtain the average grain size and the grain size distribution. The tetragonal phase contents were measured by X-ray diffraction using the calibration reported by Toraya *et al.* [12].

Transformation yielding and plasticity were characterized in three-point bending using beam specimens measuring 4 mm × 5 mm × 45 mm in dimensions and a 40 mm span. The test fixtures conformed to the specifications of the MIL standard [13]. The specimens were machined from the sintered billets by cutting with diamond blades and grinding with diamond wheels. The tensile surface was successively polished with 15, 6 and 1 μm diamond paste to achieve a surface that was adequate for surface observations of transformation plasticity. All machined and polished specimens were annealed at 1000°C for 30 min in air prior to the bend tests. There was no detectable change in the phase content after annealing. In selected specimens, strain gauges were mounted in the centre of the tensile surface to monitor the elastic and transformation strains.

Crack-tip transformation zones and crack-growth-resistance curves were studied in prepracked, annealed and reloaded single-edge-notch-bend (SENB) specimens. The relative dimensions of the specimens were according to the specifications of American Society for Testing Materials Standard E 399-83 [14]. The final dimensions of the specimens were support span, S = 60 mm, specimen width, W = 15 mm, and specimen thickness, B = 7.5 mm. This relatively large specimen size was used to meet the minimum size requirements specified in ASTM E 399-83 based on the expected range of fracture toughness and the yield stresses of the material. The SENB specimens were first notched in the centre of the beam to a depth of 1.5 mm using a 150 μm thick diamond blade, loaded in an universal testing machine to precrack to a depth of 3.0 to 3.5 mm ($a/W \sim 0.2$ to 0.25) and subsequently annealed at 1000°C for 30 min. To assess R-curve behaviour, the precracked and annealed SENB specimens were loaded incrementally, unloaded, and the crack lengths (a) and the transformation zone dimensions (zone length, l, and zone width, w) were measured with a stereo microscope and a micrometer stage. The measurements were repeated as a function of applied load and crack length. The transformation zones were photographed at various stages using an optical microscope with Nomarski interference contrast capability.

3. Experimental results and analysis

3.1. Transformation yield, plasticity and failure in three-point bending

Three-point bending was selected over four-point bending previously used [10] because the CeO_2-TZP used in this study deformed in discrete transformation bands normal to the beam axis. In four-point bending, multiple bands nucleated in the centre span and the measured yield stress and the stress–strain curve tended to vary depending upon the number and location of the transformation bands relative to the strain gauge used to monitor the strain. In contrast, a single wedge-shaped transformation band nucleated in three-point bending with a characteristic strain burst and a distinct yield stress associated with the nucleation event. Thus, yield stress could be defined more precisely in three-point bending.

Fig. 1 shows the stress–strain curve obtained in three-point bending for CeO_2-TZP material identified as IIA. The strain plotted was measured at the centre of the tensile surface using a strain gauge. The initial elastic strain rate of the outer fibres during bending was $8.0 \times 10^{-5} sec^{-1}$. The stress was calculated from the load using the conventional elastic bending formula. The stress–strain curve consisted of an initial elastic regime where the stress increased linearly up to a maximum stress which was defined as the yield stress. Yielding commenced with an increment of transformation strain which occurred at the same stress or slightly decreasing stress. This instantaneous strain increment coincided with the formation of the wedge-shaped transformation band at the centre of the bend specimen directly opposite to the loading roller. Fig. 2 shows this transformation band

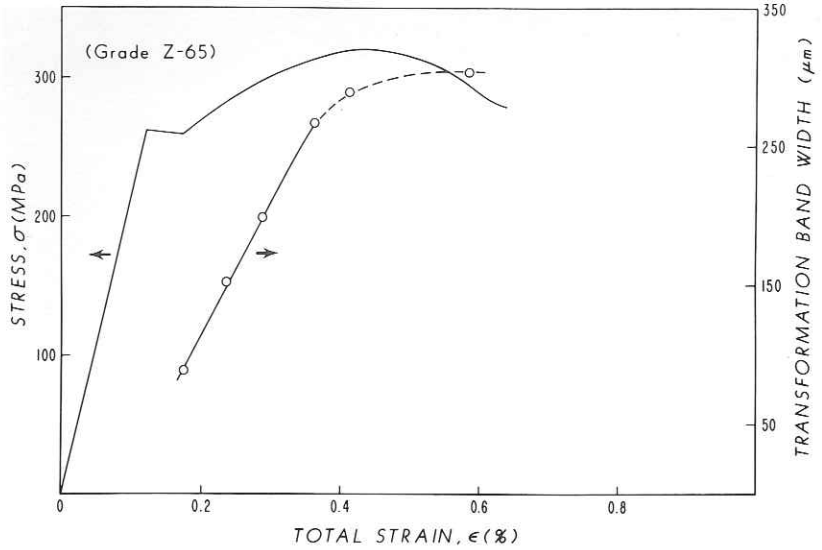

Figure 1 Elastic stress and transformation band width as functions of the measured total strain in three-point bending of CeO_2–TZP (Type IIA).

immediately after nucleation in type IIA CeO_2–TZP. In Fig. 2, the photograph labelled a shows the transformation band on the tension surface, while photograph b shows the wedge shape of the transformation band on the side surface of the beam specimen. The transformation band had the largest width on the tension surface and the width decreased in a direction toward the neutral axis. Reyes-Morel and Chen [15] have reported similar observations of discrete, wedge-shaped transformation bands in four-point bending of CeO_2–TZP. There was no transformation band on the compression side of the bend specimen and this was consistent with the much higher transformation yield stress in compression as compared to the yield stress in tension for CeO_2–TZP as reported previously [10, 15].

Further bending of the beam specimen beyond the yield point increased the surface width and depth of the transformation band. This increase of the width of the transformation band at the centre of the specimen (referred to as the primary band) as a function of the strain is also plotted in Fig. 1. The primary band width increased linearly with strain up to the maximum load corresponding to a nominal stress of about 319 MPa. Figs 3a and b show the primary transformation band at the maximum load. In addition, secondary transformation bands nucleated and grew on either side of the primary band. The stress–strain curve corresponding to the growth of the bands showed a monotonic increase of stress with decreasing work-hardening rate. Typically, in three-point bending, five independent transformation bands were observed to nucleate and grow during the inelastic bending stage.

At the maximum load, a surface crack nucleated within the primary transformation band (see Fig. 4). The surface crack extended stably beyond the maximum load until the final fracture load, which corresponds to unstable fast propagation of the surface crack. The stable growth of the surface crack was a manifestation of a rising crack-growth-resistance behaviour of the CeO_2–TZP. In the regime of surface crack nucleation and growth, the width of the primary transformation band increased much more slowly and appeared to approach a saturation width (see Fig. 1).

3.2. Effect of grain size on transformation yield stress and plasticity

Fig. 5 shows the stress–strain curves corresponding to

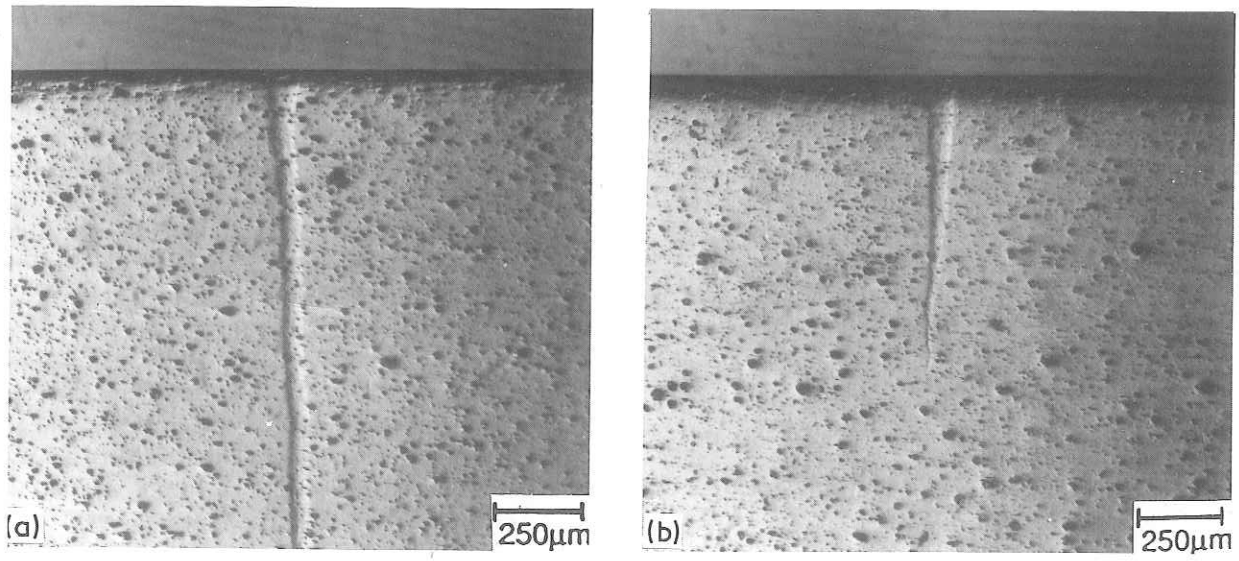

Figure 2 Primary transformation band on (a) the tension surface and (b) on the side surface of a three-point bend specimen of CeO_2TZP (Type IIA) at yield point (σ_y = 245 MPa).

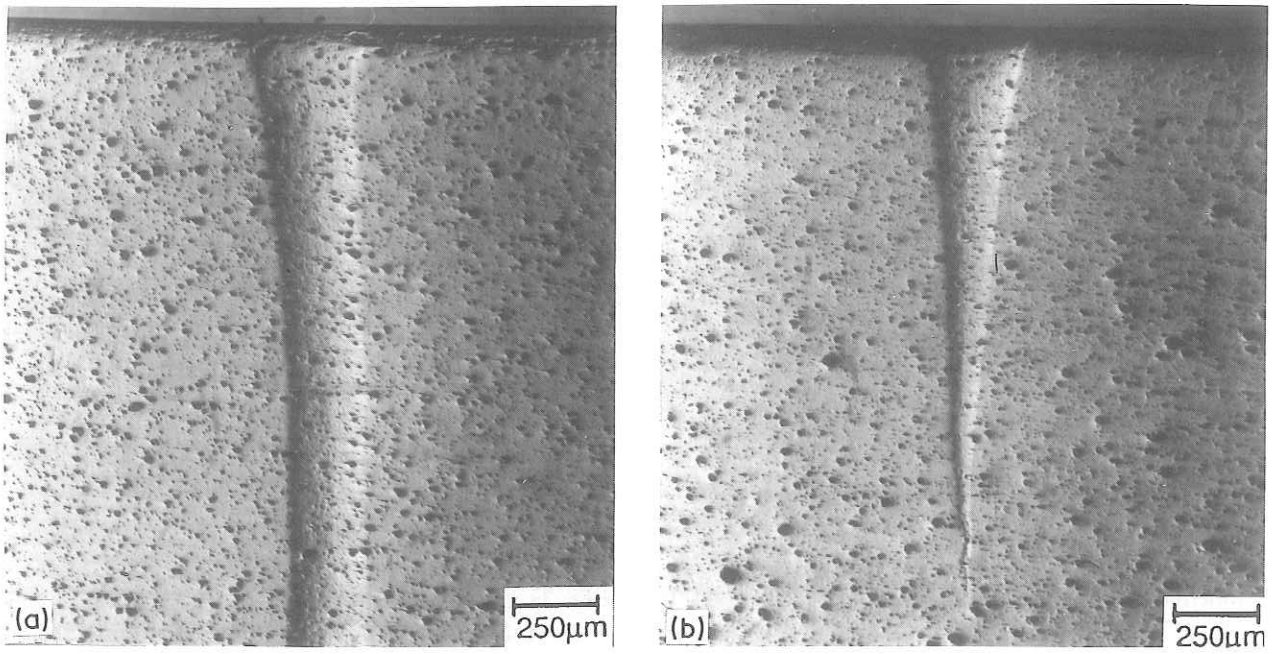

Figure 3 Primary transformation band on (a) the tension surface and (b) on the side surface of the three-point bend specimen of CeO_2TZP (Type IIA) at the maximum stress point (σ = 319 MPa).

the six different types of CeO_2–TZP designated IA, IIAA, IIA, IIB, IIC and IID. The only significant difference among these types was the average grain size (see Table I) and the grain size distribution. Small differences in grain size produced significant differences in both the transformation yield stress and the total strain to fracture. The yield stress increased from 176 to 390 MPa and the total strain to fracture decreased from 1.2% to 0.22% with a decrease in grain size from 2.18 to 1.47 μm. It is intriguing to note that these large differences in the yield stresses and the total strains to fracture occur among the six types despite the fact that volume fractions of the tetragonal phase in both sintered materials and on their fracture surfaces are not very different.

Fig. 6 shows a plot of the transformation yield stress as a function of the average grain size of the zirconia grains. The decrease of the yield stress with increase in the average grain size in Fig. 6 could be adequately described by the following equation

$$\sigma_y = A + \frac{B}{\bar{d}} \quad (1)$$

where σ_y is the yield stress defined as the elastic stress corresponding to the initial transformation burst and $\bar{d}$ is the average grain size. Optimum values for the two constants in the equation determined by regression analysis were $A = -275$ MPa and $B = 952$ MPa μm. Extrapolation based on Equation 1 suggests a critical average grain size of approximately 3.5 μm at which the yield stress would approach zero. The physical basis for choosing the inverse grain size dependence for the transformation yield stress will be discussed in a later section. The compressive yield stress versus the martensitic burst temperature (M_b) correlation established by Reyes-Morel and Chen [15] for different grades of CeO_2–TZP is also a similar manifestation of the grain size influence on transformation yield stress because compositions of the different CeO_2–TZPs were presumably the same.

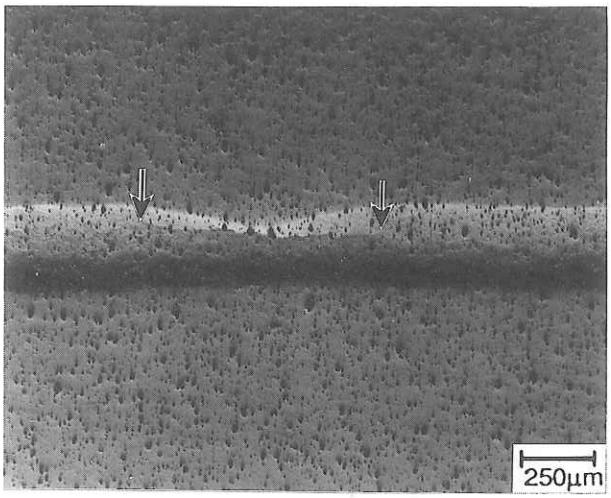

Figure 4 Surface crack within the primary transformation band in the three-point bend specimen of CeO_2TZP (Type IIA).

3.3. Effect of yield stress on crack-tip transformation zone size and crack-growth-resistance behaviour of CeO_2–TZP

Fig. 7 shows plots of the fracture toughness as functions of the normalized crack length, i.e. R-curves, for four types of CeO_2–TZPs. For all the four materials, the R-curves were measured in approximately the same crack-length range, $a/W \sim 0.2$ to 0.35. This relatively short crack length range was used to ensure sufficient elastic ligament length beyond the crack tip and the transformation zone as required by ASTM E-399 [14]. The most noteworthy result in Fig. 7 is that the R-curves for the four different types of CeO_2–TZPs are very similar. A significant amount of the fracture toughness increment was associated with increase in the size of the crack-tip transformation zone without

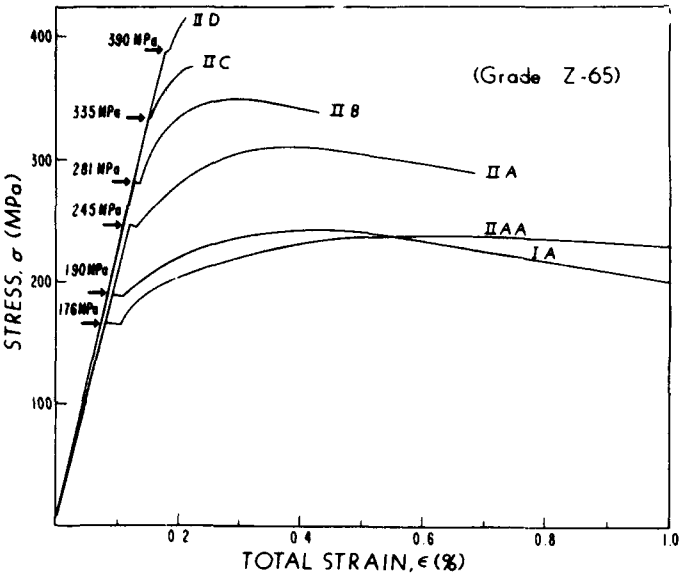

Figure 5 Stress–strain curves for six types of CeO_2TZP obtained in three-point bending.

a concurrent increase in the crack length. Beyond this stationary crack regime, the fracture toughness increased with increasing crack lengths and reached a maximum value in the range 12 to 14 MPa $m^{1/2}$. The R-curve did not show evidence of a saturation fracture toughness; instability set in when the fracture toughness was still increasing.

The similarity of the R-curves was particularly intriguing in view of the fact that crack-tip transformation zone sizes were significantly different for the four different CeO_2–TZP materials. Fig. 8 shows the transformation zones in the different CeO_2–TZPs at an applied stress intensity of 10 MPa $m^{1/2}$. The shapes of the transformation zones were similar, but the relative sizes were very different. Table II summarizes the characteristic dimensions of the transformation zones, length l, and width, w (see Fig. 8e for their definition) for the four materials at different applied stress intensities. The maximum transformation zone width measured for the type IA CeO_2–TZP ($w_{max} \sim 340\,\mu m$) was about seven times the maximum zone width in the type IIC material ($w_{max} \sim 50\,\mu m$). Despite this large difference in the transformation zone widths, the R-curves and the maximum fracture toughness observed for these two CeO_2–TZPs were nearly identical.

3.4. Analysis of the R-curves in terms of crack-shielding models

The major objective of this study was to examine the effect of the varying yield stress on the crack-tip transformation zone size and the R-curve behaviour and compare the results to crack-shielding and plastic strip-zone models. According to the crack-shielding models of transformation toughening, the crack-tip transformation zone width, w, and the extent of

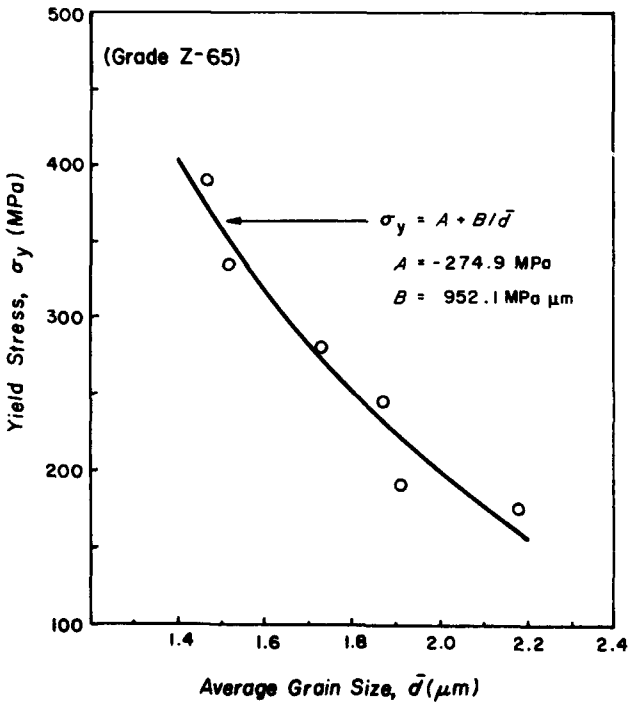

Figure 6 Variation of the transformation yield stress with average grain size for the six different types of CeO_2TZP.

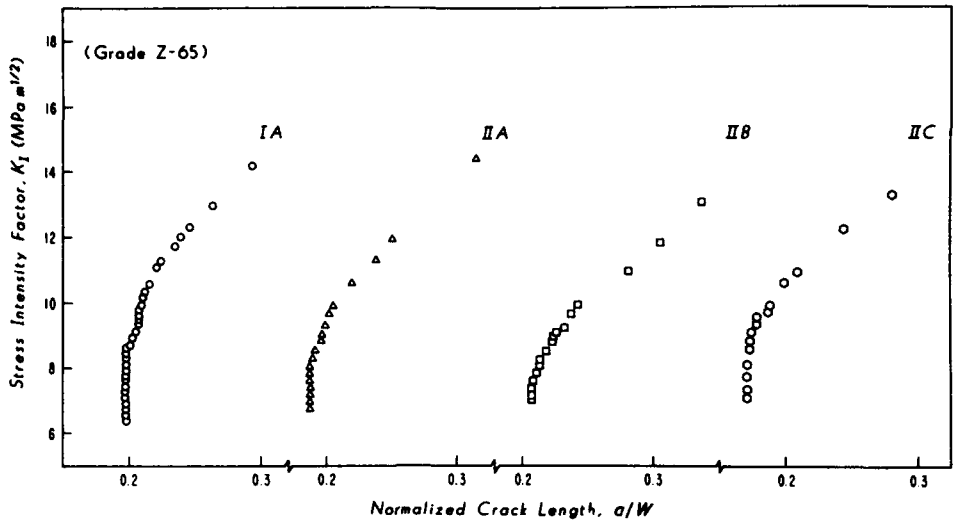

Figure 7 Crack-growth-resistance curves (R-curves) for the four types of CeO_2–TZP assessed in single-edge-notch-bend tests.

crack growth into the transformed zone, Δa, to form a transformation wake behind the crack-tip, are important parameters (among others) that determine the degree of toughening and the R-curve behaviour. The model of McMeeking and Evans [1], for example, gives the following equation for the toughness increment, ΔK_I, as a function of the normalized crack length increment, $\Delta a/w$

$$\Delta K_I = \frac{Ee^T V_f w^{1/2}}{(1-\nu)} \kappa\left(\frac{\Delta a}{w}, \nu\right) \quad (2)$$

where E is the elastic modulus of the matrix containing the zirconia particles, e^T the transformation strain, V_f the volume fraction of transformed zirconia particles, ν Poisson's ratio, and $\kappa(\Delta a/w, \nu)$ is a function whose value increases with relative crack extension and approaches an asymptotic value at $\Delta a \sim 5w$. The function κ, in effect, describes the R-curve behaviour. The magnitude of the asymptotic value is 0.215 according to the model of McMeeking and Evans [1], who considered only the dilatational component of the transformation strain. Lambropoulos [3] has proposed a model that includes both shear and dilatational strain contributions during nucleation and the predicted asymptotic value for κ in his model is 0.55 $(1-\nu)$. Swain [6] and Swain and Rose [7] have shown that measurements of the saturation fracture toughness and the zone size in Y_2O_3–TZP and MgO–PSZ ceramics are in good agreement with the above models, respectively.

Fig. 9 compares the R-curves measured for the four types of CeO_2–TZP with the prediction of the crack-shielding model of McMeeking and Evans [1]. To calculate the stress-intensity increment, ΔK_I, from the measured stress intensity at various crack lengths, a baseline fracture toughness, $K_{Ic}^M = 3.0\,\text{MPa m}^{1/2}$, was assumed for the predominantly monoclinic zirconia material in the immediate neighbourhood of the crack tip. In addition, to plot the experimental data in the same form as the theory, the following values were assumed for the constant parameters: $\nu = 0.3$, $E = 200\,\text{GPa}$, $e^T = 0.05$ and $V_f = 0.8$. Of these parameters, only the volume fraction of the transformed tetragonal zirconia in the transformation zone, V_f (assumed to be equal to the difference between the tetragonal contents of the as-sintered ceramic and the fracture surface) is likely to vary among the four types of CeO_2–TZP. The accuracy of the measurements of the tetragonal content, particularly on the fracture surface, was such that no significance could be attached to the small differences observed among the four types of zirconia. For this reason, a common value, $V_f = 0.8$, was used in the comparison in Fig. 9.

Fig. 9 shows that experimentally measured fracture toughness increments from the transformation zones are less than the prediction of the McMeeking and Evans model [1]. Type IA CeO_2–TZP, which exhibited the lowest yield stress and correspondingly the largest transformation zone, showed the maximum deviation from the theory. The fracture toughness of type IIC CeO_2–TZP was closest to the theory, but even here the discrepancy was greater than a factor of 2. In addition to this quantitative difference in the fracture toughness increments, there were several other important

TABLE II Transformation zone dimensions and stable crack extension in single edge notch beam specimens of CeO_2–TZPs

K_I (MPa m$^{1/2}$)	IA			IIA			IIB			IIC		
	w (μm)	l (μm)	Δa (μm)	w (μm)	l (μm)	Δa (μm)	w (μm)	l (μm)	Δa (μm)	w (μm)	l (μm)	Δa (μm)
7.0	41	437	0	19	130	0	19	154	0	11	79	0
8.0	81	897	0	48	486	0	33	328	70	28	221	0
9.0	125	1580	92	66	702	129	46	527	298	33	288	32
9.9	166	1961	181	87	1018	284	53	641	562	49	416	270
13.0	308	3277	1030				56	551	2083	32	305	1697

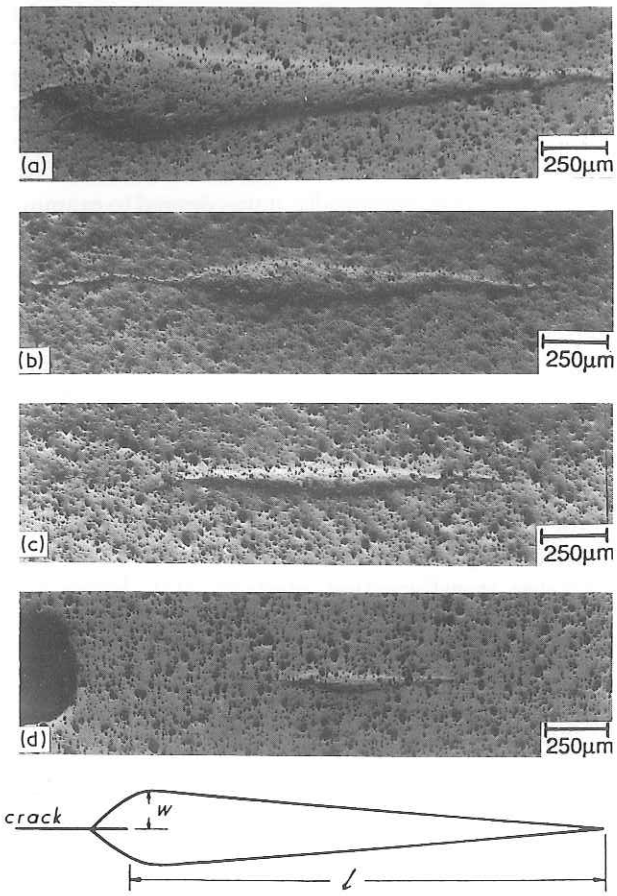

Figure 8 Crack-tip transformation zones in single-edge-notch-bend specimens of the four types of CeO_2TZP at $K_I = 10\,MPa\,m^{1/2}$: (a) type IA, (b) type IIA, (c) type IIB and (d) type IIC. (e) Schematic drawing of the transformation zone used for definition.

differences between the experimental results and the assumptions of the theoretical model. Thus, for example, in the theoretical model all of the fracture toughness increment occurs in conjuction with an increase in the crack length; in other words fracture toughness increase in crack shielding occurs only when the transformation wake builds behind the advancing crack tip. In contrast, experiments indicated that a significant fraction of the fracture toughness increase was associated with stationary crack; i.e. fracture toughness increased with increase in the size of the transformation zone without a concurrent increase in the crack length (see Table II). Secondly, the theory assumes a constant zone width, w, dictated by the transformation yield stress as the crack advances. Experiments indicated that the zone width increased with increasing crack lengths (see Table II), particularly for the low yield stress materials. The zone widths identified in Fig. 9 are the specific values at the indicated crack length increments and they are close to the final values at instability. Finally, in the theory, fracture toughness increment saturates at $\Delta a/w \sim 5$, while the experimental R-curves showed rising fracture toughness up until the point of instability. It is interesting to note in Fig. 9 that the experimental plots of the normalized fracture toughness increments, ΔK_I, show constant plateau values in the entire range of crack lengths. This is a consequence of the fact that fracture toughness of CeO_2–TZP materials typically scale with $w^{1/2}$ during a significant part of the rising R-curve behaviour. Yu and Shetty [10] have shown that this is a general consequence of the growth of the transformation zone of the same shape.

One obvious difference between the experimental results and the theoretical expectation based on fracture mechanics analysis is the shape of the transformation zones at crack tips in CeO_2–TZP materials. Yu and Shetty [10] and Rose and Swain [11] have addressed this issue in detail. The observed transformation zones are thin, elongated strips, while theoretical calculations predict more circular zones. In fact, it is this zone shape which prompted an analysis of the zone length in terms of the plastic strip zone model of Dugdale [16]. In the following paragraphs, transformation zone lengths observed in the four types of CeO_2–TZP are analysed using Dugdale's model.

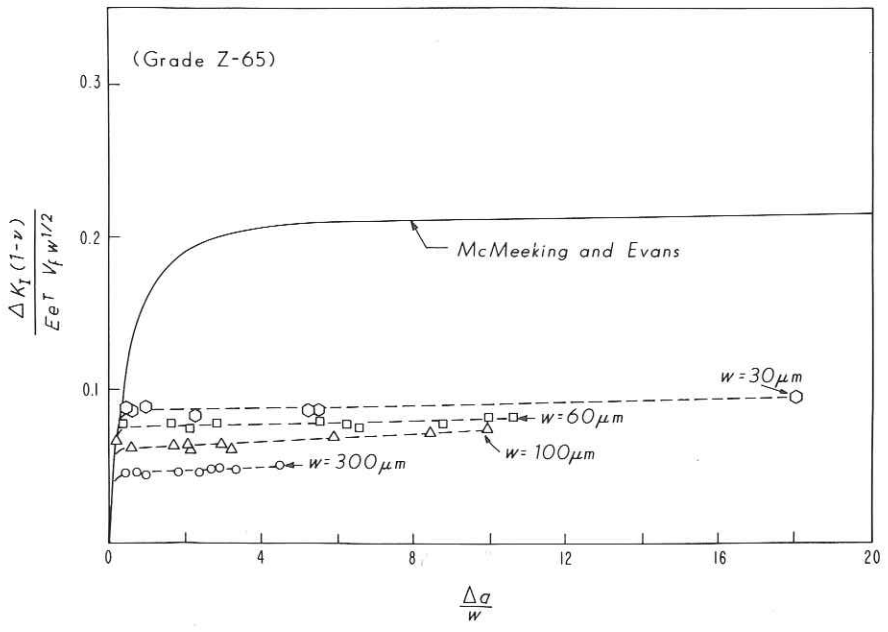

Figure 9 Comparison of R-curves measured for CeO_2–TZPs with the crack-shielding model of McMeeking and Evans [1], using single-edge-notch-bend tests.

3.5. Analysis of the transformation zone lengths in terms of the Dugdale plastic strip zone model

Dugdale [16] assumed that plasticity at a crack tip was concentrated in a strip in front of the crack. Further, the crack of length, a, with the plastic strip zone of length, l, was treated, in effect, as a crack of length $(a + l)$ in which crack closing traction of a magnitude equal to the yield stress was uniformly distributed in the strip zone. Finally, the crack-tip stress singularities from the remote stress and the crack-surface tractions were assumed to cancel to give a finite stress equal to the yield stress at the crack tip [17]. By rewriting the original Dugdale equation, which was developed for a centre-cracked panel under uniform tension, in terms of the elastic stress-intensity factor (assuming small-scale yielding condition prevails) for the single-edge-notch-beam specimen, we get the following equation for the transformation zone length ahead of the crack tip

$$\frac{l}{a + l} = 2 \sin^2 \left[\frac{\pi K_I^{eff}}{4\sigma_y [\pi(a + l)]^{1/2}} \right] \quad (3)$$

In Equation 3, K_I^{eff} is the stress intensity defined in terms of the effective crack length, $(a + l)$ and σ_y is the yield stress measured in uniaxial tension. Plastic zone length measurements in thin sheets of mild steel by Dugdale [16] and in silicon steel by Hahn and Rosenfield [18] have been found to be in agreement with the above model.

Fig. 10 compares the transformation zone length measurements in the single-edge-notch-beam specimens of the four CeO_2–TZPs with the prediction of Equation 3. Transformation zone lengths (l), crack lengths (a) and the effective stress intensity (K_I^{eff}) at different stages of both the stationary (filled points) and the stably-growing crack (open points) were used to construct the experimental plot of Fig. 10. The yield stresses measured in three-point bending were used to normalize the stress-intensity factor on the right-hand side of Equation 3. Fig. 10 shows that the zone length measurements in the CeO_2–TZPs are in good agreement with the Dugdale model.

4. Discussion

An attempt has been made in this study to vary systematically the transformation yield stress and plasticity in a commercial-grade CeO_2–TZP ceramic by varying the sintering temperature and the resulting grain-size distribution. The objective was to study the effect of the varying yield stress on the crack-tip transformation zone sizes, shapes and the R-curve behaviours. More specifically, it was desired to examine quantitatively the dependence of the fracture toughness increments during stable crack growth on the growth and size of the crack-tip transformation zones. Polycrystalline zirconia, partially stabilized with 12 mol % CeO_2, is particularly well-suited for this purpose because transformation zones are readily observed in the material using an optical microscope and Nomarski interference contrast technique.

The trend of increasing yield stress with decreasing grain size observed for CeO_2–TZP in this study is consistent with the essential characteristics of stress-activated transformation plasticity [15]. Below the tetragonal–monoclinic equilibrium temperature, both increasing stress (hydrostatic tension and/or shear) and decreasing temperature promote the transformation of the metastable tetragonal phase to the monoclinic form. Further, as discussed by Heuer *et al.* [19], Garvie and Swain [20] and others (see the review by Evans and Cannon [21]), stability of the (metastable) tetragonal zirconia phase in ceramic matrices increases, i.e. M_s temperature decreases, with decreasing grain size. An inverse linear relationship between the critical grain size and the transformation temperature (M_s) is a natural consequence in an "end-point" energy balance analysis of stability involving volume-dependent energy terms (chemical free energy and strain energy) and surface-area-dependent energy terms (interfacial energy and twin-boundary energy) [20, 21]. Thus, the inverse dependence of the transformation yield stress on the grain size (Fig. 6 and Equation 1) can be viewed as a stress equivalence to the grain-size dependence of the transformation temperature, because the applied stress is introduced in the energy balance in terms of an interaction energy modifying the strain energy term [21]. It is also equivalent to the inverse correlation between the yield stress in compression and the spontaneous martensitic transformation temperature (M_b or M_s) established for

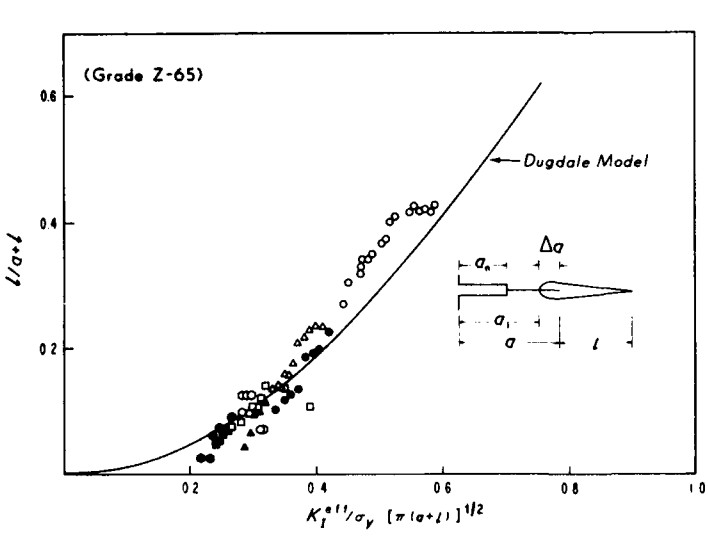

Figure 10 Comparison of the dependence of the transformation zone lengths on the applied stress intensity in CeO_2–TZPs with the Dugdale plastic strip zone model using single-edge-notch-bend tests. (●, ▲, ■, ●) Stationary cracks, (○, △, □, ○ stably extending cracks. (●, ○) IA, (▲, △) IIA, (■, □) IIB, (●, ○) IIC.

CeO_2–TZP ceramics by Reyes-Morel and Chen [15] because the M_s temperature is a measure of the stability of the tetragonal zirconia and it decreases with decreasing grain size. In this connection, the critical grain size suggested by Fig. 6 can be interpreted as the grain size of a CeO_2–TZP ceramic for which the M_s temperature is the room temperature. The interrelationship between temperature, applied stress and grain size that defines the condition for transformation has been addressed by many investigators and it has been reviewed recently by Evans and Cannon [21].

The second aspect of the transformation yielding and plasticity of CeO_2–TZP observed in the present study is the discrete nature of the transformation bands analogous to Luders bands in steels. Reyes-Morel and Chen [15] have also observed such localized transformation bands in both compression and bend specimens. From a purely end-point thermodynamics point of view as discussed above, transformation should start with the largest grains in the body and it should extend to smaller and smaller grains with increasing stress. Correspondingly, the stress–strain curve should show a gradual transition from elastic to plastic behaviour and at least in the initial stages of deformation it should be confined to isolated grains. The instantaneous formation of a transformation band of macroscopic dimensions suggests that transformation in CeO_2–TZP is a cooperative phenomenon. Grains adjacent to an already transformed grain are favoured over other isolated grains. Reyes-Morel and Chen [15] attribute this to multiple-site nucleation and call the process autocatalysis. It is interesting to note several aspects of the band formation in three-point bend specimens. Invariably, two bands nucleate at the specimen edges, propagate toward each other rapidly and join to form a single band whose length equals the bend specimen width. Secondly, once nucleated, the band grows much more easily in the depth direction than along the axial direction on the tension surface (see Figs 2 and 3). This result is despite the fact that stress gradient is much more severe in a direction perpendicular to the neutral axis than along a direction parallel to the neutral axis and on the tension surface. First, it was thought that shear stress in the beam, which is zero at the surface and increases toward the neutral axis, was responsible for this elongated zone depth. However, depth of the wedge-shaped zone in the centre span section of four-point bend specimens (where the shear stress is zero) was not significantly different from that in three-point bend specimens. Therefore, reason for the more pronounced growth of the transformation band in the thickness direction is not known.

The most significant result of this study is the relative insensitivity of the crack-growth-resistance curves to the varying yield stress and the size of the crack-tip transformation zones. This has two consequences when we compare the measured fracture toughness increments with the prediction of the crack-shielding model of McMeeking and Evans [1]. First, the fracture toughness increments measured for all the four types of CeO_2–TZP are lower than the predictions of the model (see Fig. 9). Secondly, CeO_2–TZPs with the lower yield stresses (and correspondingly larger transformation zone sizes) show greater deviation from the model prediction than the higher yield stress grades.

In the above comparison, three material parameters, which affect the normalized fracture toughness increment plotted in Fig. 9, are subject to error. These are volume fraction of transformed tetragonal phase, V_f, intrinsic fracture toughness of the transformed zone material, K_{Ic}^M and the transformation zone width, w. The value used for V_f (0.8) was based on X-ray diffraction analyses of the fracture surface and the initial sintered ceramic. The measurement on the fracture surface is subject to an error of at least 10%. In addition, fracture surface measurement gives a measure of V_f in the middle of the transformation zone. It is possible that V_f decreases within the transformation zone at locations away from the fracture surface. If this situation exists in CeO_2–TZP, then, the assumed value for V_f, which should be an average value to correspond with the assumption of the model, would be an overestimate. A smaller average value of V_f would shift the experimental points in Fig. 9 closer to the prediction of McMeeking and Evans [1]. A technique other than X-ray diffraction would be required to assess such local variations in V_f. The ΔK_I values plotted in Fig. 9 were based on an assumed fracture toughness, $K_{Ic}^M = 3\,\text{MPa m}^{1/2}$, for the transformed material in the neighbourhood of the crack tip. This is a conservatively low value and is comparable to the fracture toughness of monoclinic Y_2O_3–TZP [22]. It is unlikely that significant error was introduced in the choice of this value. The measured values of w can be in error if the measurements of the zone width on the specimen surface, where plane stress condition prevails, are not representative of the bulk of the specimens subjected to plane strain condition. To answer this question, a number of single-edge-notch-beam specimens were cut normal to the crack on a plane coinciding with the maximum width of the transformation zone. The as-cut surfaces were gently ground and polished. The transformation zones could be detected on the polished cross-section and the zone widths were found to be essentially uniform through the thickness of the SENB specimens. Thus, surface measurements of zone widths are representative of the bulk of the specimens and error in w is not likely to have caused the discrepancy in Fig. 9.

The similarity of the R-curves for the four different CeO_2–TZPs, despite the differences in their zone sizes, suggests that the transformation zones in the four types of materials do not behave the same way in terms of crack shielding. The larger zones in the lower yield stress materials are counteracted by a secondary factor to obtain a similar degree of crack shielding. Variations in V_f or different degrees of microcracking within the transformation zones are possible candidates for equalizing the crack-shielding effect for different zone sizes.

The agreement obtained between the Dugdale strip zone model and the experimental measurements in Fig. 10 is similar to our earlier result on type

IA material [10]. It is interesting to note that zone lengths in all the four types of CeO_2–TZPs superpose adequately on a single plot close to the prediction of the Dugdale model. The agreement with the Dugdale model is obtained both in the regime of the stationary crack (filled points in Fig. 10) as well as the stably growing crack (open points in Fig. 10). This result is, in one sense, not surprising because the Dugdale model, in essence, postulates a plastic zone in the shape of a thin strip ahead of the crack tip, a situation closely followed by the transformation zone in CeO_2–TZP. In another sense, however, the result is surprising. The original experiments of Dugdale [17] as well as the subsequent studies of Hahn and Rosenfield [19] have shown that in metals the Dugdale model is obeyed in thin sheets where the plastic zones are comparable to the thickness of the sheet. In contrast, the present measurements on CeO_2–TZP were on thick specimens where the specimen thickness was considerably greater than the zone size. It is this question which prompted the query about the possible difference between the transformation zones on the surface and in the bulk.

Although the original Dugdale model accounts for the length of the transformation zones in CeO_2–TZP, it is, in itself, not a substitute for transformation toughening models such as the crack shielding model. However, the Dugdale model can be adapted to include a failure criterion (such as, for example, a critical crack opening displacement) and, thus, model the saturation fracture toughness as has been done by Hahn and Rosenfield [19] and, more recently, Rose and Swain [11]. Such models have not been explicitly developed, however, to explain the rising crack-growth-resistance behaviour.

A final point concerns the R-curve behaviour pertinent to the surface cracks developed within the transformation band in the three-point bend specimens (see Fig. 4). The stable growth of the surface crack following its nucleation suggests a rising crack-growth-resistance. The R-curve behaviour corresponding to the surface crack was assessed by measuring the surface dimension of the crack, $2c$, at different loads during bending. The stress-intensity factor, K_I, for the surface crack was calculated at different stages of the stable growth by assuming a semicircular shape (radius, c) and using the following equation [23]

$$K_I = 2\sigma_b \left(\frac{c}{\pi}\right)^{1/2} F \qquad (4)$$

where σ_b is the bending stress and F is a nondimensional stress-intensity coefficient dependent on the location on the crack front and the size of the crack relative to the beam dimensions. Numerical results for F reported by Newman and Raju [23] were used to calculate stress-intensity factors at both the intersection point of the crack front with tension surface ($\phi = 0$) as well as the deepest point of the crack ($\phi = \pi/2$). The R-curves for the surface crack calculated using Equation 4 at the two crack-front locations are compared with the R-curve measured using the single-edge-notch-beam specimen in Fig. 11. It should be noted that in plotting the R-curve for the single-edge-notch-beam specimen stress-intensity is plotted as a function of the increment crack extension (Δa), while the R-curves for the surface crack are plots of K_I against c, the radius of the surface crack. There are two interesting results in Fig. 11. First, stress-intensity factors for the surface crack are significantly different at the surface point and in the interior. This is due to the assumption of a semicircular shape for the surface crack. When the size of the semicircular crack becomes a significant fraction of the bend specimen size, stress-intensity differences increase as a result of the stress gradient. In reality, crack shape may be closer to a semiellipse than a semicircle. For this case, stress-intensity would be more uniform along the crack front and in between the two extreme cases plotted in Fig. 11.

A second more interesting result in Fig. 11 is the difference between the R-curves for the surface cracks and the R-curve obtained with the single-edge-notch-

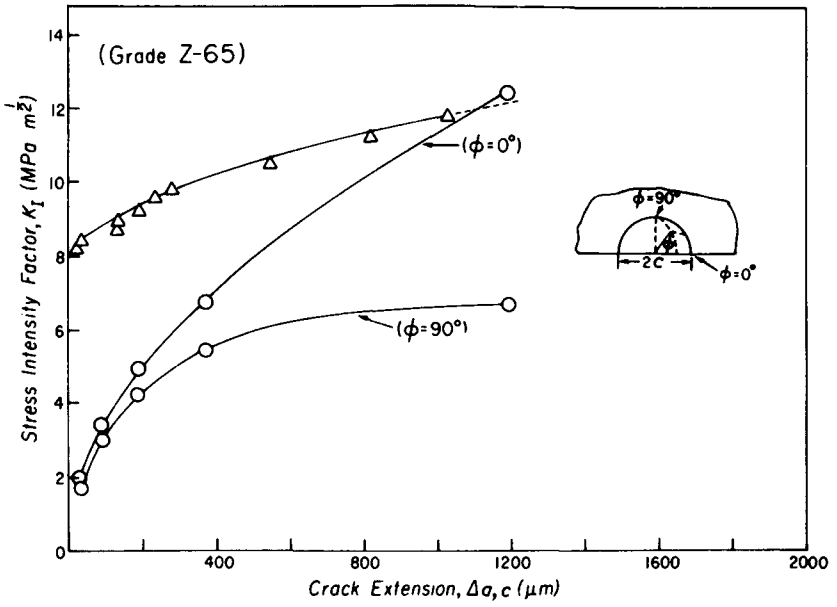

Figure 11 Comparison of the R-curve for CeO_2-TZP type IIA for a surface crack in (○) three-point-bend specimen with that obtained in (△) single-edge-notch-bend specimen: surface crack = c, edge crack = Δa.

beam specimen, particularly at small crack sizes. Similar differences have been observed in alumina [24] and MgO–PSZ [25]. The origin of the difference between the two R-curves in the case of the CeO_2–TZP is not completely clear. But there is an intrinsic difference in the relative scale and extent of the transformation zones in the two crack geometries. In the case of the single-edge-notch-beam specimen, the transformation zone is localized at the crack tip and the zone dimension is much smaller than the crack and specimen dimension. In the case of the surface crack, the crack nucleates and extends in an existing transformation band, in a manner analogous to nucleation of fatigue cracks in persistent slip bands in metals [26]. The crack-shielding effect of the transformation zones in the two crack geometries appears to be different.

5. Conclusions

1. Transformation yield stress of CeO_2–TZP measured in three-point bending increases systematically with decreasing grain size, consistent with the essential characteristics of stress-assisted transformation plasticity and the increased stability of the smaller grains.

2. The instantaneous nucleation and growth of the discrete, wedge-shaped transformation band in CeO_2–TZP suggests that transformation of grains is a cooperative phenomenon. A distinct yield stress, a yield stress plateau in strain and increasing band width and crack-tip zone sizes with decreasing yield stress are other important characteristics of transformation plasticity of CeO_2–TZP in three-point bending.

3. Significant differences in the crack-tip transformation zone sizes are observed in CeO_2–TZPs of varying yield stresses. However, R-curves measured for the different materials are not significantly different, thus suggesting that efficiency of crack-shielding apparently decreases with increasing zone size.

4. Crack-shielding models overestimate the fracture toughness increments for CeO_2–TZP based on the measured transformation zone widths. The discrepancy is greater for lower yield stress grades.

5. Dugdale's plastic strip zone model accounts properly for the transformation zone length as a function of the elastic stress-intensity factor. But the model needs further modification to account for the crack-growth-resistance behaviour.

6. R-curves estimated for surface cracks in the bend specimens differ significantly from the R-curve obtained in single-edge-notch-beam specimens, especially at small crack lengths. Differences are attributed to the different scale and extent of the transformation zones around the respective cracks and the different crack-shielding effects generated by them.

Acknowledgements

The paper is based on research supported by the Army Research Office under contract DAAL03-87-0060 at the University of Utah.

References

1. R. M. McMEEKING and A. G. EVANS, *J. Amer. Ceram. Soc.* **65** (1982) 242.
2. B. BUDIANSKY, J. W. HUTCHINSON and J. C. LAMBROPOULOS, *Int. J. Solids Structures* **19** (1983) 337.
3. J. C. LAMBROPOULOS, *J. Amer. Ceram. Soc.* **69** (1986) 218.
4. M. V. SWAIN and R. H. J. HANNINK, "R-Curve Behavior in Zirconia Ceramics", in "Science and Technology of Zirconia II", Advances in Ceramics, Vol. 12, edited by N. Claussen, M. Ruhle and A. H. Heuer (The American Ceramic Society, Westerville, Ohio, 1984) pp. 225–39.
5. D. B. MARSHALL and M. V. SWAIN, *J. Amer. Ceram. Soc.* **71** (1988) 399.
6. M. V. SWAIN, *Acta. Metall.* **33** (1985) 2083.
7. M. V. SWAIN and L. R. F. ROSE, *J. Amer. Ceram. Soc.* **69** (1986) 511.
8. R. C. GARVIE, R. H. J. HANNINK and M. V. SWAIN, *J. Mater. Sci. Lett.* **1** (1982) 437.
9. T. KOSMAC, R. WAGNER and N. CLAUSSEN, *J. Amer. Ceram. Soc.* **64** (1981) C-72.
10. C. S. YU and D. K. SHETTY, *ibid.* **72** (1989) 921.
11. L. R. F. ROSE and M. V. SWAIN, *Acta. Metall.* **36** (1988) 955.
12. H. TORAYA, M. YOSHIMURA and S. SOMIYA, *J. Amer. Ceram. Soc.* **71** (1988) 343.
13. MLD-STD-1942 (MR), "Flexural Strength of High Performance Ceramics at Ambient Temperature", November (1983).
14. ASTM E 399-83, "Standard Test Method for Plane Strain Fracture Toughness of Metallic Materials", Annual Book of ASTM Standards, Section 3, Vol. 03.01 (American Society for Testing and Materials, Philadelphia, 1984).
15. P. E. REYES-MOREL and I-WEI CHEN, *J. Amer. Ceram. Soc.* **71** (1988) 343.
16. D. S. DUGDALE, *J. Mech. Phys. Solids* **8** (1960) 100.
17. H. L. EWALDS and R. J. H. WANHILL, "Fracture Mechanics" (Edward Arnold, London, 1984) pp. 60–61.
18. G. T. HAHN and A. R. ROSENFIELD, *Acta Metall.* **13** (1965) 293.
19. A. H. HEUER, N. CLAUSSEN, W. M. KRIVEN and M. RUHLE, *J. Amer. Ceram. Soc.* **65** (1982) 642.
20. R. C. GARVIE and M. V. SWAIN, *J. Mater. Sci.* **20** (1985) 1193.
21. A. G. EVANS and R. M. CANNON, *Acta Metall.* **34** (1986) 761.
22 T. SAKUMA, Y. YOSHIZAWA and H. SUTO, *J. Mater. Sci.* **20** (1985) 2399.
23. J. C. NEWMAN Jr and I. S. RAJU, *Engng. Fract. Mech.* **15** (1981) 185.
24. R. W. STEINBRECH and O. SCHMENKEL, *J. Amer. Ceram. Soc.* **71** (1988) C-271.
25. D. B. MARSHALL and M. V. SWAIN, *J. Amer. Ceram. Soc.* **71** (1988) 399.
26. L. M. BROWN and S. L. OGIN, in "Fundamentals of Deformation and Fracture", The Eshelby Memorial Symposium, edited by B. A. Bilby, K. J. Miller and J. R. Willis (Cambridge University Press, 1985) pp. 501–29.

Received 16 January
and accepted 17 August 1989

Appendix D

Reprinted from the Journal of the American Ceramic Society, Vol. 74, No. 3, March 1991

Role of Autocatalytic Transformation in Zone Shape and Toughening of Ceria-Tetragonal-Zirconia-Alumina (Ce-TZP/Al_2O_3) Composites

Jing-Fong Tsai, Cheng-Sheng Yu, and Dinesh K. Shetty

journal

Reprinted from the Journal of the American Ceramic Society, Vol. 74, No. 3, March 1991

J. Am. Ceram. Soc., 74 [3] 678–81 (1991)

Role of Autocatalytic Transformation in Zone Shape and Toughening of Ceria–Tetragonal-Zirconia–Alumina (Ce-TZP/Al_2O_3) Composites

Jing-Fong Tsai,* Cheng-Sheng Yu,* and Dinesh K. Shetty*

Department of Materials Science and Engineering, University of Utah, Salt Lake City, Utah 84112

Stress–strain behaviors in three-point bending, transformation zones in single-edge-notch-bend specimens, and transformation toughening were studied in two types of Ce-TZP/Al_2O_3 composites. A commercial grade exhibited yield-point behavior triggered by autocatalytic transformation and elongated zones. A new grade of Ce-TZP/Al_2O_3 composite showed monotonic stress–strain behavior and a zone shape close to theoretical prediction based on a shear–dilatation yield criterion. The effects of zone sizes and shapes on fracture toughness of the two ceramic composites are shown to be qualitatively consistent with the predictions of transformation-zone shielding theories. [Key words: zirconia: partially stabilized, ceria, phase transformation, stress, crack growth resistance.]

I. Introduction

RECENT studies of transformation zones in zirconia ceramics have shown an interesting anomaly. In magnesia-partially-stabilized zirconia (Mg-PSZ) ceramics, the transformation zone fronts ahead of the crack are found to be nearly semicircular.[1] Ceria–tetragonal-zirconia–alumina (Ce-TZP/Al_2O_3) composites, on the other hand, typically exhibit thin, elongated zones with zone lengths approximately 10 times the zone widths.[2–4] These zones resemble the Dugdale zones in thin plates of steels[5] or the craze zones in polymers.[6] The lengths of the transformation zones have been shown to follow the Dugdale strip zone model.[2–4]

The two classes of zirconia ceramics also exhibit interesting differences in their stress–strain behaviors. Mg-PSZ ceramics show a gradual transition from elastic to plastic behavior,[7,8] while Ce-TZP/Al_2O_3 composites exhibit burst transformation that results in a distinct yield point and localized transformation bands in bending.[3,9] This latter behavior has been characterized as autocatalytic transformation.[9] A potential link between autocatalytic transformation and the elongated zone shape in Ce-TZP/Al_2O_3 has been speculated,[10] but no direct evidence has been reported to date.

The present communication has two objectives. First, stress–strain behaviors and crack-tip transformation zones are compared for two grades of Ce-TZP/Al_2O_3 composites to examine the role of autocatalytic transformation. Second, the influences of the transformation zone shapes and sizes on the fracture toughness of the two Ce-TZP/Al_2O_3 composites are assessed using the transformation zone shielding model.

II. Ce-TZP/Al_2O_3 Composites and Test Procedures

(1) *Ce-TZP/Al_2O_3 Composites*

The two grades of Ce-TZP/Al_2O_3 composites investigated in this study are referred as types A and M. The composites were essentially 88 wt% of 12-mol%-CeO_2–ZrO_2 with 10 wt% of Al_2O_3 and 2 wt% of minor dopants. Yu and Shetty[2,3] and Wang *et al.*[11] have described in detail processing, microstructures, and properties of types A and M, respectively.

(2) *Mechanical Tests*

Stress–strain behaviors were characterized in three-point bending using 4 mm × 5 mm × 45 mm beam specimens and a 40-mm span. A strain gauge mounted on the tension face in the center of the span was used to measure total strain, i.e., elastic and inelastic strain. Transformation zones and *R*-curves were studied in precracked single-edge-notch-bend (SENB) specimens (support span, $S = 30$ mm, specimen width, $W = 8$ mm, and thickness, $B = 4$ mm). Shapes and sizes of transformation zones at crack tips and transformation plasticity on the tension surface of the three-point bend specimens were characterized by optical microscopy using Nomarski-interference contrast. The volume fraction of the transformed monoclinic phase in the transformation zones was estimated by Raman spectroscopy.

III. Experimental Results

(1) *Stress–Strain Behavior in Three-Point Bending*

Bending moment versus strain curves obtained in three-point bending are shown in Fig. 1. The apparent flexure stresses plotted are the nominal elastic bending stresses. A marked difference was observed in the stress–strain response of the two Ce-TZP/Al_2O_3 composites. Type A showed a yield-point behavior with a characteristic strain burst followed by a work-hardening regime. The apparent yield stress corresponding to the strain burst was 260 MPa. Type M showed a gradual transition from elastic to plastic behavior. Apparent yield stress, defined at an offset plastic strain of 0.1%, was 540 MPa.

(2) *Transformation Plasticity*

In addition to the distinctly different stress–strain responses, the two Ce-TZP/Al_2O_3 composites also showed characteristic differences in the nature and distribution of transformation plasticity. Type A exhibited a distinct wedge-shaped transformation band that covered the full width of the bend specimen.[3] The surface width, w, of the band increased linearly with strain from an initial width, w_i, corresponding to the end of the yield plateau ($w_i \approx 85$ μm) up to the maximum stress where the band width was 293 μm.[3] Beyond this point, the band width saturated as a surface crack

I-W. Chen—contributing editor

Manuscript No. 197658. Received April 9, 1990; approved January 3, 1991.
The research on type A material was supported by Army Research Office under Contract No. DAAL03-87-0060 at the University of Utah. Type M composite was developed in a research program supported by the U.S. Department of Energy under Contract No. De-FG02-87ER45312 at the University of Utah.
*Member, American Ceramic Society.

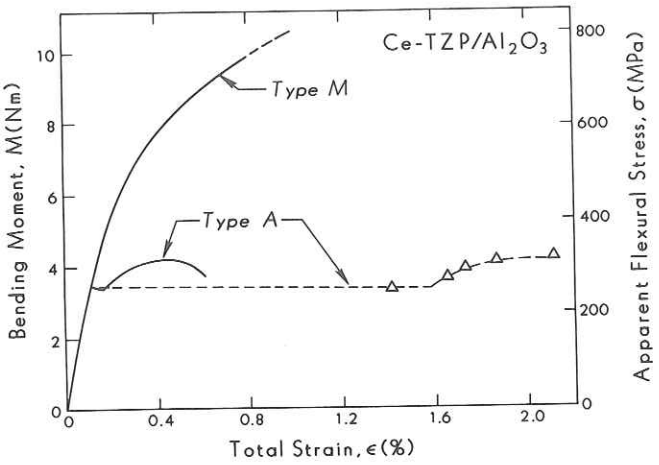

Fig. 1. Bending-moment (apparent flexure stress)–strain curves for type A and type M Ce-TZP/Al_2O_3 composites obtained in three-point bending.

initiated within the band and grew stably until instability set in at the fracture.

Since the gauge length of the strain gauge in the center of the specimen exceeded the width of the primary band, one can partition the measured total strain, ε_t, into two components; an elastic strain component, ε_e, outside the primary band and an elastic and plastic, ε_p, (i.e., transformation) strain component within the primary band as follows:

$$\varepsilon_t = \frac{w}{L}\varepsilon_p + \varepsilon_e \tag{1}$$

where L is the gauge length of the strain gauge. The three-point bend test on type A Ce-TZP/Al_2O_3 was interrupted periodically to measure the band width as a function of the strain, $w(\varepsilon_t)$. Equation (1) was then used to calculate ε_p for different values of ε_t and w with ε_e given by the elastic relation, $\varepsilon_e = \sigma_e/E$, where σ_e is the elastic bending stress and E is the Young's modulus. The discrete data points and the dashed line in Fig. 1 show the variation of this intrinsic inelastic strain within the primary transformation band.

In contrast to the discrete nature of transformation plasticity in type A, type M Ce-TZP/Al_2O_3 showed more uniformly distributed microbands of transformation over a distance of ≈12.5 mm on either side of the center of the specimen (see Ref. 11).

(3) Transformation Zone Shapes in SENB Specimens

Figures 2(A) and 3(A) show optical photographs of crack-tip transformation zones in SENB specimens of type A and type M composites, respectively, at an applied stress intensity of 10 MPa·$\sqrt{\text{m}}$. The arrow on the left in each case points to the initial crack-tip position corresponding to the precrack and the right arrow shows the extended crack tip. Figures 2(B) and 3(B) are the corresponding schematics of the zone boundaries with characteristic zone dimensions. Both the zone size and the zone shape are quite different in the two ceramics. Type A showed a relatively large zone that extended directly in front of the crack to a length roughly 10 times the zone width. Type M, on the other hand, showed a smaller, more equidimensional zone; i.e., zone length in front of the crack was comparable to the zone width.

(4) Crack-Growth-Resistance Curves

Both types of Ce-TZP/Al_2O_3 composites exhibited rising crack-growth-resistance, i.e., R-curve behavior. But there were some differences between the R-curves for the two materials. In type A material, crack growth initiated at a relatively low stress intensity, $K_I = 7.4$ MPa·$\sqrt{\text{m}}$, but toughness increased to 12.9 MPa·$\sqrt{\text{m}}$ over a crack extension,

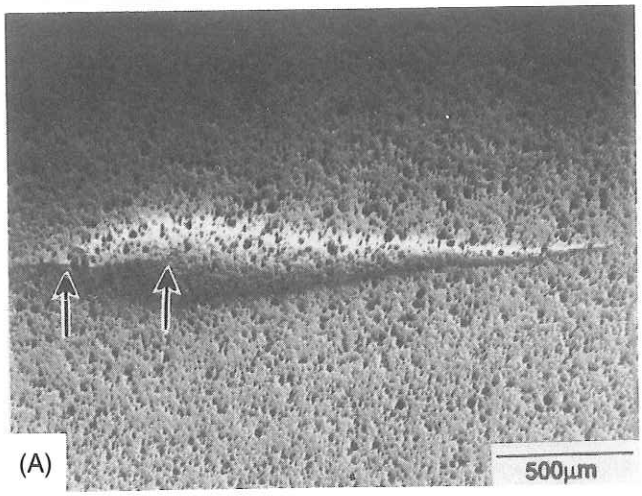

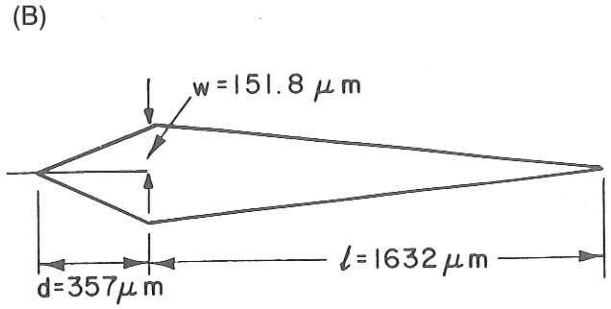

Fig. 2. (A) Transformation zone in SENB specimen of type A Ce-TZP/Al_2O_3 at $K_I = 10$ MPa·$\sqrt{\text{m}}$. (B) Schematic of the transformation zone and characteristic zone dimensions.

$\Delta a \approx 1200$ μm. In type M material, initiation fracture toughness was higher ($K_I = 8.6$ MPa·$\sqrt{\text{m}}$) but both stable crack extension ($\Delta a \approx 275$ μm) and the highest fracture toughness attained before instability ($K_I \approx 10.8$ MPa·$\sqrt{\text{m}}$) were lower.

IV. Discussion

The most interesting result of this study is the apparent link between the crack-tip transformation zone shape and the nature of the stress-induced transformation. A first-order approximation that gives a fairly accurate zone shape prediction (but not its absolute size) is based on using an applicable yield criterion for transformation yielding and the elastic stress distribution prior to transformation. Chen and Reyes-Morel[8,9] have shown that the following empirical equation adequately describes the shear and dilatation sensitivity of transformation yielding in both Mg-PSZ and Ce-TZP ceramics:

$$\frac{\sigma_e}{\sigma_e^*} + \frac{\sigma_m}{\sigma_m^*} = 1 \tag{2}$$

In Eq. (2) σ_e and σ_m are the equivalent stress and the mean hydrostatic stress, respectively, and σ_e^* and σ_m^* are the corresponding yield stress parameters. Yu and Shetty[2] have shown that the corresponding zone size and shape for a plane stress condition are given by the following equation:

$$r(\theta) = \left[\frac{2K_I\cos\frac{\theta}{2}}{3\sqrt{2\pi}\sigma_m^*} + \frac{K_I\cos\frac{\theta}{2}\left(1+3\sin^2\frac{\theta}{2}\right)^{1/2}}{\sqrt{2\pi}\sigma_e^*}\right] \tag{3}$$

The shape of the transformation zone predicted by Eq. (3) depends on the relative values of σ_m^* and σ_e^*. For $\sigma_m^* << \sigma_e^*$, i.e., dilatation-dominated yielding behavior, Eq. (3) predicts

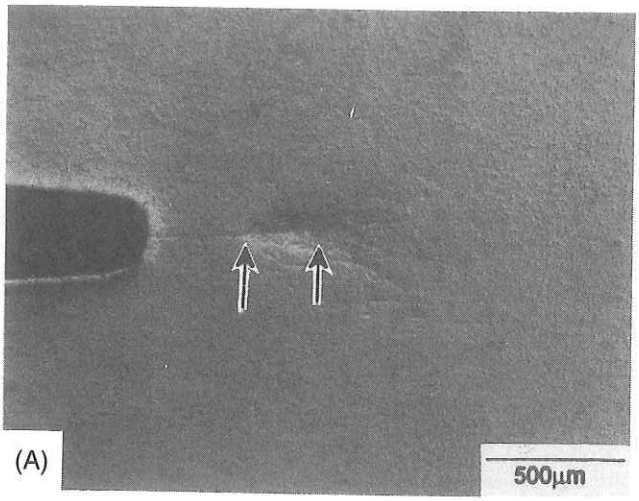

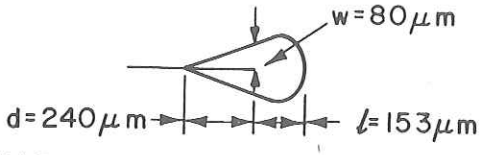

Fig. 3. (A) Transformation zone in SENB specimen of type M Ce-TZP/Al_2O_3 at an applied stress intensity, $K_I = 10$ MPa·$\sqrt{m}$. (B) Schematic of the transformation zone and characteristic zone dimensions.

a zone length in front of the crack tip ($r(\theta)$ for $\theta = 0°$) about 1.5 times the maximum zone width ($r(\theta)$ sin θ for $\theta = 60°$). For $\sigma_m^* >> \sigma_e^*$, i.e., shear-dominated yielding behavior, the zone length in front is 0.8 times the maximum zone width. For both Mg-PSZ and Ce-TZP/Al_2O_3 ceramics, transformation yield stress measurements in different stress states indicate $\sigma_m^* \approx 0.5\sigma_e^*$ to $1\sigma_e^*$ (Refs. 2, 8, 9) and the expected zone shapes should be in between the above limiting cases. The near equidimensional zone shape observed in type M Ce-TZP/Al_2O_3 is roughly in accord with this prediction.

It is not clear as yet why autocatalytic transformation leads to the elongated zone. One speculative hypothesis is that transformation zones produced by autocatalytic transformation combine the characteristics of both transformation and damage in the form of microcracks at grain boundaries and interfaces between zirconia and alumina grains. Observation of microcracks within the transformation zones in Ce-TZP[4] and observation of microcrack process zones of similar elongated shape in sandstone[12] support this hypothesis.

McMeeking and Evans[13] have developed a crack-shielding model that gives the following equation for the fracture-toughness increment, ΔK_S, due to the residual tractions on the transformation zone boundary and the crack faces:

$$\Delta K_S = \frac{e^T E V_f \sqrt{w}}{(l - \nu)} \kappa\left(\frac{l}{w}, \frac{d}{w}, \nu\right) \quad (4)$$

where e^T is the unconstrained transformation strain, E is the elastic modulus, V_f is the volume fraction of monoclinic phase in the zone, w is the zone width, l is the zone length ahead of the crack tip, d is the zone length behind the crack tip, and ν is Poisson's ratio. κ is a nondimensional stress-intensity coefficient that depends on the shape of the transformation zone both in front of the crack tip and behind. Recently, Marshall[14] calculated values of κ for the elongated zones observed in Ce-TZP and found their value to be much smaller than what was originally reported by McMeeking and Evans[13] for a steady-state zone based on a dilatational yield criterion. In the present study, it was of interest to see if a similar calculation of crack shielding could rationalize the effects of zone size and shape on the fracture toughness of the two grades of Ce-TZP/Al_2O_3 composites. The observed zone boundaries were approximated as shown in Figs. 2(B) and 3(B). In Fig. 3(B), the frontal-zone boundary was approximated as that corresponding to a dilatation yield criterion. The values of κ calculated using the weight-function method of McMeeking and Evans[13] were 0.062 and 0.134 for Ce-TZP/Al_2O_3 types A and M, respectively. Thus, the near-circular transformation zone of type M provides roughly twice the shielding as compared to the elongated zone of type A. The absolute magnitudes of the toughness increments depend on both the zone width (w) and the volume fraction of the transformed monoclinic phase (V_f). It is known that V_f typically has a maximum value at the crack tip and it decreases with distance from the tip.[1] These maximum values of V_f were determined by Raman microprobe analysis to be 0.76 and 0.53 for types A and M, respectively. These measurements, along with $E = 200$ GPa, $\nu = 0.3$, and $e^T = 0.04$, gave upper-bound estimates of $\Delta K_S = 6.62$ MPa·$\sqrt{m}$ and $\Delta K_S = 7.24$ MPa·$\sqrt{m}$ for types A and M, respectively. Thus, the high fracture toughness of type M material can be explained as being due to its more shielding-efficient zone shape, even though the zone size is much smaller and the volume fraction of the monoclinic phase is less than type A. It should be recognized, however, that these shielding calculations give only a qualitative rationalization of the relative toughness of the two zirconia ceramics. In absolute terms, the predicted toughness increments would be low if average monoclinic volume fractions within the zones are used in the calculations.

A final comment concerns the potential role of the microstructure of Ce-TZP/Al_2O_3, in particular, the size and concentration of the alumina particles, in promoting autocatalytic transformation. The microstructure of type A Ce-TZP/Al_2O_3 consisted of relatively small alumina particles ($\approx$0.5 μm) and their concentration was sufficiently high that, on an average, there was at least one alumina particle per grain of tetragonal zirconia. The type M composite had a smaller concentration of large tabular alumina grains. If the alumina–zirconia interfaces provide potent nucleation sites for martensitic transformation, a large concentration of small alumina particles might be more conducive to triggering autocatalytic transformation in adjacent grains than a smaller concentration of large alumina particles. The higher transformation temperature measured for the type A Ce-TZP/Al_2O_3 as compared to type M, despite its smaller zirconia grain size, also reflects this role of the microstructure in initiating the tetragonal to monoclinic transformation.

V. Conclusions

(1) Ce-TZP/Al_2O_3 composites that exhibit autocatalytic transformation also show elongated transformation zones, while those that exhibit monotonic transformation show more equidimensional zones consistent with shapes predicted from a combined shear–dilatation yield criterion.

(2) The relative fracture toughnesses of the two grades of Ce-TZP/Al_2O_3 composites are qualitatively consistent with the effects of zone size and shape on crack shielding. But the absolute magnitudes of predicted toughening are low as compared to the measurements.

References

[1]D. B. Marshall, M. C. Shaw, R. H. Dauskardt, R. O. Ritchie, M. J. Readey, and A. H. Heuer, "Crack-Tip Transformation Zones in Toughened Zirconia," *J. Am. Ceram. Soc.*, **73** [9] 2659–66 (1990).

[2]C-S. Yu and D. K. Shetty, "Transformation Zone Shape, Size, and Crack-

Growth-Resistance (*R*-Curve) Behavior of Ceria-Partially Stabilized Zirconia Polycrystals," *J. Am. Ceram. Soc.*, **72** [6] 921–28 (1989).

[3]C-S. Yu and D. K. Shetty, "Transformation Yielding, Plasticity, and Crack-Growth-Resistance (*R*-Curve) Behavior of CeO_2-TZP," *J. Mater. Sci.*, **25**, 2025–35 (1990).

[4]L. R. F. Rose and M.V. Swain, "Transformation Zone Shape in Ceria-Partially-Stabilized Zirconia," *Acta Metall.*, **36** [4] 955–62 (1988).

[5]D. S. Dugdale, "Yielding of Steel Sheets Containing Slits," *J. Mech. Phys. Solids*, **8**, 100–104 (1960).

[6]A. J. Kinloch, "Micromechanisms of Crack Extension in Polymers," *Met. Sci.*, **14** [8–9] 305–18 (1980).

[7]D. B. Marshall, "Strength Characteristics of Transformation-Toughened Zirconia," *J. Am. Ceram. Soc.*, **69** [3] 173–80 (1986).

[8]I-W. Chen and P. E. Reyes-Morel, "Implications of Transformation Plasticity in ZrO_2-Containing Ceramics: I, Shear and Dilatation Effects," *J. Am. Ceram. Soc.*, **69** [3] 181–89 (1986).

[9]P. E. Reyes-Morel and I-W. Chen, "Transformation Plasticity of CeO_2-Stabilized Tetragonal Zirconia Polycrystals: I, Stress Assistance and Autocatalysis," *J. Am. Ceram. Soc.*, **71** [5] 343–53 (1988).

[10]I-W. Chen, J. Pan, F. Li, and J. S. Cherng, "A Critical Assessment of Crack Tip Plastic Zone in Transformation Toughened Zirconia Ceramics"; presented at the 91st Annual Meeting of the American Ceramic Society, Indianapolis, IN, April 25, 1989 (Basic Science Division, Paper No.80-B-89).

[11]J-S. Wang, J-F. Tsai, D. K. Shetty, and A.V. Virkar, "Effect of MnO on the Microstructures, Phase Stability, and Mechanical Properties of Ceria-Partially-Stabilized Zirconia (Ce-TZP) and Ce-TZP–Al_2O_3 Composites," *J. Mater. Res.*, **5** [9] 1948–57 (1990).

[12]R. G. Hoagland, G.T. Hahn, and A. R. Rosenfield, "Influence of Microstructure on Fracture Propagation in Rock," *Rock Mech.*, **5**, 77–106 (1973).

[13]R. M. McMeeking and A. G. Evans, "Mechanics of Transformation Toughening in Brittle Materials," *J. Am. Ceram. Soc.*, **65** [5] 242–46 (1982).

[14]D. B. Marshall, "Crack Shielding in Ceria-Partially-Stabilized Zirconia," *J. Am. Ceram. Soc.*, **73** [10] 3119–21 (1990). □

journal

J. Am. Ceram. Soc., 75 [11] 2991–94 (1992)

Transformation Zone Shape Effects on Crack Shielding in Ceria-Partially-Stabilized Zirconia (Ce-TZP)–Alumina Composites

Cheng-Sheng Yu* and Dinesh K. Shetty*

Department of Materials Science and Engineering, University of Utah, Salt Lake City, Utah 84112

Michael C. Shaw* and David B. Marshall*

Rockwell International Science Center, Thousand Oaks, California 91360

Crack tip shielding is evaluated for observed transformation zones in Ce-TZP/Al_2O_3 composites, in which the transformation zone sizes were changed significantly by varying the sintering temperature to control the transformation yield stress. The calculated shielding effects are consistent with an observed insensitivity of crack resistance curves to transformation zone size; smaller zones in materials with higher yield stress were associated with larger ratios of wake length to zone width and correspondingly higher normalized shielding stress intensity factors. Shielding due to the dilatational component of the transformation strain accounted for most of the toughening observed in these materials.

I. Introduction

In a recent study, Yu and Shetty[1] measured crack resistance curves (*R*-curves) in a series of Ce-TZP/Al_2O_3 materials that had been sintered at various temperatures to vary the transformation yield stress within the range 190 to 390 MPa. The specimen geometry used for these measurements allowed stable crack growth for the initial, rising part of the resistance curve (typically for crack extensions of 1 to 2 mm). However, unstable crack growth occurred before reaching a steady-state toughness. The widths of the transformation zones at the instability points varied from ~30 μm in the material with the highest yield stress to 300 μm in the material with the lowest yield stress. Despite this large variation in zone size, the *R*-curves were almost the same in all of the materials, with instability occurring at an applied stress intensity factor of ~15 MPa·$m^{1/2}$.

Calculations of the crack tip shielding due to the observed transformation zones in the material with the lowest yield stress have shown that the measured stress intensity factors were consistent with most of the toughening being due to shielding associated with the dilatational component of the transformation strain.[2] In this paper we present more extensive calculations to investigate whether the measured *R*-curves for these materials are consistent with shielding, and especially to rationalize the observed insensitivity of the *R*-curves to the transformation yield stress.

II. Materials and Test Procedures

The processing, microstructures, and mechanical properties of the Ce-TZP/Al_2O_3 materials used in this study are described elsewhere.[1,3] The nominal compositions were 12 mol% CeO_2–ZrO_2 + 10 wt% Al_2O_3 + 2 wt% proprietary dopant. The same notation as in a previous paper[1] is used to identify materials fabricated from two powder batches (I and II) and sintered at 1500°, 1475°, and 1450°C (A, B, and C) (Table I).

R-curves were measured using single-edge-notched bend specimens as described elsewhere.[1] In all cases the specimens were precracked under monotonic loading and then annealed to eliminate the transformation zone. The *R*-curves were then evaluated using incremental loading, with unloading at various stages to allow measurement of the transformation zone. The beam dimensions were 60 mm × 15 mm × 7.5 mm and the notch depth was 1.5 mm. All *R*-curve data were obtained from cracks of length between 0.2 and 0.3 of the specimen width.

The transformation zone dimensions were measured from optical Nomarski interference micrographs which highlight surface uplift caused by dilatation within the zone. The relative concentrations of monoclinic and tetragonal phases adjacent to the cracks were measured by X-ray diffraction from the fracture surfaces.[4] In a material made from a third batch of powder and annealed at 1500°C (i.e., type IIIA), Raman spectroscopy was used to measure the relative distributions of monoclinic and tetragonal phases within transformation zones.[5] These measurements were obtained using a microprobe system (~2 μm lateral resolution) which was scanned along several lines traversing transformation zones that were formed during interrupted *R*-curve tests.

III. Zone Shapes and *R*-Curves

The large differences in sizes of the crack tip transformation zones in the various Ce-TZP/Al_2O_3 materials at given applied stress intensity factor, K_a, are shown in Fig. 1. For the purpose of the shielding calculations in the following section, the zone shapes can be approximated as shown in Fig. 1(E), with triangular shapes ahead of and behind the crack tip. The zone size is then characterized by the width *w*, and the shape by the normalized lengths *l*/*w* and *d*/*w*.

The measured *R*-curves for these four materials are shown in Fig. 2(A), and the corresponding zone dimensions are shown in Figs. 2(B) to (D). Despite the large differences in zone width at given K_a, all of the *R*-curves are almost the same. The parameter *l*/*w*, which defines the frontal zone shape, is roughly constant during crack growth and is the same for all materials, most

Table I. Ce-TZP/Al_2O_3 Composites

Composite type	Sintering temperature (°C)	Yield stress (MPa)	*f**
IA	1500	190 ± 5	0.85
IIA	1500	236 ± 13	0.82
IIB	1475	280 ± 6	0.81
IIC	1450	326 ± 9	0.78

*Volume fraction of monoclinic phase on the fracture surface, determined from X-ray diffraction analysis.

I-W. Chen—contributing editor

Manuscript No. 195917. Received March 9, 1992; approved July 2, 1992.
This research was supported at the University of Utah by the Army Research Office under Contract No. DAAL03-87-0060 and at Rockwell Science Center by the U.S. Air Force Office of Scientific Research under Contract No. F49620-89-C-0031.
*Member, American Ceramic Society.

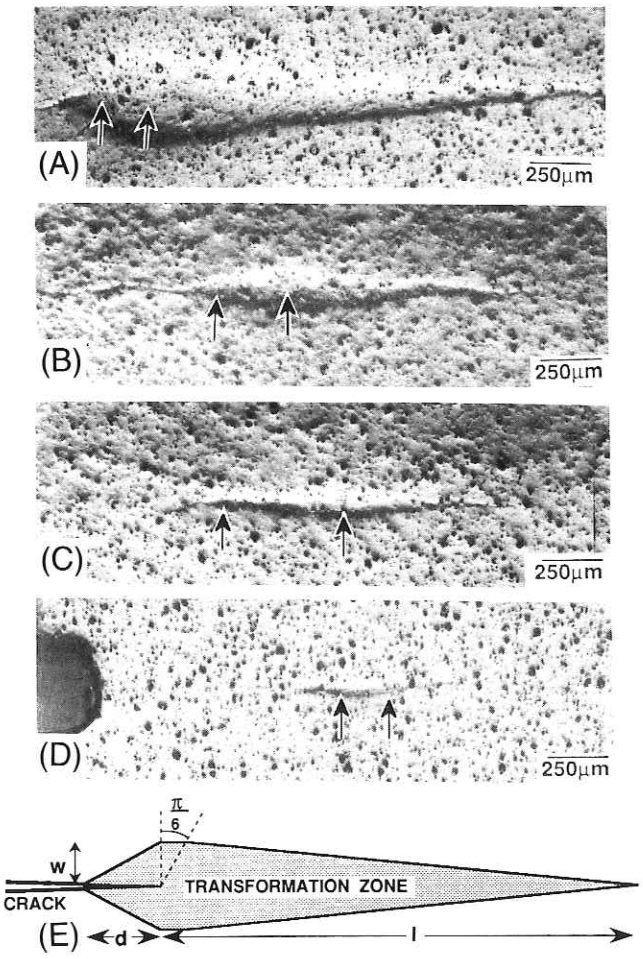

Fig. 1. Nomarski interference micrographs showing crack tip transformation zones in SENB specimens of four types of Ce-TZP/Al_2O_3 composites, at applied stress intensity factor of 10 MPa·$m^{1/2}$: (A) type IA, (B) type IIA, (C) type IIB, (D) type IIC, (E) schematic of zone shape. Arrows indicate positions of crack tip before loading and when micrographs were obtained.

values falling within the range 9 to 13. The wake zone parameter w/d decreases with crack extension for a given material and increases with decreasing yield stress at given crack extension.

The variation of the volume fraction of monoclinic phase with distance from the crack, as measured by Raman spectroscopy, is shown in Fig. 3. A continuous decrease in f with distance is evident, similar to that reported in MgO–ZrO_2 materials,[5] with a significant amount of transformed material lying outside the zone boundary that was inferred from the Nomarski interference image. This difference arises because the contrast in Nomarski interference is caused by changes in *inclination* of the surface rather than absolute surface displacement; the highest contrast occurs where f changes most rapidly. X-ray measurements from the fracture surfaces of the specimens used for Figs. 1 and 2 (Table I) suggest that the fraction of monoclinic phase adjacent to the crack decreases slightly with increasing yield stress. However, these measurements represent values averaged over the penetration depth of the X-rays (~20 μm). For the material with the lowest yield stress, the variation in f over the penetration depth is not significant. However, for the other materials, with smaller zone widths, a significant decrease in f occurs within the penetration depth (assuming that the zone profile of Fig. 3 scales with the zone width). With this spatial variation in f accounted for, the X-ray results would indicate that the value of f at the fracture surface is approximately the same for all of the materials ($f \approx 0.8$).

IV. Crack Schielding Calculations

For a transformation zone with the shape depicted in Fig. 1(E), containing a uniform volume fraction, f, of transformed material with a net hydrostatic transformation strain, e^T, the shielding stress intensity factor, K_s, can be written[6]

$$\frac{K_s(1-\nu)}{e^T E f\sqrt{w}} = \kappa\left(\frac{w}{l}, \frac{w}{d}\right) \tag{1}$$

where ν is Poisson's ratio, E is Young's modulus, and κ is a function of the zone shape parameters.* The function κ can be evaluated using the weight function method of McMeeking and Evans,[6] as described for zones of similar shape in Ref. 2. This expression can be readily modified to account for nonuniform f within the zone, if contours of constant f are geometrically similar. In that case, $f\sqrt{w}$ in Eq. (1) is replaced by

$$f\sqrt{w} \rightarrow \int_0^\infty \frac{f(x)}{2\sqrt{x}}\,dx \equiv f_0\sqrt{w}\int_0^\infty \frac{g(x/w)}{2\sqrt{x/w}}\,d(x/w) \tag{2}$$

where $f(x)$ is the volume fraction of transformed material as a function of distance, x, from the crack. In the normalized expression on the right side of Eq. (2), f_0 is the value of $f(x)$ adjacent to the crack ($x = 0$), $g(x/w)$ is the normalized function $f(x/w)/f_0$, and w is a length scale that can be chosen arbitrarily. For the following calculations we take w as the zone width measured by Nomarski interference (as indicated in Fig. 3), and assume that $g(x/w)$ is given by Fig. 3 for all of the materials. Then, evaluation of the integral in Eq. (2) gives

$$\int_0^\infty \frac{g(x/w)}{2\sqrt{x/w}}\,d(x/w) = 0.9 \tag{3}$$

With $f_0 = 0.8$ from the X-ray measurements, Eqs. (1), (2), and (3) give

$$K_s = \frac{e^T E f'\sqrt{w}}{(1-\nu)}\kappa\left(\frac{w}{l}, \frac{w}{d}\right) \tag{4}$$

where $f' = 0.7$.

The shielding stress intensity factors evaluated from Eq. (4) using the measured values of zone parameters w, w/d, and l/w (Figs. 2(B) to (D)), with $E = 200$ GPa, $\nu = 0.3$, and $e^T = 0.04$, are compared with the measured R-curve data in Fig. 4(A). The values of K_s fall on a curve with shape that is similar to that of the R-curve but displaced by a constant amount to smaller values of K. The differences, $K_a - K_s$, for all of the data are plotted in Fig. 4(B). The difference is approximately constant, most values falling within the range 4 to 6 MPa·$m^{1/2}$.

V. Discussion

The crack resistance, $K_a = K_R$, at any point on the R-curve is given by the sum of the following contributions: the toughness, K_0, of the transformed ZrO_2; the shielding stress intensity factor, K_s, due to the dilatational component of the transformation strain; shielding due to the shear component of the transformation strain; and contributions from other toughening mechanisms. The value of K_0 would be expected to be ~3 MPa·$m^{1/2}$. Therefore, since the results in Fig. 4 show that $K_R - K_s \approx 4$ to 6 MPa·$m^{1/2}$, it is evident that the measured values of K_R are almost fully accounted for by the sum of K_0 and K_s. The results also indicate that the observed insensitivity of the R-curves to the transformation yield stress (i.e., transformation zone size) is consistent with the values of K_s calculated with the observed zone sizes and shapes.

*For the zone shape of Fig. 1(E), κ is not strictly independent of ν as it is for the zones analyzed by McMeeking and Evans.[6] However, the variation with ν is very weak (<2% for $\nu = 0.2$ to 0.3).

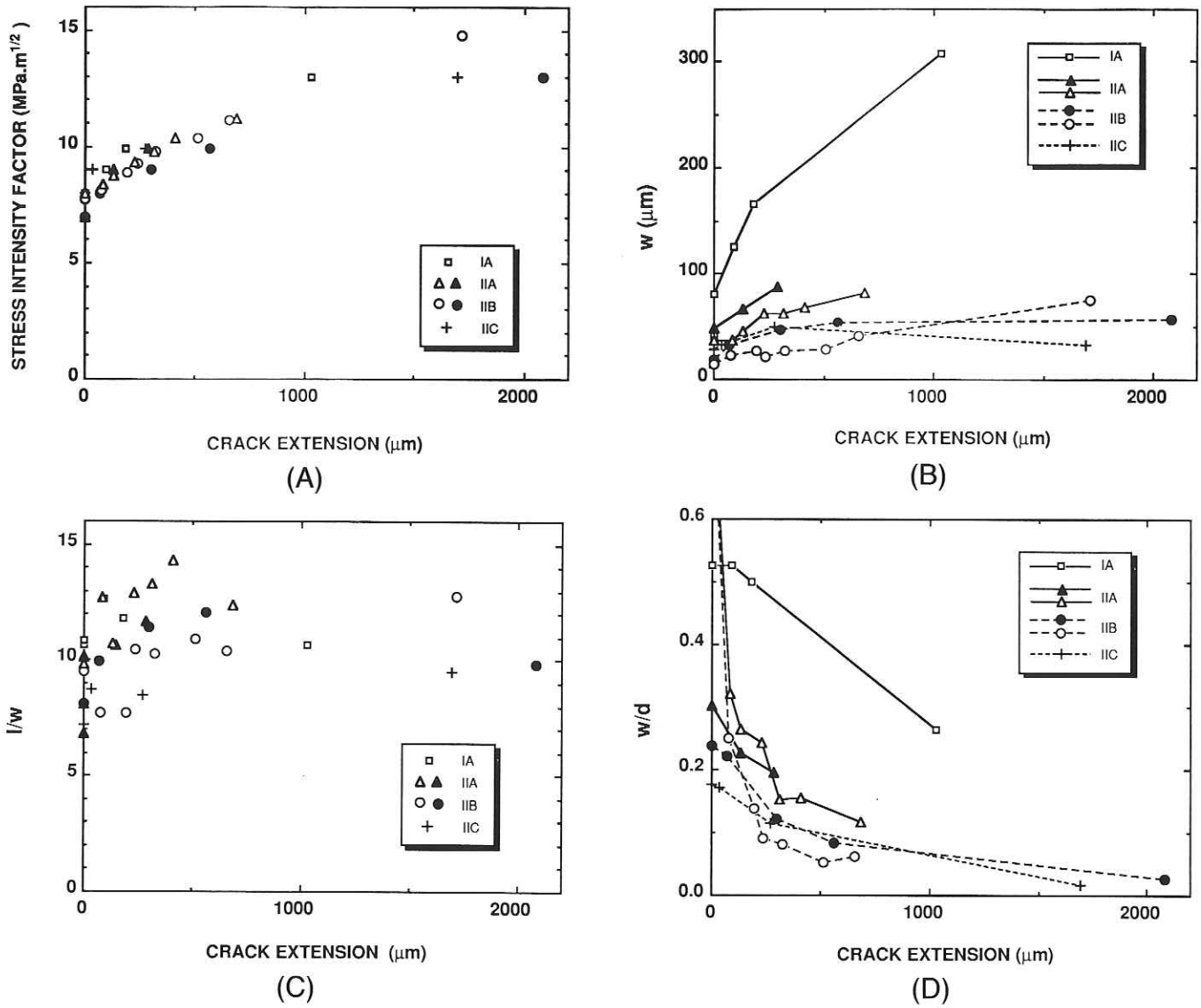

Fig. 2. (A) Crack resistance curves for the materials of Fig. 1, measured using single-edge-notched-beam specimens. (B–D) Transformation zone dimensions (as defined in Fig. 1(E)) corresponding to the data of (A).

The insensitivity of K_R to transformation yield stress warrants further examination. During initial loading in these experiments, the transformation zone extends behind the crack tip a distance d_0 before the crack begins to grow, as indicated in Fig. 1(E). After the crack extends by Δa, the length, d, of the wake zone is

$$d = d_0 + \Delta a \tag{5}$$

where the values of d_0 range from 80 to 150 μm (but not systematically with yield stress). Thus, if we take d_0 as approximately constant (valid for sufficiently large crack extensions), the value of d at given crack extension is approximately the same for all materials. Moreover the values of l/w are approximately the same for all of the zones measured in this study (Fig. 2). Therefore, the relative zone shapes in different materials at given crack extension are roughly as shown schematically in the inset of Fig. 5, with materials of smaller yield stress having the larger zones. The tendency for K_s to increase with increasing zone size ($K_s \propto \sqrt{w}$, Eq. (1)) is opposed by the effect of changing zone shape, which causes κ in Eq. (1) to decrease (as the zone gets larger in changing to materials with lower yield stress, the frontal shape, as defined by l/w, remains constant, but the relative extent of the wake region (d/w) decreases (Fig. 2)). The combined effect of these two opposing changes in K_s is conveniently assessed by rewriting Eq. (4) as

$$K_s = \frac{e^T E f' \sqrt{d}}{(1-\nu)}\left[\sqrt{\frac{w}{d}}\,\kappa\left(\frac{w}{d},\frac{w}{l}\right)\right] \tag{6}$$

so that K_s is proportional to the term in square brackets at given Δa (i.e., given d). This term is plotted in Fig. 5 as a function of w/d for fixed $l/w = 13$. Over the ranges of w/d observed in the four materials of this study (as marked in Fig. 5), this term varies slowly, thus explaining the observed insensitivity of K_s to the value of the w/d.

With the value of $[\sqrt{w/d}\,\kappa(w/d,w/l)]$ given by Fig. 5, Eqs. (5) and (6) provide an approximate expression for the R-curve:

$$K_s = \left\{\frac{e^T E f'}{1-\nu}\left[\sqrt{\frac{w}{d}}\,\kappa\left(\frac{w}{d},\frac{w}{l}\right)\right]\right\}\sqrt{d_0 + \Delta a} \tag{7}$$

The edges of the shaded regions in Fig. 4(A) are defined by Eq. (7), evaluated using values of e^T, E, ν, and f' as defined earlier, and with $[\sqrt{w/d}\,\kappa(w/d,w/l)] = 0.022$ and 0.035, representing the approximate extremes within the ranges of w/d indicated in Fig. 5.

Materials with w/d far out of the range of the present experiments would not exhibit the insensitivity of the R-curve to yield stress, since the curve in Fig. 5 decreases rapidly with changing

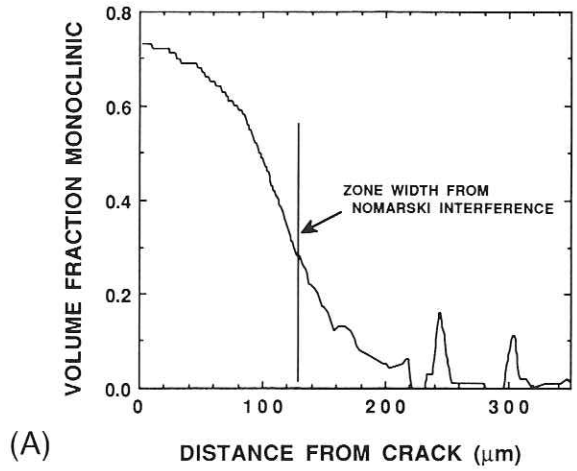

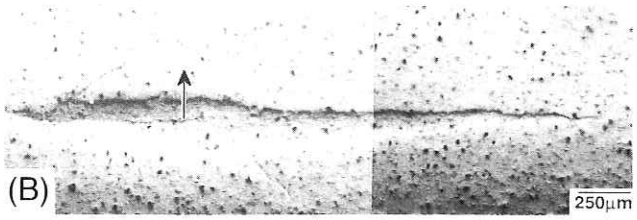

Fig. 3. (A) Variation of volume fraction of monoclinic phase adjacent to crack in type IIIA Ce-TZP/Al_2O_3 composite, measured by Raman spectroscopy. (B) Crack tip transformation zone used for (A) with arrow showing scan line.

w/d outside this range. Moreover, since the slope of the *R*-curve is proportional to $[\sqrt{w/d}\ \kappa(w/d,w/l)]$, materials with *w/d* out of the range of the present experiments would be expected to have *R*-curves of *lower* slope. Finally, we emphasize that all of the results discussed here pertain to the initial, rising part of the *R*-curve, where the zone shapes are approximately as depicted in Fig. 1(E). At larger crack extensions, the *R*-curves would be expected to diverge and approach steady-state values, corresponding to transformation zones with uniform widths over the crack wakes. The steady-state values of K_R would be expected to increase with increasing zone size.

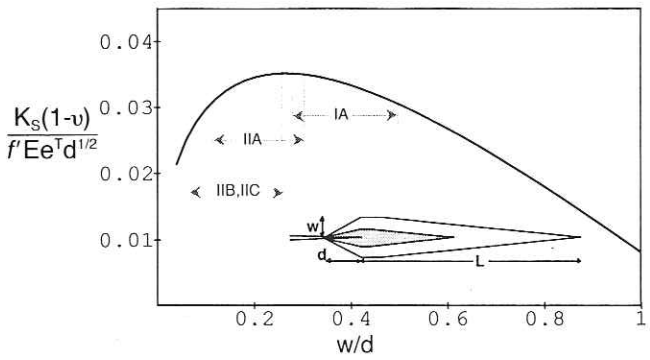

Fig. 5. Variation of shielding stress intensity factor with zone shape parameter, *w/d* (for *l/w* = 13). Inset shows relative zone sizes and shapes at given crack extension in Ce-TZP/Al_2O_3 materials of different yield stress (larger zone corresponding to smaller yield stress).

VI. Conclusions

(1) The insensitivity of measured initial rising portions of *R*-curves in Ce-TZP/Al_2O_3 materials to variations in transformation zone size is consistent with the calculated effect of zone *shape* on crack shielding. The smaller zones were more efficient in shielding the crack tip because of their larger ratio of wake length to zone width.

(2) Most of the measured toughening in Ce-TZP/Al_2O_3 can be accounted for by crack tip shielding due to the dilatational component of the martensitic tetragonal-to-monoclinic transformation.

References

[1]C. S. Yu and D. K. Shetty, "Transformation Yielding, Plasticity and Crack-Growth-Resistance (*R*-Curve) Behavior of CeO_2-TZP," *J. Mater. Sci.*, **25**, 2025–35 (1990).

[2]D. B. Marshall, "Crack Shielding in Ceria-Partially-Stabilized Zirconia," *J. Am. Ceram. Soc.*, **73** [10] 3119–21 (1990).

[3]J. F. Tsai, C. S. Yu, and D. K. Shetty, "Fatigue Crack Propagation in Ceria-Partially-Stabilized Zirconia (Ce-TZP)–Alumina Composites," *J. Am. Ceram. Soc.*, **73** [10] 2992–3001 (1990).

[4]H. Toraya, M. Yoshimura, and S. Somiya, "Calibration Curve for Quantitative Analysis of the Monoclinic–Tetragonal ZrO_2 System by X-ray Diffraction," *J. Am. Ceram. Soc.*, **67** [6] C-119–C-121 (1984).

[5]D. B. Marshall, M. C. Shaw, R. H. Dauskardt, R. O. Ritchie, M. J. Readey, and A. H. Heuer, "Crack-Tip Transformation Zones in Toughened Zirconia," *J. Am. Ceram. Soc.*, **73** [9] 2659–66 (1990).

[6]R. M. McMeeking and A. G. Evans, "Mechanics of Transformation-Toughening in Brittle Materials," *J. Am. Ceram. Soc.*, **65** [5] 242–46 (1982). □

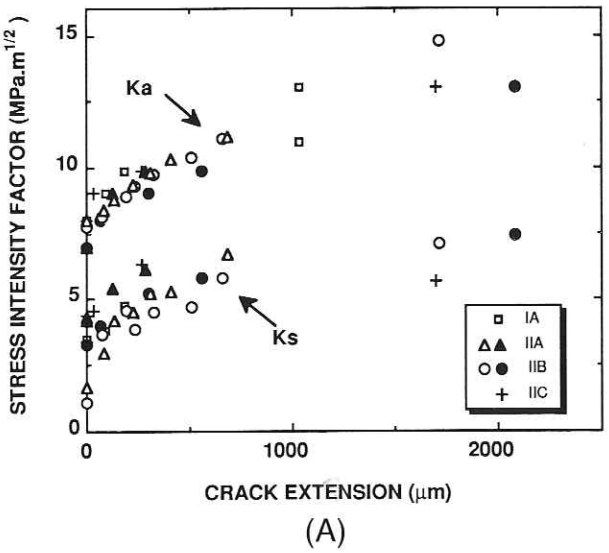

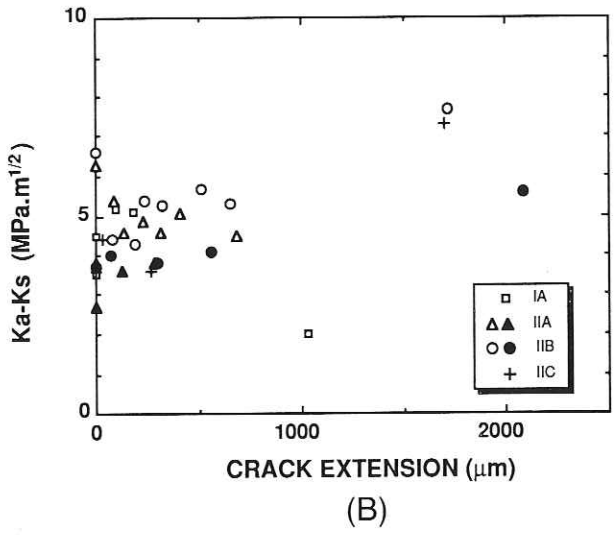

Fig. 4. (A) Comparison of resistance curve data (K_a) from Fig. 2(A) and calculated shielding stress intensity factors (K_s). Shaded bands are representations of Eq. (7). (B) Differences between measured applied stress intensity factors and the calculated shielding stress intensity factors.

journal

J. Am. Ceram. Soc., 73 [10] 2992–3001 (1990)

Fatigue Crack Propagation in Ceria-Partially-Stabilized Zirconia (Ce-TZP)–Alumina Composites

Jing-Fong Tsai,* Cheng-Sheng Yu,* and Dinesh K. Shetty*

Department of Materials Science and Engineering, University of Utah, Salt Lake City, Utah 84112

Fatigue crack propagation rates in tension–tension load cycling were measured in ZrO_2–12 mol% CeO_2–10 wt% Al_2O_3 ceramics using precracked and annealed compact tension specimens. The fatigue crack growth behavior was examined for Ce-TZPs of different transformation yield stresses obtained by sintering for 2 h at temperatures of 1500°C (type A), 1475°C (type B), 1450°C (type C), and 1425°C (type D). The threshold stress-intensity range, ΔK_{th}, for initiation of fatigue crack propagation increased systematically with decreasing transformation yield stress obtained with increasing sintering temperature. However, the critical stress-intensity range for fast fracture, ΔK_c, as well as the stress-intensity exponent in a power-law correlation (log (da/dN) vs log ΔK) were relatively insensitive to the transformation yield stress. The fatigue crack growth behavior was also strongly influenced by the history of crack shielding via the development of the crack-tip transformation zones. In particular, the threshold stress-intensity range, ΔK_{th}, increased with increasing size of the transformation zone formed in prior quasi-static loading. Crack growth rates under sustained peak loads were also measured and found to be significantly lower and occurred at higher peak stress intensities as compared to the fatigue crack growth rates. Calculations of crack shielding from the transformation zones indicated that the enhanced crack growth susceptibility of Ce-TZP ceramics in fatigue is not due to reduced zone shielding. Alternate mechanisms that can lead to reduced crack shielding in tension–tension cyclic loading and result in higher crack-growth rates are explored. [Key words: fatigue, crack growth, zirconia—tetragonal polycrystals, transformation, crack growth.]

I. Introduction

FATIGUE crack growth behavior of structural ceramics has been of interest ever since the development of such advanced ceramics as Si_3N_4, SiC, and partially stabilized ZrO_2. In the mid 1970s, Evans *et al.*[1–3] studied crack propagation under cyclic loading in Si_3N_4, porcelain, and glass. Analysis of the crack growth data, however, revealed that the observed phenomenon of cyclic crack growth was essentially a cyclic manifestation of stress corrosion cracking; i.e., the measured crack growth rates under cyclic loading could be rationalized on the basis of sustained load crack growth rates and the time variation of load during cycling. Therefore, it was concluded that these ceramics did not exhibit genuine fatigue effect on crack propagation in the same manner as metals. This conclusion was also supported by the observation that the measured crack growth rates were independent of the frequency of applied cyclic loading.[3] The absence of the fatigue effect was rationalized as being due to the absence of appreciable crack tip plasticity in most ceramics.[4]

In addition to the direct crack growth measurements cited above, fatigue effects in ceramics have been examined by measuring failure times under cyclic loading,[5–10] i.e., by establishing the traditional S–N curves under cyclic loading. Although time-dependent strength degradation was observed in most of these studies, only a limited number of these studies critically examined the life times under cyclic loading with the corresponding life times under static loading. Results obtained on polycrystalline alumina by Krohn and Hasselman,[5] Chen and Knapp,[7] and Guiu[8] showed evidence for shorter life times under cyclic loading as compared to life times under peak sustained loads. The differences in the life times were, however, small, especially in relation to the large scatter in the measured life times, and the statistical significance of the differences was not clearly established. The results obtained by Matsuo *et al.*[9] and Fett *et al.*[10] on Si_3N_4, on the other hand, showed no evidence of cyclic enhancement of strength degradation. In fact, life times measured under cyclic loads in the experiments of Fett *et al.*[10] were greater than the predictions based on the sustained load crack growth data.

Thus, it was the perception generally that structural ceramics did not suffer from a true fatigue phenomenon as observed in metals. Recent developments have effected a change in this perception. First, Suresh *et al.*[11–13] have shown that application of cyclic compressive stresses to notched specimens of ceramics can lead to stable crack growth in the plane of the notch in a direction normal to the far-field compression axis. This cyclic-stress-induced crack growth is believed to be caused by a notch-tip tensile residual stress that develops on unloading the far-field compressive stress. The extent of cyclic crack growth is, however, limited and the crack growth terminates after a finite extension of the crack.

Swain and Zelizko[14] have recently shown that failure times for two commercial grades of magnesia-partially-stabilized zirconia (Mg-PSZ) under rotational bending fatigue are very much smaller than the corresponding failure times under constant peak bending loads. The differences in the life times as well as in the stress exponent of the failure times were very significant. However, cyclic bending tests did not show much deviation in the failure times as compared to static bending tests. This implied that tension–compression load cycling was more damaging than tension–tension (or compression–compression) load cycling in Mg-PSZ.

More direct evidence of enhanced crack growth in cyclic loading as compared to peak static loading in Mg-PSZ has been reported by Dauskardt *et al.*[15–17] Several aspects of their results point to a true fatigue crack-growth phenomenon in Mg-PSZ. First, tension–tension load cycling of compact tension specimens produced crack growth rates that were several orders of magnitude greater than the crack growth rates at peak sustained loads. Therefore, fatigue crack growth in Mg-PSZ cannot be a direct cyclic manifestation of the crack growth observed under sustained loading, such as that reported by Becher.[18] Secondly, load cycling produced significant crack growth rates at stress intensities well below the range of stress intensities required for crack growth under sus-

D. Marshall—contributing editor

Manuscript No. 197869. Received January 3, 1990; approved July 6, 1990.
Based on research supported by the Army Research Office under Contract No. DAAL03-87-0060 at the University of Utah.
*Member, American Ceramic Society.

tained loading. Finally, the slope of the log (crack velocity)–log (stress intensity) plot for cyclic loading was significantly smaller than the corresponding slope for sustained loading. All of these results suggest that Mg-PSZ exhibits a fatigue crack growth phenomenon analogous to the behavior of metals. Interestingly, a fatigue study by Sylva and Suresh[19] in Mg-PSZ using precracked single-edge-notch beam specimens did not show similar crack growth characteristics. Crack growth was highly discontinuous and periodic crack arrest occurred after growth over small distances.

The present paper reports the results of an experimental investigation of fatigue crack growth in CeO_2-partially-stabilized ZrO_2 ceramics containing 10 wt% Al_2O_3. The objective of this study was to see if tetragonal polycrystalline zirconia ceramics are also susceptible to enhanced fatigue crack growth under tension–tension cyclic loading in the same manner as the Mg-PSZ ceramics. It is shown that Ce-TZP ceramics also exhibit true fatigue crack growth behavior in tension–tension load cycling with significantly higher crack growth rates as compared to sustained load crack growth at constant peak loads. The fatigue behavior of Ce-TZP ceramics is also characterized by a well-defined threshold stress-intensity range (ΔK_{th}) that decreases systematically with increasing transformation yield stress and fatigue crack growth exponents that were much smaller than those obtained for Mg-PSZ ceramics. The fatigue behavior was also sensitive to the history of crack shielding via the development of the crack-tip transformation zones. Potential differences in crack shielding due to both transformation zones as well as crack-face contact shielding mechanisms are examined to account for the enhanced crack growth of Ce-TZPs in cyclic loading.

II. Ce-TZP Ceramics and Test Procedures

(1) CeO_2-Partially-Stabilized Zirconia Ceramics

Ce-TZP powder of the nominal composition, 90 wt% of (12 mol% CeO_2 and 88 mol% ZrO_2) and 10 wt% Al_2O_3, was obtained from a commercial source.* The as-received powder was sieved on a 70-μm screen before the powder was first die-pressed at 34.5 MPa and then isostatically cold-pressed at 207 MPa. The green compacts were sintered in air for 2 h at one of four temperatures: 1500°C (type A), 1475°C (type B), 1450°C (type C), and 1425°C (type D). The sintered billets were cut and ground to the required specimen shape and size and annealed at 1000°C for 30 min before using them for characterization of microstructures, phase contents, phase stability, and fatigue crack propagation behaviors.

(2) Characterization of Microstructures, Transformation Zones, Phase Contents, and Phase Stability

Microstructures were characterized by scanning electron microscopy using ground and polished specimens that were thermally etched for 40 min at a temperature that was 100°C below the sintering temperature. The grain sizes were determined by intercept length measurements on scanning electron micrographs of polished and thermally etched surfaces.[20] Approximately 700 grain intercept lengths were measured for each material to obtain the mean grain size and the grain size distribution. Only the intergranular alumina particles were considered as the second phase in assessing the grain size of the tetragonal zirconia phase in the two-phase microstructures.[20]

Shapes and sizes of transformation zones at crack tips were assessed by optical microscopy using Nomarski interference technique. Volume fractions of the tetragonal phase on annealed and fracture surfaces were determined by X-ray diffraction using the calibration and procedure described by Toraya *et al.*[21] In addition, Raman spectroscopy was used to assess local variations of the monoclinic phase content within the transformation zones as described by Dauskardt *et al.*[17] Stability of the tetragonal zirconia phase was characterized by measuring the burst transformation temperature (M_b). Strain gages were mounted on right square cylinder (4 mm × 4 mm × 10 mm) specimens and the specimen-gage assemblies were cooled uniformly using a liquid N_2 cooling arrangement. Burst transformation temperature was indicated by a sudden burst of strain on a strain–temperature record.

(3) Transformation Yielding and Plasticity in Three-Point Bending

The stress–strain behaviors of the different types of Ce-TZPs, including transformation yield stresses and inelastic strains to fracture, were characterized in three-point bending using strain-gaged specimens. Typical bend specimens were 3 mm × 4 mm × 45 mm in dimensions. The tension surfaces were polished to enable observations of discrete transformation bands. Yu and Shetty[22,23] have described the test procedures and results in detail.

(4) Quasi-Static, Fatigue, and Sustained Load Crack Growth Tests

All crack-growth measurements under quasi-static (at constant load-point deflection rate), fatigue (tension–tension cyclic loading between two fixed load limits), and sustained (constant) loads were made using compact tension specimens. The geometry of the specimens followed the specifications given in ASTM standards E-561[24] and E-647.[25] The specific dimensions were width, W = 25.4 mm, and thickness, B = 7.5 mm. Relatively thick specimens were used in all the crack-growth tests so as to satisfy the minimum thickness requirements specified in the above standards. Prior to testing, all specimens were precracked by quasi-static or fatigue loading so that the initial crack length increment, Δa_i, was approximately 1.5 mm and then annealed at 1000°C for 30 min.

Quasi-static crack growth tests were conducted in a screw-driven universal testing machine† at a constant crosshead displacement rate of 0.05 mm/min and ambient environmental conditions (22°C, 40% relative humidity). The tests were periodically interrupted and specimens unloaded to measure the crack lengths and record the crack-tip transformation zones. From the loads at each interruption and the corresponding crack lengths, applied stress-intensity factors for stable crack growth were calculated using the equations given in the ASTM standards to establish the crack-growth-resistance behaviors (R-curves) for the different Ce-TZPs.

Fatigue crack growth rates and sustained load crack growth rates were measured on precracked and annealed compact tension specimens using a servohydraulic testing machine.‡ For the fatigue tests, load was cycled between a maximum (P_{max}) and a minimum tension load (P_{min}) following a sinusoidal profile at 30 Hz frequency. The load ratio, $R = P_{min}/P_{max}$, was maintained at 0.1 in all the fatigue tests. The tests were conducted at ambient laboratory conditions, and the number of cycles applied for incremental crack extensions, Δa = 0.1 to 0.2 mm, were recorded during fatigue crack extension. Crack lengths were monitored on both faces of the compact specimen using a pair of traveling microscopes. Crack lengths, number of cycles, and the applied loads were used to generate log (da/dN) vs log ΔK plots using the incremental polynominal method described in Ref. 25. For sustained load crack growth tests, the applied load was maintained on the specimens, and the crack growth was monitored as a function of time. The selection of the initial load for either the fatigue crack growth tests or the sustained load

*Grade Z-65, Ceramatec, Salt Lake City, UT.

†Model 1125, Instron, Canton, MA.
‡880 material test system, MTS, Minneapolis, MN.

crack growth tests was initially based on trial and error to get a measurable crack growth rate of 10^{-10} m/cycle or 10^{-9} m/s.

III. Experimental Results

(1) Microstructures, Phase Contents, and Phase Stability of Ce-TZP Ceramics

Figure 1 shows microstructures of type A and type C Ce-TZPs. There was only a slight difference in the mean grain size of the tetragonal zirconia phase, 1.87 μm for type A and 1.52 μm for type C. The initial phase contents of all the four types of sintered and annealed Ce-TZPs were nearly identical, greater than 98 vol% tetragonal phase. However, stability of the tetragonal phase varied significantly with small variation in the mean grain size, and this was reflected in the variation of the burst transformation temperature, 4°C for type A and −48°C for type D.

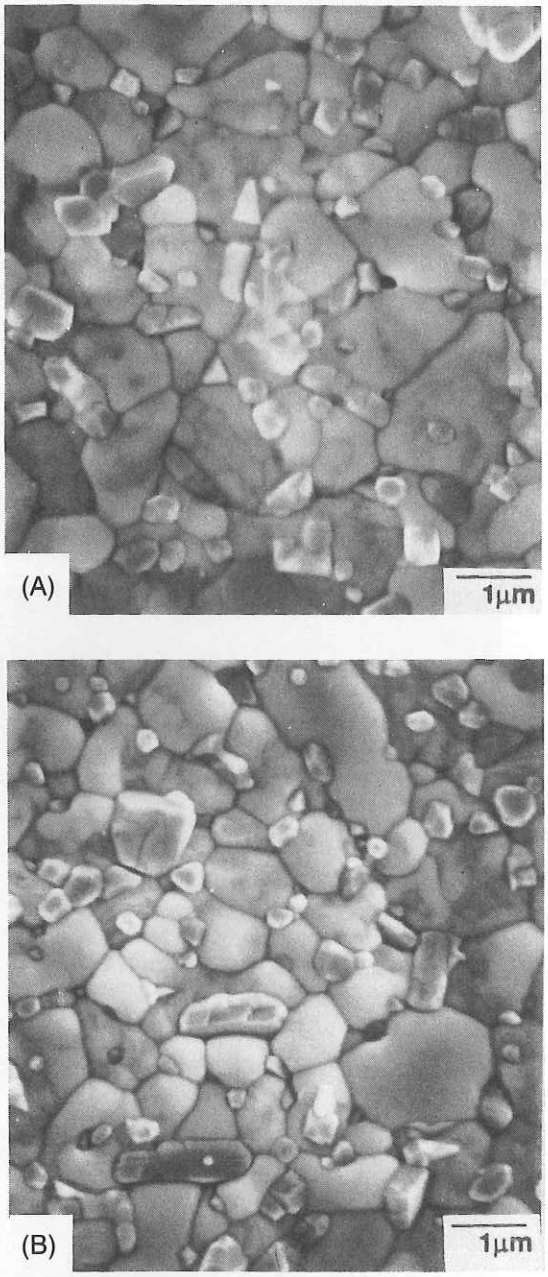

Fig. 1. Microstructures of Ce-TZP ceramics sintered at (A) 1500°C and (B) 1450°C for 2 h.

Table I summarizes the mean grain sizes of the tetragonal zirconia phase, phase contents on annealed and fracture surfaces (vol% of tetragonal phase), burst transformation temperature (M_b), and transformation yield stress for all the four types of ceramics. There were significant differences in the M_b temperatures and yield stresses, but the other properties were very similar.

(2) Transformation Yielding and Plasticity in Three-Point Bending

Figure 2 shows stress–strain curves for the four types of Ce-TZPs as measured in three-point bending at a constant deflection rate (δ = 0.05 mm/min). The stresses plotted in the figure are the nominal elastic bending stresses. The strain was measured on the tension face at the center of the beam using strain gages. The Ce-TZP ceramics showed distinct yield points (indicated by arrows in Fig. 2) corresponding to instantaneous formation of wedge-shaped transformation bands that spanned the width of the beam. Yu and Shetty[23] have described the details of the development of this primary and other secondary transformation bands and the nucleation and stable growth of a surface crack within the primary band that leads to final fracture.

The transformation yield stress increased from 244 (type A) to 405 MPa (type D) with decreasing mean grain size. There was also a corresponding decrease in the total transformation strain prior to fracture, accompanied by the formation of transformation bands of smaller width.[23]

(3) Crack-Growth-Resistance (R-Curve) Behaviors of Ce-TZPs

Figure 3 shows representative compact tension specimens used in the measurements of R-curves, fatigue crack growth rates, and sustained load crack growth rates. The R-curves measured for the type A and type D Ce-TZPs are shown in Fig. 4. There were only modest differences between the two R-curves. Crack growth initiated at slightly lower K_I value and there was more stable crack extension in the type D Ce-TZP as compared to the type A material. However, the slopes of the R-curves at a given crack extension and the maximum fracture toughness values reached before instability were comparable in the two ceramics. The R-curves for type B and type C Ce-TZPs were similar and were in between the R-curves of types A and D. They are not shown in Fig. 4, to ensure clarity.

One question that might be raised regarding the procedure used in this study for measuring the R-curves is whether the periodic unloading used to measure crack lengths has any effect on the R-curves. Singh and Shetty[26] measured R-curves for type A Ce-TZP by measuring crack lengths using microcircuit grids during quasi-static loading (without unloading) of single-edge-notch-bend specimens. The R-curve assessed by continuous loading was identical to the R-curve obtained by periodic unloading to measure crack lengths. It was, therefore, concluded that periodic unloading did not affect the R-curves measured in this study.

Figure 5(A) shows a Nomarski interference photograph of the crack-tip transformation zone in type A Ce-TZP compact specimen at K_I = 12 MPa·m$^{1/2}$. Compact specimens of types B, C, and D Ce-TZPs showed similar, but much smaller zones. The arrows on the photograph point to the initial (after precracking) and the final crack-tip positions. The elongated shape of the transformation zone shown in Fig. 5(A) is similar to the earlier observations of Yu and Shetty[22,23] in single-edge-notch-bend specimens and Rose and Swain[27] in double-cantilever beam specimens. The R-curves shown in Fig. 4 are also qualitatively similar to the R-curves measured by Yu and Shetty[22,23] using precracked single-edge-notch-bend specimens. However, Rose and Swain[27] observed a saturation plateau in their R-curve for a Ce-TZP measured with double-cantilever beam (DCB) specimen, while no true satu-

Table I. Grain Sizes, Phase Contents, Burst Temperatures, and Yield Stresses for Ce-TZPs Sintered at Four Different Temperatures

Type	Sintering temperature (°C)	Mean grain size (μm)	Phase content (as annealed) (%)	Burst temperature (°C)	Yield stress (MPa)	Phase content (fracture surface) (%)
A	1500	1.87	98	4	249 ± 5	18
B	1475	1.73	99	−8	296 ± 5	19
C	1450	1.52	99	−25	353 ± 8	22
D	1425	1.47	99	−48	405 ± 10	27

ration was observed in the present study or the earlier studies of Yu and Shetty.[22,23]

Figure 5(B) is a schematic of the zone with the shape approximated by two triangular zones, one ahead of the crack tip and one behind. The size and shape of the zone are characterized by the parameters l (zone length ahead of the crack tip), d (zone length behind the crack tip), and w (maximum zone width at the crack tip). The magnitudes of the zone size parameters are indicated on the figure. These zone size and shape parameters are used in a later section to estimate crack shielding arising from the dilatational strains in the transformation zone.

(4) Fatigue Crack Growth Rates in Ce-TZPs

Figure 6 summarizes fatigue crack growth rates (da/dN) as functions of the stress-intensity range (ΔK_I) on log–log plots for the four types of Ce-TZPs. Fatigue crack growth plots showed three distinct characteristics. All the four types showed well-defined fatigue thresholds (ΔK_{th}) corresponding to crack growth rates below 10^{-9} m/cycle. Above these thresholds, crack growth rates increased rapidly at first, then more gradually at crack growth rates above 10^{-7} m/cycle, reaching a minimum slope in the log (da/dN) vs log ΔK_I plots. These minimum slopes, i.e., exponents of stress-intensity ranges, were very similar for the four Ce-TZPs, $n \sim 8$ to 11, in the fatigue crack growth rate range, 10^{-7} to 10^{-5} m/cycle. However, the fatigue thresholds decreased systematically with increasing yield stress and at a given stress-intensity range (for example, $\Delta K_I = 9$ MPa · m$^{1/2}$) the crack growth rates increased with increasing yield stress. Finally, all the four Ce-TZPs showed unstable fast fracture at approximately the same stress-intensity range, $\Delta K_c \sim 14$ MPa · m$^{1/2}$. This behavior is equivalent to the nearly identical peak fracture toughness obtained for type A and type D Ce-TZPs in the R-curve measurements (see Fig. 4).

Figure 7(A) shows a Nomarski interference photograph of a crack-tip transformation zone in a fatigue crack growth specimen of type A Ce-TZP. Again, the photograph was taken when the maximum stress-intensity reached 12 MPa · m$^{1/2}$ during a constant load range fatigue test. Figure 7(B) shows the characteristic dimensions of the zone on a schematic. Comparison of the transformation zone of Fig. 7 with the corresponding zone in the quasi-statically loaded specimen (Fig. 5) shows that zone length ahead of the crack tip was smaller in the fatigue specimen ($l \sim 1.43$ mm) relative to the R-curve specimen ($l \sim 2.16$ mm), even though these comparisons were made at the same maximum applied K_I. Similarly, the zone width in the fatigue specimen was slightly smaller than the corresponding width in the R-curve specimen. It was also evident from the initial and the final crack-tip positions that total crack extension under tension–tension cyclic loading was much greater than the corresponding crack growth in quasi-static loading.

(5) Fracture Surfaces of Quasi-Static and Fatigue Crack Growth Specimens

The scanning electron micrographs in Fig. 8 compare the fracture surfaces in quasi-static and fatigue crack growth speci-

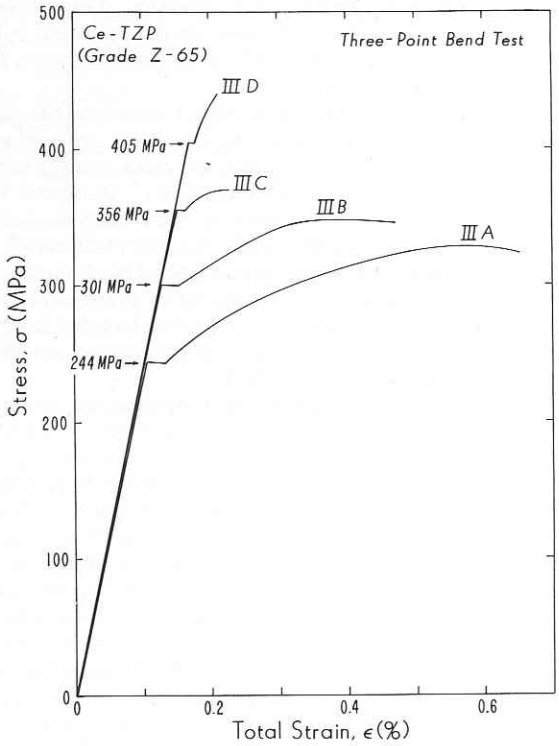

Fig. 2. Stress–strain curves for Ce-TZPs measured in three-point bending.

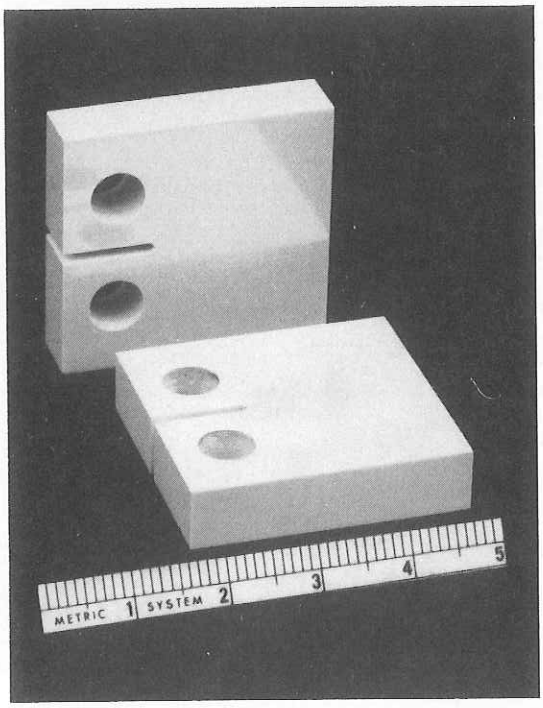

Fig. 3. Compact tension specimens of Ce-TZP used in R-curve, fatigue crack growth, and sustained load crack growth measurements.

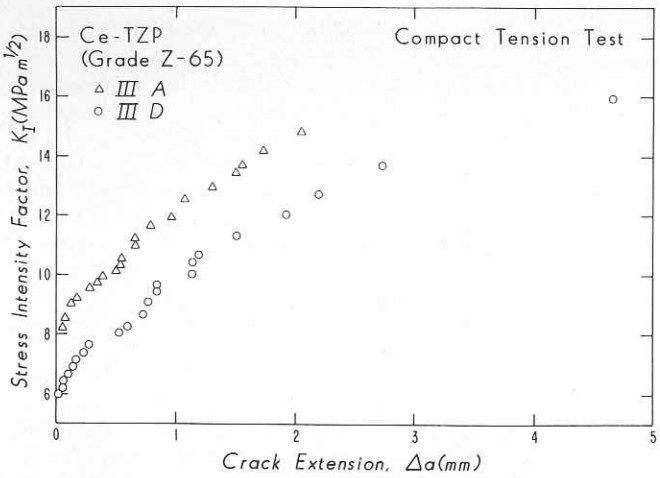

Fig. 4. Crack-growth-resistance (*R*-curve) behaviors of Ce-TZPs measured in quasi-static loading of compact tension specimens.

mens of type A Ce-TZP. The fracture surface of the quasi-statically loaded specimen (Fig. 8(A)) showed predominantly intergranular fracture with some evidence of transgranular fracture in some grains. Grain faces appeared "clean" and sharp. Grain faces showed the presence of large alumina particles. By contrast, fracture surface of the fatigue crack growth specimen (Fig. 8(B)) showed rounded or smoothened grain faces and edges. The alumina particles that appeared on the grain faces were much smaller and appeared to be partially buried in the zirconia grains. Similar differences on the fracture surfaces were observed in types B, C, and D Ce-TZPs.

(6) Comparison of Fatigue Crack Growth and Sustained Load Crack Growth Behaviors

A critical question that naturally arises in a fatigue crack growth study such as the present one is whether the observed crack growth behavior is a genuine fatigue crack growth phenomenon or is simply a manifestation of environmentally induced subcritical crack growth under varying load. To answer this question, crack growth tests were conducted in which precracked compact tension specimens were loaded to a maximum load in the servohydraulic machine, and then the loads were held constant. The initial loads were selected such that a small crack extension (~100 μm) could be measured in a reasonable period of time (~12 h). The crack growth rates measured under these sustained loads are compared with the corresponding crack growth rates under tension–tension cyclic loads in Fig. 9 for type A and type D Ce-TZPs. It should be noted in Fig. 9 that crack growth rates are plotted as functions of the maximum stress intensity at any stage of crack growth. The plots of crack growth rates under sustained loads were qualitatively similar to the fatigue crack growth plots. However, sustained load crack growth plots were shifted to higher values of K_{max}. The threshold stress intensity for crack growth as well as stress intensity for a specific crack growth rate was higher for sustained loading than tension–tension cyclic loading. The results of Fig. 9, therefore, suggest that Ce-TZP ceramics exhibit a genuine fatigue crack growth phenomenon, and the crack growth under cyclic loading cannot be explained as a cyclic manifestation of sustained load crack growth behavior.

The threshold stress intensity, K_{th}, measured in fatigue and sustained load crack growth tests is plotted versus the transformation yield stress in Fig. 10. The data clearly show that the threshold stress-intensity increases with decreasing transformation yield stress in both the fatigue and the sustained load tests. The magnitudes of the threshold stress intensities were higher in the sustained load tests as compared to the fatigue tests for all four types of Ce-TZPs.

Figure 11(A) shows a Nomarski photograph of a crack-tip transformation zone in a type A Ce-TZP compact tension specimen that was subjected to sustained load crack growth to $K_{max} = 12$ MPa · m$^{1/2}$. The three arrows on the photograph beginning at left indicate the initial crack length after precracking and annealing, the crack length on application of the sustained load, and the crack length after sustained-load crack growth to $K = 12$ MPa · m$^{1/2}$. Figure 11(B) is the corresponding schematic with the characteristic zone dimensions. Comparison of Fig. 11 with the corresponding zones of Figs. 5 and 7 indicated that both the zone length ahead of the crack (l) and the zone width (w) for the sustained load crack growth specimen were comparable to and in between the corresponding zone dimensions in the quasi-static (Fig. 5) and fatigue (Fig. 7) specimens. It is interesting to note, however, that unlike the quasi-static and the fatigue specimens the maximum zone width in the sustained load specimen did not occur at the final crack-tip position. It occurred at the crack-tip

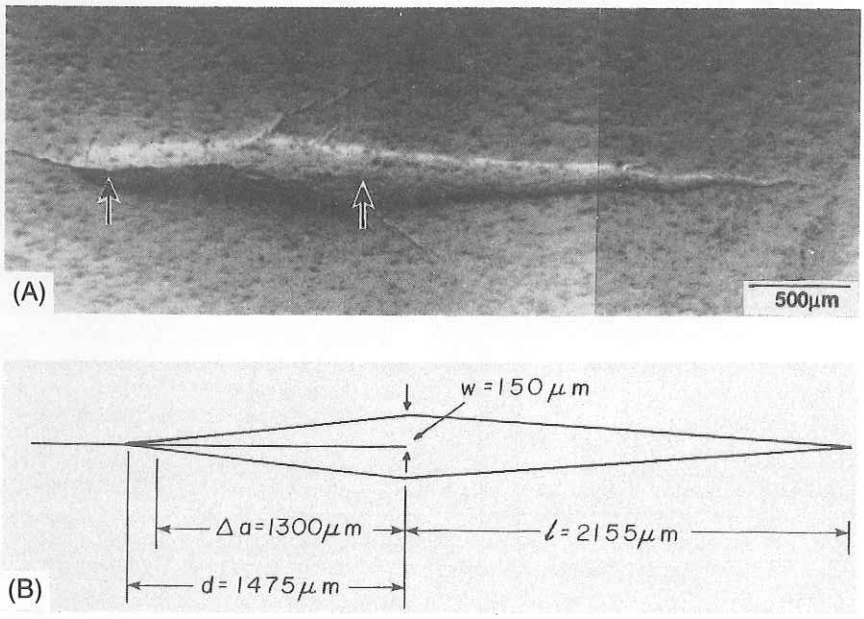

Fig. 5. (A) Transformation zone in a quasi-statically loaded compact tension specimen of type A Ce-TZP at $K_I = 12$ MPa · m$^{1/2}$. Arrows point to the initial and final crack-tip positions. (B) Schematic of the transformation zone and characteristic zone dimensions.

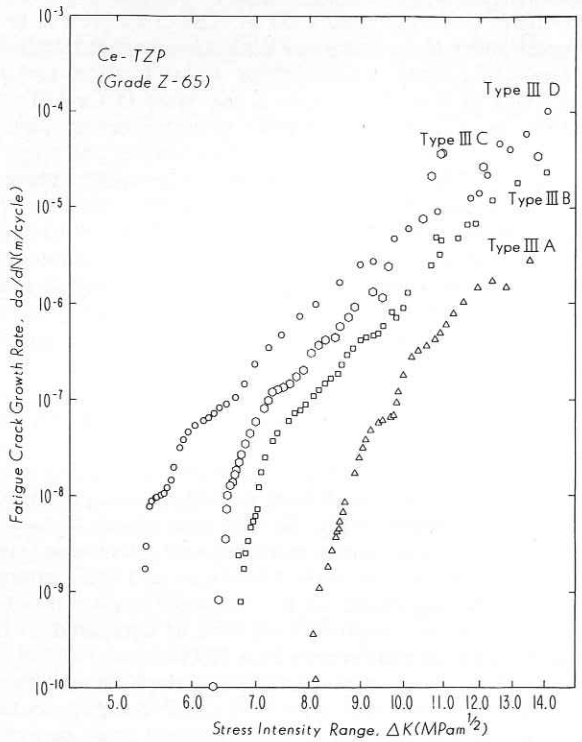

Fig. 6. Fatigue crack growth rates (da/dN) as functions of stress-intensity range (ΔK_I) for four types of Ce-TZPs.

position immediately after the application of the sustained load. Also, crack extension under sustained load was nearly half of the crack extension observed under cyclic fatigue. Potential implications of these zone size and shape differences in terms of their influence on crack shielding will be addressed later.

(7) Influence of Preformed Crack-Tip Transformation Zone on Fatigue Crack Growth Response

The crack growth rate plots of Fig. 6 represent the fatigue behavior of precracked and annealed compact specimens. In such specimens, material resistance to crack growth increases during fatigue crack extension because of the R-curve behavior. In other words, plots of Fig. 6 represent fatigue response of Ce-TZPs superposed over a rising crack-growth-resistance behavior. Since the Ce-TZPs of this study did not show a true saturation fracture toughness, a steady-state fatigue response could not be established. It was of interest, however, to examine the influence of a preformed crack-tip transformation zone on subsequent fatigue response. For this purpose, a type A Ce-TZP compact specimen was precracked, annealed, and then quasi-statically loaded to $K_{max} = 12\ \text{MPa}\cdot\text{m}^{1/2}$ to develop a crack-tip transformation zone similar to the one shown in Fig. 5. The specimen was subsequently loaded in cyclic tension following essentially the same procedure as that used for the annealed compact specimens. Based on the crack length after the initial quasi-static loading, a cyclic maximum load, P_{max}, was chosen to give $\Delta K = 8\ \text{MPa}\cdot\text{m}^{1/2}$ in the fatigue test. After applying 100 000 load cycles at this maximum load, the load was incrementally increased if there was no measurable increase in the crack length. This procedure was repeated until measurable crack growth rate ($\sim 10^{-10}$ m/cycle) was detected. At this point, the maximum load was fixed and fatigue crack growth was monitored at fixed cyclic load range.

Figure 12 compares fatigue crack growth in a "fresh" annealed compact specimen of type A Ce-TZP with the fatigue crack growth response of a compact specimen quasi-statically preloaded to $12\ \text{MPa}\cdot\text{m}^{1/2}$. The preloaded compact specimen showed an increased fatigue threshold stress-intensity range, $\Delta K_{th} \sim 10.8\ \text{MPa}\cdot\text{m}^{1/2}$ as compared to a threshold stress-intensity range of $\sim 8\ \text{MPa}\cdot\text{m}^{1/2}$ for the annealed specimen. It is interesting to note that the peak stress intensity corresponding to the higher threshold, $K_{max} = 12\ \text{MPa}\cdot\text{m}^{1/2}$, exactly matches the crack growth resistance initially developed in the specimen during quasi-static loading. A second interesting feature of the fatigue response was the sharp rise in the crack growth rate just above the fatigue threshold until the crack growth rate in the preloaded specimen reached the crack growth rate in the annealed specimen, and beyond this point the fatigue crack growth behaviors were nearly identical in the two specimens. Thus, the compact specimen with the preexisting transformation zone showed a clear transition from the higher threshold to the normal fatigue response.

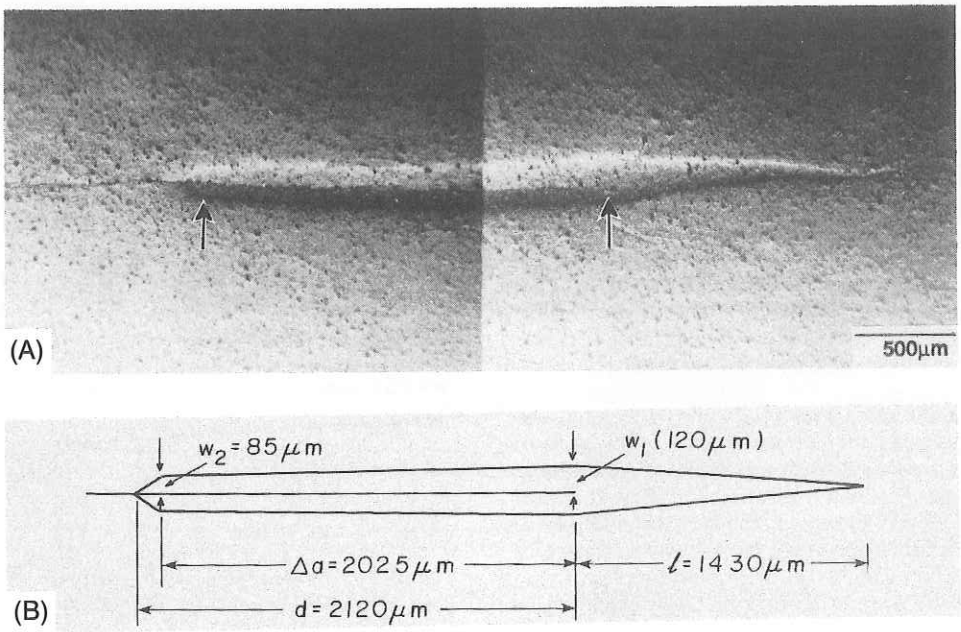

Fig. 7. (A) Transformation zone in a compact tension specimen of type A Ce-TZP after fatigue crack growth to $K_I = 12\ \text{MPa}\cdot\text{m}^{1/2}$. Arrows point to the initial and final crack-tip positions. (B) Schematic of the transformation zone and characteristic zone dimensions.

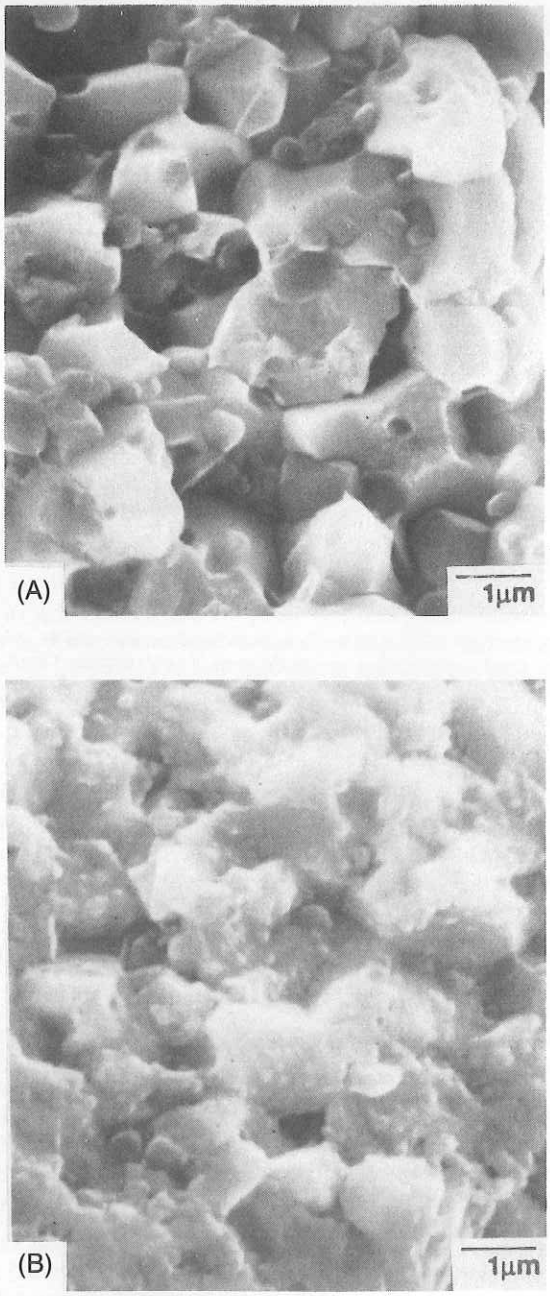

Fig. 8. Fracture surfaces of (A) quasi-static crack growth (*R*-curve) specimen and (B) fatigue crack growth specimen of type A Ce-TZP.

IV. Discussion

The results of the present study have shown that Ce-TZP ceramics are susceptible to a true fatigue crack growth phenomenon. Characteristics of fatigue crack growth in Ce-TZP included significantly higher crack growth rates in tension–tension cyclic loading relative to crack growth rates under sustained loading at the same peak stress intensities (Fig. 9) and fatigue threshold stress intensities that were lower than the corresponding thresholds for sustained load crack growth (Fig. 10). Minimum stress-intensity exponents in the fatigue crack growth plots were not very sensitive to different sintering conditions of Ce-TZP. However, the threshold stress intensity for initiation of fatigue crack growth was sensitive to both the transformation yield stress determined by the sintering conditions as well as prior history of crack shielding as determined by a preformed crack-tip transformation zone.

Although some of the above characteristics of the fatigue behavior of Ce-TZP ceramics are similar to those reported for

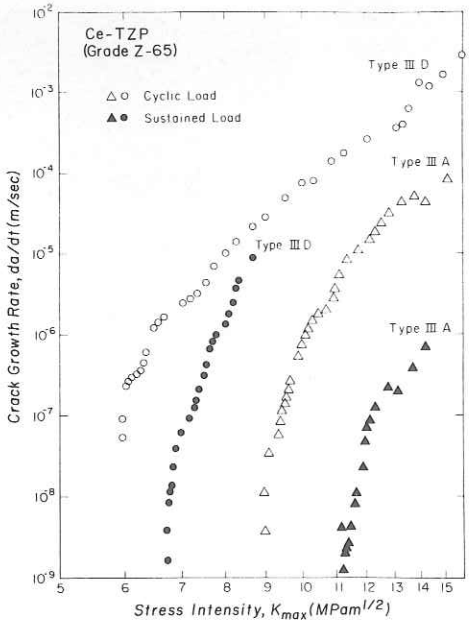

Fig. 9. Comparison of fatigue crack growth rates and sustained load crack growth rates for types A and D Ce-TZPs.

Mg-PSZ,[17] there were many interesting differences as well. Plots of log (da/dN) vs ΔK for Mg-PSZ exhibited single linear stages with large exponents in the range 21 to 42. There was no evidence of a clear fatigue threshold. Fatigue crack growth plots of Ce-TZP obtained in this study (Fig. 6) were highly nonlinear with well-defined thresholds and minimum stress-intensity exponents in the range 8 to 11. It is important to note a fundamental difference in the experimental approaches of the two studies. Dauskardt *et al.*[15–17] exclusively studied fatigue behavior of Mg-PSZ ceramics that were precracked and loaded to a steady-state crack growth regime with a saturation fracture toughness and corresponding steady-state crack-tip transformation zone size. On the other hand, fatigue crack growth plots of Fig. 6 of this study represent fatigue behavior of Ce-TZP during a crack-growth regime with simultaneous buildup of crack-growth resistance from the growing crack-tip transformation zone. In this sense, the fatigue plot shown in Fig. 12 (filled points) for the specimen preloaded to $K = 12$ MPa · m$^{1/2}$ in quasi-static loading should be closer to the fatigue behavior of Mg-PSZ reported by Dauskardt *et al.*[17] However, as seen in Fig. 12, even the

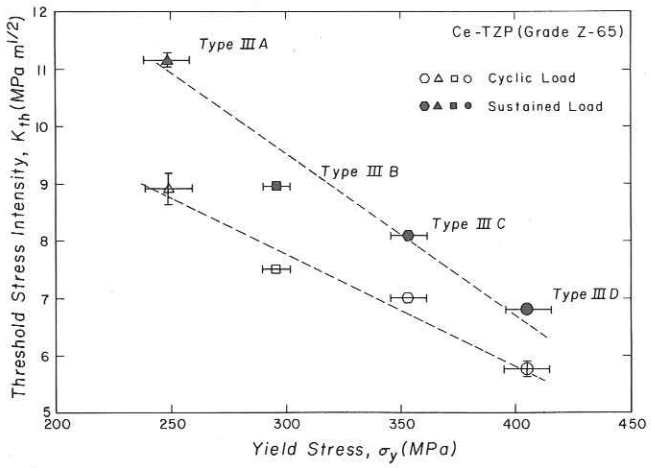

Fig. 10. Variation of threshold stress intensity with transformation yield stress of Ce-TZPs in fatigue and sustained load crack growth.

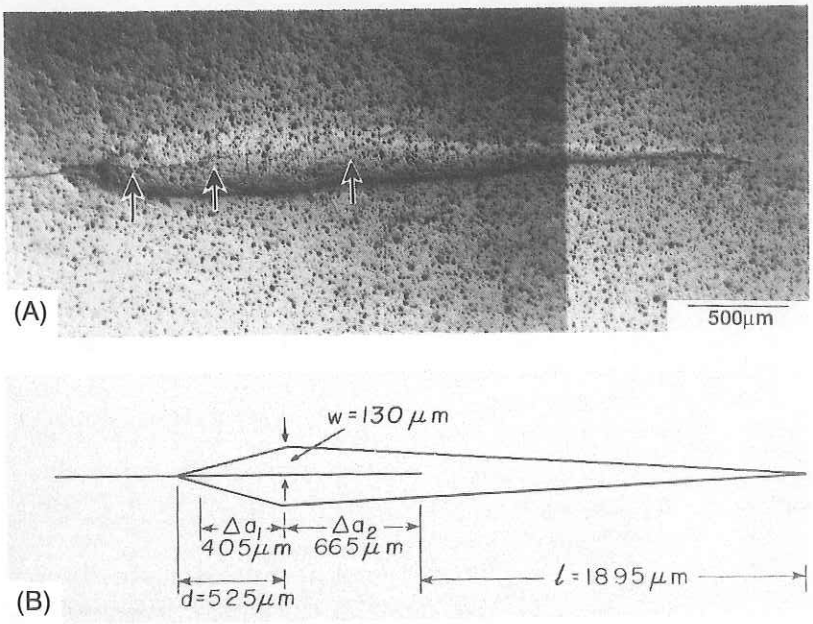

Fig. 11. (A) Transformation zone in a compact tension specimen of type A Ce-TZP subjected to sustained load crack growth to K_I = 12 MPa · $m^{1/2}$. The three arrows from the left point to initial crack-tip position, crack-tip position on application of the sustained load, and crack-tip position after subcritical crack growth, respectively. (B) Schematic of the transformation zone and characteristic zone dimensions.

preloaded Ce-TZP exhibits a well-defined threshold (albeit a higher one) and a low stress-intensity exponent at high crack-growth rates. Thus, it appears that there are some genuine differences in the fatigue responses of Mg-PSZ and Ce-TZP ceramics.

Differences between Mg-PSZ and Ce-TZP ceramics were also evident in other areas of this study. Unlike Mg-PSZ, Ce-TZP ceramics used in the present study did not exhibit true steady-state plateau fracture toughness. The crack-growth-resistance behaviors of Ce-TZPs sintered at different temperatures were similar, particularly the maximum fracture toughness measured before instability. There was a similar behavior in fatigue in that fast fracture occurred at approximately

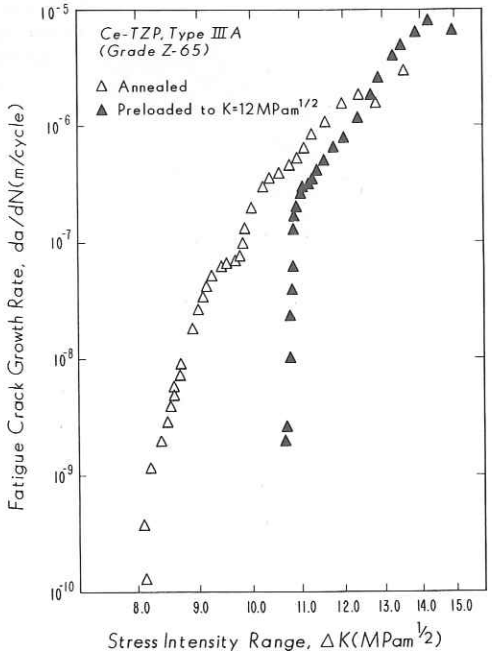

Fig. 12. Comparison of fatigue crack growth behavior of annealed and quasi-statically preloaded compact tension specimens of type A Ce-TZP.

the same critical stress-intensity range (ΔK_c) for different Ce-TZPs. The Ce-TZPs sintered at different temperatures, however, did exhibit very different transformation yield stresses and total transformation plasticity before fracture. Thus, the variation in the relative susceptibilities to fatigue or sustained load crack growth among the different grades (as indicated by the variation in the threshold stress intensities) correlated better with the transformation yield stress (Fig. 7) rather than the saturation or peak fracture toughness.

The most significant difference between Mg-PSZ and Ce-TZP ceramics is in the shape of the transformation zones at crack tips. In Mg-PSZ, transformation zones ahead of the crack tip are nearly semicircular.[17] Such a shape is consistent with a combined shear/dilatation yield criterion. In contrast, Ce-TZPs used in this study showed elongated zones resembling craze zones in polymers. Zones of similar shapes have been reported in earlier studies by Yu and Shetty[22,23] and Rose and Swain.[27] The reason for this unexpected zone shape is not clear. However, a recent study by Tsai *et al.*[28] has shown that the elongated zone shape appears to be associated with the autocatalytic nature of the phase transformation in certain Ce-TZPs. This was supported by evidence of more circular transformation zones in Ce-TZPs that exhibited homogeneous transformation of the metastable tetragonal zirconia. Ongoing research is currently examining the role of the microstructure, specifically, size and distribution of second-phase alumina particles, in triggering autocatalytic transformation in Ce-TZP. It is also of interest to compare both fatigue and sustained load crack growth behaviors in Ce-TZPs that exhibit autocatalytic and homogeneous phase transformations.

There are several potential crack-tip mechanisms that could be responsible for the enhanced crack growth rates in tension–tension fatigue of ceramics (see Evans[4] and Ritchie[29] for a discussion of these mechanisms). In transformation-toughened zirconia ceramics, a mechanism of interest is possible difference in crack-tip shielding from the transformation zone due to either differences in size or shape of the zones or differences in transformation strains or volume fraction of the monoclinic phase in the zones developed in fatigue and sustained loads. To investigate this possibility, crack shielding calculations were made for specific zone shapes and sizes observed in quasi-static (Fig. 5), fatigue (Fig. 7), and sustained load (Fig. 11) crack-growth specimens following the method

Table II. Crack Shielding From Transformation Zones in Quasi-Static, Fatigue, and Sustained Load Crack Growth Specimens of Type A Ce-TZP at $K = 12$ MPa·m$^{1/2}$

Specimen	$\frac{\Delta K(1-\nu)}{e^T V_f E w^{1/2}}$	V_f*	$\Delta K^\dagger$ (MPa·m$^{1/2}$)
Quasi-static (Fig. 5)	−0.091	0.75	−8.90
Fatigue (Fig. 7)	−0.119	0.73	−10.12
Sustained (Fig. 11)	−0.095	0.75	−8.68

*Volume fraction of monoclinic phase in the vicinity of the crack tip determined by Raman spectroscopy. †Calculated assuming $\nu = 0.25$, $e^T = 0.04$, $E = 200$ GPa, and w from the appropriate zone figures.

of McMeeking and Evans.[30] Recent calculations of Marshall[31] have demonstrated the strong influence transformation zone shapes have on the degree of crack shielding in addition to the effect of size. For this reason, observed sizes and shapes of the zones, closely approximated by the schematics in Figs. 5, 7, and 11, were employed in calculating crack shielding from zone boundary tractions resulting from an assumed uniform dilatation strain in the transformation zones. The procedure for this calculation, which involves the use of weight functions, is described in Refs. 30 and 31. The final results are summarized in Table II. Several results are noteworthy. First, normalized crack shielding from the elongated zones of Ce-TZP is nearly half of the asymptotic value calculated by McMeeking and Evans[30] for a steady-state zone with a near circular frontal zone shape defined by a critical hydrostatic stress. This effect of reduction in crack shielding with increasing aspect ratio of the zone front has been discussed by Marshall.[31] Secondly, calculated shielding for the zone in the fatigue crack growth specimen is, in fact, slightly greater than the corresponding crack shieldings in the quasi-static and the sustained load specimens. This result is largely due to the much longer zone extension behind the crack tip in the fatigue specimen as compared to the other two specimens. The absolute values of crack shielding, i.e., values of ΔK, also indicate the same trend. It should be pointed out, however, that calculated values of ΔK are overestimates because the volume fraction of the monoclinic phase used in the calculations was measured close to the crack tip. It is known from Raman spectroscopy measurements that volume fraction of the monoclinic phase decreases with distance from the crack plane. A final point of interest in Table II is that values of V_f are nearly identical for the three specimens. It appears, therefore, that reverse transformation due to load cycling is not very significant in the fatigue specimens. All of the above results suggest that enhanced crack growth during tension–tension load cycling is very likely not due to a decreased crack shielding from the transformation zone.

Even though calculated crack shielding from the transformation zones was nearly identical for the fatigue and sustained load crack growth specimens, they showed an interesting difference in residual crack opening following loading to $K_{max} = 12$ MPa·m$^{1/2}$ and then unloading. Figures 13(A) and (B) compare the crack opening behind the crack tip in the fatigue and the sustained load specimens. It is interesting to note significantly greater residual crack opening in the fatigue specimen as compared to the sustained load specimen. This observation suggests that there may be secondary shielding (or antishielding) mechanisms operating in Ce-TZP ceramics that may have different degrees of effectiveness in fatigue and sustained loading. Ritchie[29] has classified these mechanisms under the category of contact shielding. Two mechanisms in this category are relevant to Ce-TZP ceramics. First, scanning electron microscope observations of cracks, such as those shown in Fig. 13, showed evidence of crack bridging by grains. The lengths of the bridging zones were much greater in the sustained load specimen (~60 μm) as compared to the fatigue specimen (~15 μm). The repeated displacement of the crack faces during fatigue loading may have caused fracture of the bridging grains and overall reduction in crack-tip shielding. Wedging action of grain debris on fatigue fracture surface is another potential mechanism responsible for reduced crack shielding or enhanced residual crack opening in fatigue specimens. Differences in the fracture surfaces of the fatigue and the quasi-static crack growth specimens (Figs. 8(A) and (B)) are consistent with such a mechanism. Current research is focused on quantitatively assessing the contributions of such contact shielding mechanisms to establish their role in cyclic-stress-accelerated crack growth in Ce-TZP ceramics.

V. Conclusions

(1) Ce-TZP ceramics exhibit true cyclic-stress-induced fatigue crack growth behavior characterized by significantly higher crack growth rates in tension–tension cyclic loading as compared to crack growth rates under peak static loading and fatigue threshold stress intensities lower than thresholds for sustained load crack growth.

(2) Resistance to fatigue crack growth in Ce-TZP, as indicated by the threshold stress-intensity range, can be en-

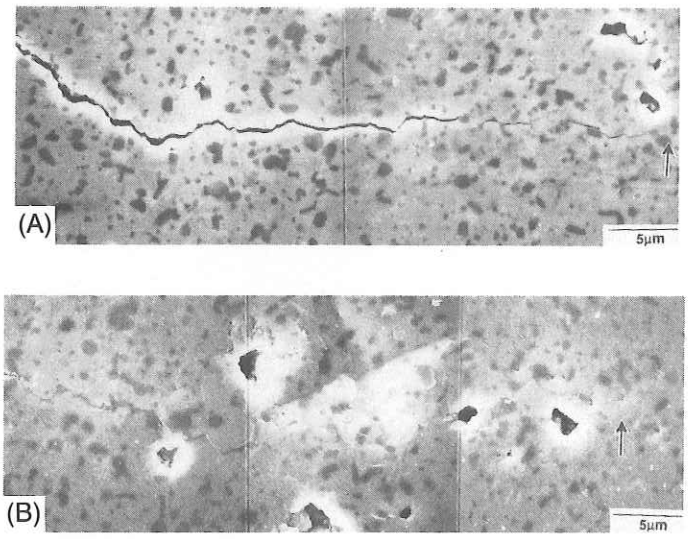

Fig. 13. Scanning electron micrographs of cracks in compact tension specimens after loading to $K_{max} = 12$ MPa·m$^{1/2}$ and unloading: (A) fatigue crack growth specimen, (B) sustained load crack growth specimen. Arrows point to the crack tips.

hanced either by decreasing the transformation yield stress by sintering at higher temperatures or by preforming a crack-tip transformation zone by prior quasi-static loading.

(3) The enhanced crack growth in fatigue in Ce-TZPs is not due to reduced crack shielding from the transformation zone.

(4) Evidence of increased residual crack opening noted in fatigue specimens is consistent with reduced crack shielding. But the reduction in crack shielding is likely to be caused by a shorter crack-tip bridging zone and/or wedging action of grain debris on the fatigue fracture surface.

Acknowledgments: The authors are grateful to Dr. David B. Marshall, Rockwell Science Center, for the Raman spectroscopy measurements of the phase compositions within transformation zones.

References

[1]A. G. Evans and E. R. Fuller, "Crack Propagation in Ceramic Materials under Cyclic Loading Conditions," *Metall. Trans.,* **5** [1] 27–33 (1974).

[2]A. G. Evans, L. R. Russell, and D.W. Richerson, "Slow Crack Growth in Ceramic Materials at Elevated Temperatures," *Metall. Trans. A,* **6** [4] 707–16 (1975).

[3]A. G. Evans and M. Linzer, "High-Frequency Cyclic Crack Propagation in Ceramic Materials," *Int. J. Fract.,* **12** [2] 217–22 (1976).

[4]A. G. Evans, "Fatigue in Ceramics," *Int. J. Fract.,* **16** [6] 485–98 (1980).

[5]D. A. Krohn and D. P. H. Hasselman, "Static and Cyclic Fatigue Behavior of a Polycrystalline Alumina," *J. Am. Ceram. Soc.,* **55** [4] 208–10 (1972).

[6]R. Kossowsky, "Cyclic Fatigue of Hot-pressed Si_3N_4," *J. Am. Ceram. Soc.,* **56** [10] 531–35 (1973).

[7]C. P. Chen and W. J. Knapp, "Fatigue Fracture of an Alumina Ceramic at Several Temperatures"; p. 691 in Fracture Mechanics of Ceramics, Vol. 2. Edited by R. C. Bradt, D. P. H. Hasselman, and F. F. Lange. Plenum Press, New York, 1974.

[8]F. Guiu, "Cyclic Fatigue of Polycrystalline Alumina in Direct Push-Pull," *J. Mater. Sci.,* **13**, 1357–61 (1978).

[9]Y. Matsuo, Y. Hattori, Y. Katayama, and I. Fukuura, "Cyclic Fatigue Behavior of Ceramics"; pp. 515–22 in Progress in Nitrogen Ceramics. Edited by F. L. Riley. Martinus Nijhoff Publishers, Boston, MA, 1983.

[10]T. Fett, G. Himsolt, and D. Munz, "Cyclic Fatigue of Hot-Pressed Si_3N_4 at High Temperatures," *Adv. Ceram. Mater.,* **1** [2] 179–84 (1986).

[11]L. Ewart and S. Suresh, "Dynamic Fatigue Crack Growth in Polycrystalline Alumina under Cyclic Compression," *J. Mater. Sci.,* **5**, 774–78 (1986).

[12]L. Ewart and S. Suresh, "Crack Propagation in Ceramics under Cyclic Loads," *J. Mater. Sci.,* **22**, 1173–92 (1987).

[13]S. Suresh and J. R. Brockenbrough, "Theory and Experiments of Fracture in Cyclic Compression: Single Phase Ceramics, Transforming Ceramics, and Ceramic Composites," *Acta Metall.,* **36** [6] 1455–70 (1988).

[14]M.V. Swain and V. Zelizko, "Comparison of Static and Cyclic Fatigue on Mg-PSZ Alloys"; pp. 595–606 in Advances in Ceramics, Vol. 24B, Science and Technology of Zirconia III. Edited by S. Somiya, N. Yamamoto, and H. Hanagida. The American Ceramic Society, Westerville, OH, 1988.

[15]R. H. Dauskardt, W. Yu, and R. O. Ritchie, "Fatigue Crack Propagation in Transformation-Toughened Zirconia Ceramic," *J. Am. Ceram. Soc.,* **70** [10] C-248–C-252 (1987).

[16]R. H. Dauskardt, D. B. Marshall, and R. O. Ritchie, "Cyclic Fatigue Crack Propagation in Ceramics: Behavior in Overaged and Partially Stabilized MgO–Zirconia"; in Proceedings of a Joint Symposia on Fracture Mechanics/Structural Mechanics, Materials Research Society International Meeting on Advanced Materials, Ikebukuro, Tokyo, Japan, June, 1988. Material Research Society, Pittsburgh, PA.

[17]R. H. Dauskardt, D. B. Marshall, and R. O. Ritchie, "Cyclic Fatigue-Crack Propagation in Magnesia-Partially-Stabilized Zirconia Ceramics," *J. Am. Ceram. Soc.,* **73** [4] 893–903 (1990).

[18]P. F. Becher, "Subcritical Crack Growth in Partially Stabilized ZrO_2 (MgO)," *J. Mater. Sci.,* **21** [1] 297–300 (1984).

[19]L. A. Sylva and S. Suresh, "Crack Growth in Transforming Ceramics under Cyclic Tensile Loads," *J. Mater. Sci.,* **24**, 1729–38 (1989).

[20]J. C. Wurst and J. A. Nelson, "Lineal Intercept Technique for Measuring Grain Size in Two-Phase Polycrystalline Ceramics," *J. Am. Ceram. Soc.,* **55** [2] 109 (1972).

[21]H. Toraya, M. Yoshimura, and S. Somiya, "Calibration Curve for Quantitative Analysis of the Monoclinic-Tetragonal ZrO_2 System by X-Ray Diffraction," *J. Am. Ceram. Soc.,* **67** [6] C-119–C-121 (1984).

[22]C. S. Yu and D. K. Shetty, "Transformation Zone Shape, Size, and Crack-Growth-Resistance (*R*-Curve) Behavior of Ceria-Partially-Stabilized Zirconia Polycrystals," *J. Am. Ceram. Soc.,* **72** [6] 921–28 (1989).

[23]C. S. Yu and D. K. Shetty, "Transformation Yielding, Plasticity, and Crack-Growth-Resistance (*R*-Curve) Behavior of CeO_2-TZP," *J. Mater. Sci.,* **25**, 2025–2035 (1990).

[24]ASTM E 561-81, Standard Practice for *R*-Curve Determination; pp. 612–32 in Annual Book of ASTM Standards, Sect. 3, Metals Test Methods and Analytical Procedures. American Society for Testing and Materials, Philadelphia, PA, 1984.

[25]ASTM E 647-83, Standard Test Method for Constant-Load-Amplitude Fatigue Crack Growth Rates Above 10^{-8} m/cycle; pp. 711–31 in Annual Book of ASTM Standards, Sect. 3, Metals Test Methods and Analytical Procedures. American Society for Testing and Procedures, Philadelphia, PA, 1983.

[26]D. Singh and D. K. Shetty, "Application of Microcircuit Grids in Crack-Growth-Resistance (*R*-Curve) and Subcritical Crack Growth Measurements in Ceramics"; presented at the 91st Annual Meeting of the American Ceramic Society, Indianapolis, IN, April 25, 1989 (Basic Science Division, Paper No. 68-8-89).

[27]L. R. F. Rose and M.V. Swain, "Transformation Zone Shape in Ceria-Partially-Stabilized Zirconia," *Acta Metall.,* **36** [4] 955–62 (1988).

[28]J. F. Tsai, C. S. Yu, and D. K. Shetty, "Autocatalytic Phase Transformation and the Zone Shape in Ceria-Partially-Stabilized Zirconia (Ce-TZP)/Al_2O_3 Composites"; unpublished work.

[29]R. O. Ritchie, "Mechanisms of Fatigue Crack Propagation in Metals, Ceramics, and Composites: Role of Crack Tip Shielding," *Mater. Sci. Eng.,* **A103**, 15–28 (1988).

[30]R. M. McMeeking and A. G. Evans, "Mechanics of Transformation–Toughening in Brittle Materials," *J. Am. Ceram. Soc.,* **65** [5] 242–46 (1982).

[31]D. B. Marshall, "Crack Shielding in Ceria-Partially-Stabilized Zirconia"; unpublished work. □